RESEARCH MEMORANDUM

PRELIMINARY INVESTIGATION OF PUMPING AND THRUST CHARACTERISTICS OF FULL-SIZE COOLING-AIR EJECTORS AT SEVERAL EXHAUST-GAS TEMPERATURES

By W. K. Greathouse

Lewis Flight Propulsion Laboratory
Cleveland, Ohio

NATIONAL ADVISORY COMMITTEE
FOR AERONAUTICS

WASHINGTON
April 9, 1954

NACA RM E54A18

NATIONAL ADVISORY COMMITTEE FOR AERONAUTICS

RESEARCH MEMORANDUM

PRELIMINARY INVESTIGATION OF PUMPING AND THRUST CHARACTERISTICS OF FULL-SIZE COOLING-AIR EJECTORS AT SEVERAL EXHAUST-GAS TEMPERATURES

By W. K. Greathouse

SUMMARY

An experimental investigation was made to determine the performance of seven full-size ejector configurations operating over a range of secondary to primary air-flow ratio from zero to about 0.30, at primary total- to ambient-pressure ratios up to 5.0, and at various primary gas temperatures from 1120° to 3700° R. The tests were performed on a turbojet-engine and afterburner assembly in an altitude test chamber. Ejector-shroud to primary-nozzle-exit diameter ratios of 1.048, 1.095, 1.195, and 1.60 were tested with cylindrical-type ejector shrouds, and a diameter ratio of 1.10 was tested with a conical-type ejector shroud. Spacing ratio was varied from 0.213 to 0.810 for the cylindrical ejector with a diameter ratio of 1.095.

The weight-flow ratio of the cylindrical ejectors increased with primary gas temperature in such a manner that the pumping characteristics were almost generalized by the corrected weight-flow ratio parameter $(W_s/W_p)\sqrt{T_s/T_p}$, which applied especially well for ejectors having a short shroud length relative to the diameter ratio. Pumping performance of the conical ejector investigated did not correlate at various primary gas temperatures on the basis of the corrected weight-flow ratio parameter.

The variation in gross ejector-thrust ratio with the different levels of afterburning gas temperature was not consistent. Thrust ratio with afterburning, however, was generally higher than without afterburning, but the total variation for any one ejector configuration did not exceed 5 percent when compared over a range of corrected weight-flow ratio at a primary pressure ratio of 5.0.

At very low values of weight-flow ratio, the cylindrical-type ejector showed better air-handling capacity than a conical-type ejector of the same diameter and spacing ratio, and this trend was reversed at

higher flow ratios. The thrust ratio of the cylindrical type was slightly higher than that of the conical-type ejector at the same weight-flow ratio. Reverse secondary flow was indicated as more likely to occur with the conical-type ejector.

INTRODUCTION

The air ejector has been established as an effective means of supplying cooling air for aircraft engine installations. Because of the many variables which affect ejector performance, there is considerable need at the present time for experimental ejector test data to aid in the design and selection of ejector configurations. References 1 to 4 present ejector-performance data of conical and cylindrical models over a range of ejector geometry and operating pressure ratio for cold (540° R) primary- and secondary-air temperatures. Pumping characteristics of turbojet-engine ejectors (with a 16-in. primary nozzle-exit diameter) operating at primary gas temperatures from 1260° to 1660° R and at primary pressure ratios up to only 1.8 are compared in reference 5 with pumping characteristics of geometrically similar 1/4-scale model ejectors operating with cold (540° R) air. A corrected weight-flow parameter $(W_s/W_p)\sqrt{T_s/T_p}$ was developed in reference 5, and, by use of this parameter, a good correlation was obtained between the hot and cold ejector tests for the ejector configurations that had short mixing lengths. Subsequent ejector tests performed on a full-scale afterburning engine (ref. 6) indicated that the corrected weight-flow ratio parameter did not correlate engine-ejector and model-ejector pumping characteristics at afterburning gas temperatures and high pressure ratios.

The NACA Lewis laboratory is therefore conducting a program to determine the effects of temperature on both ejector pumping and thrust characteristics. This phase of the investigation covers the experimental results obtained from tests of full-size ejectors on a turbojet-engine and afterburner assembly in one of the NACA Lewis altitude test chambers.

Pumping and thrust performance of six cylindrical-type ejectors and one conical-type ejector are presented at primary total- to ambient-pressure ratios from 1.75 to 5.0 with primary-gas temperatures from 1120° to 3700° R. These ejector data are presented in terms of secondary to primary weight-flow ratio, primary-gas to secondary-air temperature ratio, and gross ejector thrust to primary nozzle thrust ratio, and are plotted as functions of the operational variables, primary pressure ratio and secondary pressure ratio. Cross plots of data are made to show how well the ejector performance was correlated by the corrected weight-flow ratio parameter $(W_s/W_p)\sqrt{T_s/T_p}$ and to indicate the effects of diameter ratio and spacing ratio at specific operating conditions.

[redacted]

Primary nozzle-exit diameters of 21.10 and 15.75 inches were used with several ejector shrouds to provide diameter ratios of 1.048, 1.095, 1.195, and 1.60 for the six cylindrical ejectors and a diameter ratio of 1.10 for the one conical ejector. Spacing ratio varied from 0.213 to 0.810 for the various ejectors.

APPARATUS

Test Facility

Ejector tests of this investigation were performed on an engine-afterburner assembly installed in an altitude chamber as shown in figures 1(a) and (b). The J34-WE-22 turbojet engine and afterburner were rigidly mounted on a platform that was suspended from the top of the altitude chamber by means of steel flexure plates. Force was transmitted from the platform to a thrust-measuring unit calibrated to read the total thrust force with an accuracy of $\pm 1\frac{1}{2}$ percent. A more complete description of the engine and altitude test chamber is reported in reference 7.

Afterburner

The afterburner shell (fig. 2(a)) was made of 1/8-inch Inconel sheet and was 61 inches long. Inconel channels on the outside surface (fig. 2(b)) provided support and served as spaces for the cooling shroud, which was installed as shown in figure 3. Dimensions of the afterburner were the same for all ejector configurations, and the primary nozzle-exit diameters and half-cone angles are shown in figure 2(a).

Ejector Configurations

A typical cylindrical-ejector shroud is shown in figure 4(a), and 4(b) shows a conical-ejector shroud. These shrouds were also made of Inconel and could be coupled to the cooling-shroud afterburner assembly (fig. 3) by means of a quick-disconnect, clamped flange joint. Seven ejector shrouds were attached to the cooling-shroud flange to provide the following ejector configurations:

Ejector configuration	Type of ejector	Diameter ratio, D_s/D_p	Spacing ratio, L/D_p
A	Cylindrical	1.048	0.445
B	Cylindrical	1.095	.213
C	Cylindrical	1.095	.408
D	Cylindrical	1.095	.810
E	Cylindrical	1.195	.403
F	Cylindrical	1.60	.587
G	Conical	1.10	.408

Diagrams giving the basic dimensions of each ejector configuration are shown in figure 5. Also shown is the basic engine configuration used for calibrating the primary nozzle in terms of mass flow and thrust.

Instrumentation

Primary total and static pressures were measured 20 inches upstream of the primary nozzle exit (station p) by a water-cooled rake and wall-pressure taps, respectively. The 12 total-pressure probes on the rake (fig. 6) were spaced at intervals of equal flow areas.

Secondary total pressure P_s was measured by 10 probes at station s spaced in the secondary flow passage, as indicated in figure 7. Axial location of the P_s probes (station s) was 1/2 inch upstream of the minimum secondary-flow area for ejector configurations A to E. For configuration F the secondary total pressure was measured 1/2 inch upstream from the cylindrical portion of the ejector shroud, and for configuration G the measurement was made 1/2 inch upstream of the conical portion of the ejector shroud (see fig. 5). Ambient pressure (exhaust pressure) was taken with four equally spaced static tubes located on the outside lip of the ejector shroud, as shown in figure 4(a). Static pressures along the ejector shroud were measured by wall static taps (fig. 4) spaced over the entire shroud length.

Primary gas temperature for nonafterburning operation was measured by 48 thermocouples at the turbine outlet. With the afterburner in operation, primary gas temperature was calculated as described in appendix B.

Secondary total temperature was measured with four equally spaced temperature probes located at station s, as in figure 7.

Various skin temperatures were measured on the afterburner and ejector to calculate nozzle thermal expansion and to locate hot spots in the afterburner shell. Engine air flow was calculated in the conventional manner by using measured pressures and temperatures and a calibrated venturi engine-inlet assembly. Primary-stream weight flow was calculated as the sum of engine-inlet air flow and total fuel flow, minus calibrated leakage air flow. Secondary-air flow was measured with A.S.M.E. standard flat-plate orifices.

PROCEDURE

Ejector geometry was varied over a range of diameter ratio (from 1.048 to 1.195) and spacing ratio (from 0.213 to 0.810) by simply changing the ejector shroud and using the same 21.1-inch-diameter primary nozzle. The large diameter ratio of 1.60 (configuration F) was obtained by using a 15.75-inch primary nozzle.

Operational variables involved were primary total pressure P_p, secondary total pressure P_s, primary total temperature T_p, secondary total temperature T_s, primary air flow W_p, secondary air flow W_s, and ambient pressure p_0. The variables P_p, T_p, and W_p were held nearly constant for a given test by adjusting engine-inlet pressure, inlet temperature, engine speed, and afterburner fuel-air ratio. Then, one method of performing the test was to set P_p/p_0 by changing p_0 and varying W_s to obtain a range of W_s/W_p, T_p/T_s, and P_s/p_0. Another method was to set W_s and vary p_0 to obtain a range of P_s/p_0 and P_p/p_0 for which T_p/T_s and W_s/W_p were practically constant.

Each ejector configuration was investigated over a range of W_s/W_p, T_p/T_s, P_s/p_0, and P_p/p_0 at the nominal values of primary gas temperatures in table I. Tests with zero secondary flow ($W_s = 0$) were performed over a range of pressure ratio for each ejector configuration at primary gas temperatures of 540° and 1120° R, except for configuration G which was operated at primary gas temperatures of 1120° and 2200° R with zero secondary flow.

Thrust was measured for all the ejector tests except when the engine was windmilling ($T_p = 540°$ R). Large ram forces acting on the windmilling engine made the measurement of ejector thrust impractical.

Calibration of the 21.1-inch nozzle was made with the ejector removed (basic engine configuration, fig. 5(a)) at gas temperatures of 1120°, 3000°, and 3700° R to determine flow and thrust coefficients over a range of pressure ratio. The 15.75-inch nozzle was calibrated at a gas temperature of 1500° R only.

Clear unleaded gasoline (H/C of about 0.180) was used as engine fuel and JP-4 (H/C of about 0.170) was used for afterburner fuel throughout the investigation.

RESULTS AND DISCUSSION

Pumping and thrust characteristics of a full-size ejector are reported herein as determined from experimental test results. The symbols and various parameters used are defined in appendix A. Thrust and discharge coefficients of the primary nozzles are also presented for use in calculation of net ejector thrust for a specific flight plan.

Primary-Nozzle Performance

Results of the primary-nozzle calibrations are shown in figures 8 and 9 along with calculated thrust curves ($\gamma = 1.365$) for an ideal convergent nozzle and for an ideal nozzle having complete isentropic expansion. The thrust parameter F_j/p_0A_p for the 21.1-inch nozzle (fig. 8) was higher at the gas temperature of 1120° R (nonafterburning) than at gas temperatures of 3000° and 3700° R (with afterburning). This change in thrust is not only a result of the change in gas properties due to the change in temperature level, but is also a result of various primary-stream characteristics such as velocity profiles and possibly gas whirl from the engine associated with different levels of afterburner operation.

Primary-nozzle thrust coefficients in figure 10 are the ratio of measured thrust to the thrust of an ideal convergent nozzle calculated as described in appendix B. The thrust coefficient of the 21.1-inch nozzle for nonafterburning at T_p of 1120° R was about 2 percent higher than with afterburning at T_p of 3000° or 3700° R, probably because of the previously mentioned differences in primary-stream characteristics. A lower thrust coefficient (about 1 percent lower) was obtained with the 15.75-inch nozzle than with the 21.1-inch nozzle. Since the gas temperatures (1500° and 1120° R) and operating conditions of the two nozzles were not radically different (both were evaluated at nonafterburning conditions), the lower thrust coefficient can probably be attributed to the greater convergence angle of the 15.75-inch nozzle. Discharge coefficients for the 21.1-inch and 15.75-inch nozzles in figure 11 show essentially the same trends as the thrust coefficients in figure 10. Calculation of the discharge coefficient is presented in appendix B.

Either nozzle coefficients or the nozzle calibration curves, or both, can be used to calculate absolute values of primary gas flow, secondary air flow, primary-nozzle thrust, and ejector thrust from the ejector-performance curves presented herein.

Ejector Performance

The ejector test data are grouped according to configuration in figures 12 to 36. Each group (except for configuration F) contains experimental ejector-performance data at three or more primary gas temperatures. At each primary gas temperature, ejector pumping characteristics are presented as measured values of weight-flow ratio W_s/W_p against secondary pressure ratio P_s/p_0 for constant values of primary pressure ratio P_p/p_0. Ejector gross-thrust ratio F_{ej}/F_j is plotted over the range of primary pressure ratio for various constant values of weight-flow ratio. Ejector-thrust ratio is the ratio of ejector gross thrust to the gross thrust of the primary nozzle operating at approximately the same gas temperature and at the same over-all pressure ratio without the ejector shroud. The ratio of primary gas temperature to secondary air temperature T_p/T_s is presented in the same manner as weight-flow ratio so that the corrected weight-flow ratio parameter $(W_s/W_p)\sqrt{T_s/T_p}$ can be determined at any ejector operating condition investigated. The minimum weight-flow ratio for afterburning (T_p from 2000° to 3700° R) conditions was dictated by cooling requirements necessary to keep the primary nozzle and afterburner skin temperature at a safe level (1600° F). Values of weight-flow ratio with nonafterburning (T_p = 1120° R) were therefore carried well into the range required with afterburning in order to allow comparison of the ejector at various operating gas temperatures. All ejector configurations were tested with zero secondary flow (upstream secondary passage blocked) at the nonafterburning temperature, and the resulting secondary pressure ratios and ejector-thrust ratios are presented herein.

3162

Typical Ejector Characteristics

Pumping characteristics of ejector configuration A in figure 12 show the usual ejector action for zero-secondary-flow conditions in that secondary pressure ratio P_s/p_0 was reduced to a minimum and then increased approximately linearly as primary pressure ratio P_p/p_0 was increased. The linear relation between P_s/p_0 and P_p/p_0 existed after the primary jet expanded to intercept the ejector shroud and formed a stable supersonic flow upstream of any internal shock as described in reference 4. The area above zero-secondary-flow curves (such as fig. 12) defines combinations of primary and secondary pressure ratios at which the ejector will operate with some secondary air flow. The area below the zero-flow curve represents operating conditions for which reverse flow would occur (ref. 3) if the ejector were subjected to such combinations of pressure ratio. The primary pressure ratio at which secondary flow is exactly zero for a given pressure ratio across the entire secondary system is called the "cut-off point", and the locus of these cut-off points is, of course, defined by the zero-secondary-flow curve.

Pumping characteristics of configuration A with secondary flow are shown in figure 13(a) for the nonafterburning gas temperature of 1120° R, in figure 13(b) for afterburning gas temperatures from 3000° to 3200° R, and in figure 13(c) for afterburning gas temperatures from 3600° to 3700° R. The temperature ratio T_p/T_s at which the ejector operated is shown in figure 14(a) to (c) for the respective parts of figure 13(a) to (c).

Thrust performance of configuration A is shown in figure 15(a) to (c) for the three primary gas temperatures previously mentioned. Data points are not shown because the thrust curves (except for $W_s/W_p = 0$) were cross-plotted. The thrust ratio at zero secondary flow (fig. 15(a) is similar to that of a convergent-divergent nozzle in that relatively large thrust losses resulted from overexpansion and shock losses when the primary ratio was at a certain value (P_p/p_0 of about 1.75 in this case). Overexpansion of the primary stream was effectively reduced by the addition of secondary flow (fig. 15(a)) and thus enabled more of the ideally available primary thrust to be recovered. Thrust was also added by the secondary mass flow and velocity, and consequently the gross thrust of the ejector system continuously increased with weight-flow ratio as shown in figure 15. It should be noted, however, that net ejector thrust will not continuously increase with increased weight-flow ratio because of the secondary-air inlet momentum. In other words, at a fixed flight condition, net-thrust ratio will maximize with weight-flow ratio.

3162

Ejector performance data for configurations B, C, D, and E (figs. 16 through 33) are presented in the same general manner as were data for configuration A. Some ejectors were not tested with a primary gas temperature of 3700° R (because of excessive nozzle skin temperature), and therefore performance data at a gas temperature of about 2000° R are included for these configurations. Configuration F represents a large diameter-ratio ejector such as might exist with a fixed ejector shroud when the nozzle of an afterburning engine is in the closed position. Tests of this ejector (figs. 34 to 36) were performed only at the nonafterburning gas temperature of 1500° R. The secondary pressure ratio is not presented in figure 34 (configuration F) for values of weight-flow ratio above 0.086 because of unreliable secondary-pressure measurements which resulted from supersonic flow and shock in the secondary passage.

Performance data for the one conical ejector investigated (configuration G) are presented in figures 37 to 40.

Effect of Operating Temperatures on Ejector Flow Characteristics

Ejector flow theory (ref. 5) shows that the weight-flow ratio W_s/W_p of an ejector will increase with increased temperature ratio T_p/T_s if operating pressures P_p/p_0 and P_s/p_0 are held constant. The manner in which W_s/W_p increases with T_p/T_s for a turbojet-engine ejector is a function of many secondary variables that also change with temperature level (because of the change in engine or afterburner operation necessary to obtain the temperature level). Some of these secondary variables are the velocity and temperature gradients across the primary stream and the gas properties of the primary stream resulting from the addition of various amounts of fuel. However, the corrected weight-flow ratio $(W_s/W_p)\sqrt{T_s/T_p}$, as developed in reference 5, serves as an approximate parameter to correlate flow characteristics of an ejector operating at different temperatures.

In order to compare values of measured weight-flow ratio and also to indicate the degree of correlation that can be obtained by use of the corrected weight-flow ratio, these two parameters are plotted in figures 41 to 46 over a range of secondary pressure ratio (parts (a)) and a range of primary pressure ratio (parts (b)) for the various ejector configurations operating at afterburning and nonafterburning gas temperatures. At a specific operating pressure ratio, the measured weight-flow ratio (represented by dashed lines) for all the ejector configurations increased with an increase from the nonafterburning gas temperature (1120° R) to the lowest afterburning gas temperature (about 2000° or 3000° R). For the afterburning range of gas temperature (2000° to 3700° R), measured weight-flow ratio increased with increased gas temperature (except for configurations A and G), but the rate of increase of weight-flow ratio with temperature was not as great as for the change from nonafterburning to afterburning operation. However, configuration A (the smallest diameter ratio investigated, $D_s/D_p = 1.048$) and configuration G (the one conical-type ejector tested) showed a decrease in measured weight-flow ratio with an increase in afterburning gas temperature. The curves of figures 41 to 46 thus indicate that measured ejector weight-flow ratio (for specific operating pressure ratios) is not only a function of operating temperature but is also influenced by (1) changes in secondary variables necessary to obtain various operating temperatures and (2) the geometry of the ejector configuration.

The solid lines in figures 41 to 46 show air-flow characteristics of the various ejectors in terms of corrected weight-flow ratio $(W_s/W_p)\sqrt{T_s/T_p}$, and a comparison of these curves indicates the degree of correlation obtained by using only a temperature-ratio correction factor. A good correlation was obtained for two of the cylindrical ejectors (configuration B, fig. 42, and configuration C, fig. 43) in that the corrected

weight-flow ratio curves grouped together (maximum spread of less than 0.01 $(W_s/W_p)\sqrt{T_s/T_p}$ scale units) over the range of operating gas temperature from 1120° to 3200° R. For the cylindrical configurations A, D, and E the corrected weight-flow ratio curves (figs. 41, 44, and 45) at afterburning temperatures are below the curve for the nonafterburning temperature, which means that the afterburning data were essentially "overcorrected" by the temperature-ratio correction factor $\sqrt{T_s/T_p}$. The conical-ejector (configuration G) curves in figure 46 show a much larger "overcorrection" than occurred for any of the cylindrical-type ejectors. It can be noted that the measured weight-flow ratio curves of the conical ejector grouped closer than the corrected weight-flow ratio curves.

To give an over-all view of how the corrected weight-flow ratio applied to cylindrical ejectors of various diameter and spacing ratios, figure 47 is presented as the difference in corrected weight-flow ratio $\left(\Delta \frac{W_s}{W_p}\sqrt{\frac{T_s}{T_p}}\right)$ that resulted between nonafterburning operation at 1120° R and afterburning operation at 3000° to 3200° R, for fixed operating pressure ratios ($P_p/p_0 = 3.5$ and $P_s/p_0 = 2.5$). It is indicated that $\left(\Delta \frac{W_s}{W_p}\sqrt{\frac{T_s}{T_p}}\right)$ increased from 0.0005 to 0.008 units as spacing ratio was changed from 0.213 to 0.810 with the diameter ratio constant at 1.095.

For a constant spacing ratio of about 0.4, $\left(\Delta \frac{W_s}{W_p}\sqrt{\frac{T_s}{T_p}}\right)$ decreased greatly as diameter ratio was changed from 1.048 to 1.095 and increased only slightly with a diameter-ratio change from 1.095 to 1.195. Thus, for the gas-temperature range (1120° to 3200° R) and operating pressure ratios ($P_p/p_0 = 3.5$ and $P_s/p_0 = 2.5$) of figure 47, it appears that airflow characteristics were practically generalized for the cylindrical-type ejector with a short mixing length relative to the diameter ratio (L/D_p of 0.40 or less and D_s/D_p of 1.10 or greater, configurations B and C), but were not generalized for the cylindrical ejector having an L/D_p greater than 0.40 (configuration D) or a D_s/D_p less than 1.10 (configuration A).

Effect of Operating Temperature on Ejector-Thrust Ratio

The effect of operating temperature on ejector-thrust ratio is presented in figure 48 for a range of corrected weight-flow ratio at the primary pressure ratio of 5.0 (highest P_p/p_0 investigated). These curves were cross-plotted from the corresponding thrust data previously

presented. A higher thrust ratio at the afterburning temperatures (2000° to 3700° R) than at the nonafterburning temperature (1120° R) is indicated as a general trend in figure 48 for all the ejector configurations when compared at the same corrected weight-flow ratio. For the afterburning temperature range only, the variation of thrust ratio with primary gas temperature is shown to be unsystematic, and pronounced trends are not apparent because the accuracy of the thrust-measuring system was only about $\pm 1\frac{1}{2}$ percent. It is of interest to note that the gross-thrust ratio (at a given value of $(W_s/W_p)\sqrt{T_s/T_p}$) of any specific ejector configuration in figure 48 did not vary with gas temperature more than 0.04 thrust-ratio units (less than 5 percent of engine thrust) over the range (0.01 to 0.18) of corrected weight-flow ratio presented.

Effect of Geometry on Ejector Performance

Ejector performance is, of course, affected by changes in ejector geometry because expansion processes of both the primary and secondary streams are affected, as well as the amount of mixing between the two streams. In order to show the effects of changes in ejector geometry, a brief comparison of pumping and thrust characteristics was made for the various ejector configurations at the nonafterburning gas temperatures of 1120° R in figures 49 to 51.

Diameter ratio. - Changes in diameter ratio at a constant spacing ratio of about 0.4 showed in figure 49(a) that the ejector with the largest diameter ratio (D_s/D_p = 1.195) had the best pumping characteristics for weight-flow ratios of both 0.03 and 0.07 in that the flow ratios were handled at a lower level of secondary pressure ratio. In figure 49(a), operational limits (cut-off point) of the ejectors were shifted to a higher range of primary pressure ratio with increased diameter ratio as indicated by the zero-secondary-flow curves.

Thrust characteristics of the three ejectors with spacing ratio of 0.4 in figure 49(b) indicate that the highest thrust ratio at a weight-flow ratio of 0.07 was attained by the ejector with the medium diameter ratio (D_s/D_p = 1.095). This effect is likely the result of a more efficient expansion of the primary stream with the diameter ratio of 1.095 at W_s/W_p of 0.07 than with the other two diameter ratios. That is, the expansion ratio of the primary stream is essentially controlled by the physical size of the ejector and the amount of secondary flow.

Spacing ratio. - The effects of changes in spacing ratio on ejector pumping and thrust characteristics at a diameter ratio of 1.095 are shown in figures 50(a) and (b), respectively. The longest ejector (L/D_p = 0.81) had the best pumping characteristics at the flow ratio W_s/W_p of 0.7, but

for the lower flow ratio of 0.03 the shortest ejector ($L/D_p = 0.213$) had a slightly better air-handling capacity (fig. 50(a)) when operating above a primary pressure ratio of 3.0. About the same thrust ratio occurred (fig. 50(b)) at a weight-flow ratio of 0.07 for the short-length ejector ($L/D_p = 0.213$) and the medium-length ejector ($L/D_p = 0.408$). The thrust ratio of the longest ejector ($L/D_p = 0.81$) was about 2 to 3 percent lower than for the other two ejectors at the flow ratio of 0.07. The maximum thrust losses at zero secondary flow (fig. 50(b)) and the maximum suction pressure (fig. 50(b)) developed by the ejectors with the diameter ratios of 1.095 increased as spacing ratio was increased. This effect, of course, resulted because the primary jet expanded to fill the shroud exit of the longer ejector at a primary pressure ratio somewhat lower than the primary pressure required to fill the shroud exit of the two shorter ejectors.

3162

Comparison of cylindrical and conical ejector. - Performance of the one conical-type ejector investigated (configuration G) is compared in figure 51 with the performance of a cylindrical ejector (configuration C) having almost the same diameter ratio and spacing ratio and operating at the same nonafterburning gas temperature of 1120° R. The large differences in pumping characteristics (fig. 51(a)) that occurred with the different type of ejector can be explained by considering the type of flow believed to be present in the conical- and cylindrical-type ejector shrouds at different levels of weight-flow ratio. At a weight-flow ratio of zero, the primary jet can expand to strike the conical-shroud wall well upstream of the shroud exit and cause a portion of the primary stream to be deflected upstream along the shroud wall with a consequent rise in secondary pressure. To maintain equilibrium, the deflected flow is entrained by the primary jet and a continuous circulation is set up. Thus, the conical ejector is essentially pumping a certain amount of secondary flow, even though the over-all weight-flow ratio is zero. The circulating flow should be a function of the conical-shroud geometry and would probably increase with increased shroud cone angle. The cylindrical shroud (cone angle of zero) would have the least circulation, and a lower secondary pressure would result as indicated in figure 51(a). At some low value of weight-flow ratio, the circulation within the conical shroud could be partially eliminated by the presence of a small secondary flow, and the pumping characteristics of the conical and cylindrical ejector could approach each other as indicated in figure 51(a) at W_s/W_p of 0.01. At a sufficiently large weight-flow ratio ($W_s/W_p = 0.05$, fig. 51(a)), the circulation would, of course, be completely stopped and the conical ejector could pump the same secondary flow at a lower level of secondary pressure ratio than the cylindrical ejector because the exposed shearing surface of the primary jet is greater for the conical ejector. It can also be noted from the slope and position of the zero-secondary-flow curves in figure 51(a) that reverse flow at a given primary pressure ratio is more likely to occur with a conical-ejector shroud than with a cylindrical-ejector shroud.

The comparison of thrust ratio in figure 51(b) indicates that the thrust of the cylindrical ejector was generally slightly higher than the thrust of the conical ejector.

Type of Flow Present in Full-Scale Ejector

Wall static-pressure measurements taken along the shroud of the longest ejector investigated (configuration D) at the primary gas temperature of 1120° R are presented in figures 52 to 54 for weight-flow ratios of 0, 0.031, and 0.112, respectively.

At the weight-flow ratio of zero shown in figure 52, curves a and b indicate that the primary jet was diffused subsonically to exhaust pressure when the primary pressure ratio was relatively low (P_p/p_0 = 1.44 and 1.63). Between the P_p/p_0 of 1.63 (curve b) and 1.72 (curve c), the primary jet completely filled the ejector shroud and rapidly changed to a supersonic type of flow as represented by curve c. Curve c shows that the supersonic primary jet expanded to strike the shroud wall slightly downstream of the primary nozzle exit and caused a sharp rise in wall pressure due to impingement and possibly oblique shock near the boundary layer. The second sharp pressure rise shown in curve c was indicated as a form of normal shock that occurred from overexpansion of the core of the primary stream. Downstream of the normal shock, the primary stream diffused to almost exhaust pressure before leaving the ejector shroud. Increased primary pressure ratios allowed the normal shock to progressively move downstream (curves e to h) until the flow throughout the entire shroud length became supersonic (curves i and j) and the internal shroud pressures became independent of the external exhaust pressure.

Wall pressures plotted for a constant weight-flow ratio of 0.031 in figure 53 show that the relatively small secondary flow somewhat suppressed an overexpansion of the primary stream (by forming a semi-physical boundary), and thus oblique shock was eliminated and normal shock occurred farther downstream than for the case of zero secondary flow in figure 52 at the same primary pressure ratio.

The cylindrical-shroud wall pressures in figure 54 indicate that at the weight-flow ratio of 0.112, internal shock in the primary stream was almost eliminated. Choking of the secondary-flow passage, however, must have occurred at the minimum secondary-flow area because of the abrupt changes in wall pressure measured just downstream of the minimum secondary-flow area. Supersonic flow and then some sort of shock system in the secondary passage (fig. 54) occurred near the primary nozzle exit.

Wall-pressure profiles of figures 52 and 54 thus show that expansion (and hence internal shock) of the primary ejector stream can be essentially controlled by changes in the ejector weight-flow ratio. The usefulness of such a control would, of course, be to increase the thrust available from the primary stream by eliminating some of the overexpansion losses at high pressure ratios.

Application of Data

The data presented throughout this report are experimental and give the performance of specific full-size ejector configurations operating at afterburning and nonafterburning temperature conditions over a range of mass flow and pressure. Ejectors having flow passages and nozzle shapes similar to these experimental ejectors should give essentially the same performance at comparable operating conditions. However, ejectors with radically different geometries (such as size and shape of secondary-flow passage and primary nozzle) can give greatly different performance even though diameter ratio and spacing ratio are the same. It should also be recognized that performance of an engine and ejector assembly can change somewhat if the same ejector is used with another engine having radically different velocity and temperature profiles at the engine exhaust nozzle.

Ejector performance in an aircraft installation is controlled by the scoop, duct, and cooling passage through which the secondary air must flow. A desirable characteristic of the secondary system is, of course, to supply only the required secondary flow at the highest possible secondary total pressure. Since the thrust ratio F_{ej}/F_j presented herein is in terms of gross measured thrust (jet thrust), the inlet momentum of the primary and secondary flow must be accounted for in order to arrive at the value of net thrust for a specific flight speed.

CONCLUDING REMARKS

An investigation was made to determine the pumping and thrust performance of seven full-size ejector configurations operating on a turbojet-engine and afterburner assembly at a nonafterburning gas temperature (1120° R) and at several afterburning gas temperatures (2000° to 3700° R). The tests were performed over a range of secondary to primary air-flow ratio from zero to about 0.30 at primary pressure ratios from 1.75 to 5.0. Six cylindrical-type ejectors having diameter ratios from 1.048 to 1.60 and spacing ratios from 0.213 to 0.810 were tested. One conical-type ejector with a diameter ratio of 1.10 and a spacing ratio of 0.408 was also tested.

The experimental test results of the investigation presented herein indicate that ejector weight-flow ratio (for specific operating pressure ratios) is not only a function of operating temperature but is also influenced by secondary factors caused by a change in the mode of operation from nonafterburning to afterburning conditions. However, the corrected weight-flow ratio served to correlate air-flow characteristics of cylindrical ejectors with short mixing lengths relative to the diameter ratio (spacing ratios $\leq$ 0.40 and diameter ratios $\geq$ 1.10) for the range of operating gas temperature from 1120° to 3200° R.

3162

The variation in gross-thrust ratio with primary gas temperature was not consistent. It was indicated, however, that thrust ratio at a specific corrected weight-flow ratio was changed more by changing from nonafterburning to afterburning conditions than by changing only primary gas temperature. The gross ejector-thrust ratio with afterburning temperatures from 2000° to 3700° R was generally higher than for the nonafterburning temperature of 1120° R when compared at a primary pressure ratio of 5.0 over a range of corrected weight-flow ratio from 0.01 to 0.18, but the total variation did not exceed 5 percent for any ejector configuration investigated.

Of the cylindrical ejectors investigated at a spacing ratio of about 0.4 (diameter ratios of 1.048, 1.095, and 1.195), the ejector with the largest diameter ratio was indicated to have the best pumping characteristics, and the highest thrust ratio was indicated for the ejector with the medium diameter ratio.

Changes in spacing (spacing ratios of 0.213, 0.408, and 0.81) at a constant diameter ratio of 1.095 showed that the longest cylindrical ejector had the best pumping characteristics at the ejector weight-flow ratio of 0.07, but at the flow ratio of 0.03 the shortest ejector had a slightly better air-handling capacity when operating above the primary pressure ratio of 3.0. Gross-thrust ratios of the short and medium length ejectors (spacing ratios of 0.213 and 0.408) were about the same at a weight-flow ratio of 0.07, but thrust of the long ejector (spacing ratio of 0.81) was 2 or 3 percent lower than for the two shorter ejectors.

A cylindrical-type ejector showed better pumping characteristics than a conical-type ejector of the same diameter ratios and spacing ratios at a very low value of weight-flow ratio (weight-flow ratio below 0.01). This trend was reversed at higher values of weight-flow ratio. The thrust ratio of the cylindrical-type ejector was generally slightly higher than for the conical-type ejector. Reverse secondary flow was indicated as more likely to occur with the conical-type ejector.

Typical ejector wall-pressure profiles showed that increasing amounts of secondary flow tended to suppress and move downstream the shocks indicated in the primary stream. Secondary air served as a semi-physical boundary which essentially controlled or altered the primary-stream expansion process.

Lewis Flight Propulsion Laboratory
National Advisory Committee for Aeronautics
Cleveland, Ohio, January 25, 1954

3162

[redacted]

APPENDIX A

SYMBOLS

The following symbols are used in this report:

A	area, sq ft
C_D	primary nozzle discharge coefficient, ratio of measured mass flow to isentropic mass flow
C_F	primary nozzle thrust coefficient, ratio of measured jet thrust to thrust available with isentropic flow in convergent nozzle
D_p	exit diameter of primary nozzle, in.
D_s	exit diameter of ejector shroud, in.
F	jet thrust (gross thrust), lb
g	acceleration due to gravity, 32.17 ft/sec^2
L	axial distance between exit planes of primary nozzle and ejector shroud, in.
P	total pressure, lb/sq ft abs
p	static pressure, lb/sq ft abs
R	gas constant, 53.4 ft-lb/(lb)(^oR)
T	total temperature, ^oR
V	velocity, ft/sec
W	weight flow, lb/sec
γ	ratio of specific heats of gas

Subscripts:

a	engine inlet air
c	critical flow
cn	conical nozzle

ej	ejector jet
f_1	engine fuel
f_2	afterburner fuel
i	isentropic
in	engine inlet
j	primary jet
l	leakage
lip	primary nozzle-exit lip
p	primary stream or primary nozzle
s	secondary stream or ejector nozzle
w	wall of ejector nozzle
0	ambient or exhaust conditions
1	conditions upstream of engine nozzle
2	conditions at exit of engine nozzle

APPENDIX B

CALCULATION OF PRIMARY GAS TEMPERATURE AND NOZZLE FLOW COEFFICIENTS

The diagram below represents the turbojet engine and the primary-nozzle assembly:

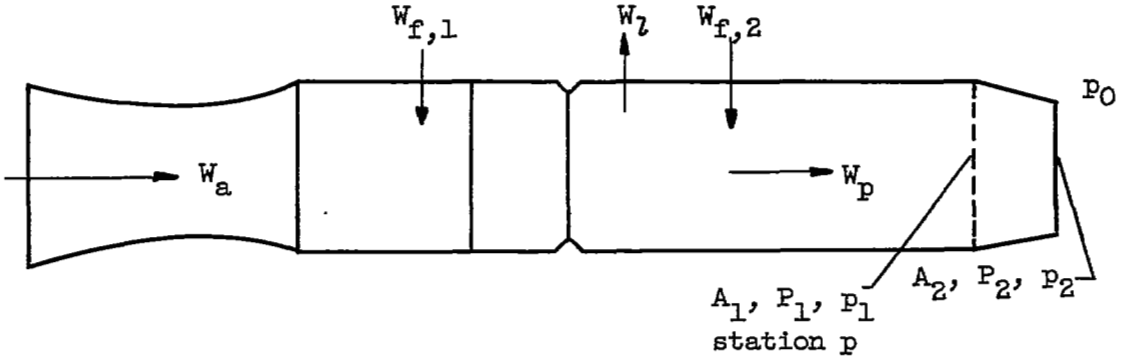

The primary mass flow W_p was the sum of engine air flow W_a plus engine fuel flow $W_{f,1}$ plus afterburner fuel flow $W_{f,2}$ minus leakage flow W_l. Primary gas temperature was calculated for afterburning conditions from measurements taken at station p as

$$T_1 = T_p = \left(\frac{p_1 A_1}{W_p}\right)^2 \frac{2\gamma_1 g}{R(\gamma_1 - 1)} \left(\frac{P_1}{p_1}\right)^{\frac{\gamma_1 - 1}{\gamma_1}} \left[\left(\frac{P_1}{p_1}\right)^{\frac{\gamma_1 - 1}{\gamma_1}} - 1\right] \tag{B1}$$

The value of γ_1 was assumed for a trial calculation of T_p. The calculation was repeated using γ_1 based on the value of T_p from the previous calculation, until T_p and γ_1 corresponded at the existing known fuel-air ratio.

The discharge coefficient of the primary nozzle was calculated from tests with the ejector shroud removed by using the following:

$$C_D = \frac{\text{Measured mass flow}}{\text{Isentropic mass flow}}$$

$$C_D = \frac{W_p}{P_1 A_2} \sqrt{\frac{RT_p}{g}} \left[\frac{P_1}{p_2}\right] \left[\frac{pA}{W\sqrt{\frac{RT}{g}}}\right]_i \tag{B2}$$

[redacted]

where the parameter $\left[\frac{pA}{W\sqrt{\frac{RT}{g}}}\right]_i$ was taken from one-dimensional isentropic-flow tables (ref. 8) at known values of γ_p and P_1/p_0. The quantity $\left[P_1/p_2\right]$ equaled P_1/p_0 for subcritical flow, or $\left[P_1/p_2\right]$ equaled $\left(\frac{\gamma_1 + 1}{2}\right)^{\frac{\gamma_1}{\gamma_1 - 1}}$ for critical flow. The value W_p was measured, and T_p was taken as a calculated value at station p.

3162

The thrust coefficient C_F of the primary nozzle was calculated as the ratio of measured jet thrust F_j to the ideal thrust of a convergent nozzle F_{cn} as follows:

$$C_F = \frac{F_j}{F_{cn}}$$

where

$$F_{cn} = \left(\frac{W_i}{g}\right) V_i \quad \text{for subcritical flow}$$

$$F_{cn} = \left(\frac{W_i}{g}\right)_c V_e \quad \text{for critical flow}$$

and

$$\frac{W_i}{g} = \text{isentropic mass flow}$$

$$\left(\frac{W_i}{g}\right)_c = \text{critical isentropic mass flow}$$

V_i = isentropic velocity with complete expansion to ambient pressure

V_e = effective isentropic velocity of a choked convergent nozzle

$$\text{or} \quad V_e = V_c + \frac{A_2(p_2 - p_0)}{\left(\frac{W_i}{g}\right)_c}$$

V_c = critical isentropic velocity

A_2, p_2, and p_0 are as previously defined

The preceding mass flows and velocities were calculated by using one-dimensional isentropic-flow tables (ref. 8) at the known values of γ_p and nozzle pressure ratio.

3162

REFERENCES

1. Greathouse, W. K., and Hollister, D. P.: Preliminary Air-~~Force~~ Flow and Thrust Calibrations of Several Conical Cooling-Air Ejectors with a Primary to Secondary Temperature Ratio of 1.0. I - Diameter Ratios of 1.21 and 1.10. NACA RM E52E21, 1952.

2. Greathouse, W. K., and Hollister, D. P.: Preliminary Air-Flow and Thrust Calibrations of Several Conical Cooling-Air Ejectors with a Primary to Secondary Temperature Ratio of 1.0. II - Diameter Ratios of 1.06 and 1.40. NACA RM E52F26, 1952.

3. Greathouse, W. K., and Hollister, D. P.: Air-Flow and Thrust Characteristics of Several Cylindrical Cooling-Air Ejectors with a Primary to Secondary Temperature Ratio of 1.0. NACA RM E52L24, 1953.

4. Kochendorfer, Fred D., and Rousso, Morris D.: Performance Characteristics of Aircraft Cooling Ejectors Having Short Cylindrical Shrouds. NACA RM E51E01, 1951.

5. Wilsted, H. D., Huddleston, S. C., and Ellis, C. W.: Effect of Temperature on Performance of Several Ejector Configurations. NACA RM E9E16, 1949.

6. Wallner, Lewis E., and Jansen, Emmert T.: Full-Scale Investigation of Cooling Shroud and Ejector Nozzle for a Turbojet Engine - Afterburner Installation. NACA RM E51J04, 1951.

7. Huntley, S. C., Auble, Carmon M., and Useller, James W.: Altitude Performance Investigation of a High-Temperature Afterburner. NACA RM E53D22, 1953.

8. Turner, L. Richard, Addie, Albert N., and Zimmerman, Richard H.: Charts for the Analysis of One-Dimensional Steady Compressible Flow. NACA TN 1419, 1948.

TABLE I. - EJECTOR TEST CONDITIONS

Configuration	Diameter ratio, D_s/D_p	Spacing ratio, L/D_p	Primary gas temperature, $^{\circ}R$	Primary pressure ratio, P_p/p_0	Secondary pressure ratio, P_s/p_0	Measured weight-flow ratio, W_s/W_p
A	1.048	0.445	1120	1.75 to 5.0	0.5 to 6.0	0 to 0.29
	1.048	.445	3000 to 3200	1.75 to 5.0	1.1 to 5.0	.04 to .27
	1.048	.445	3600 to 3700	2.0 to 5.0	1.6 to 4.8	.14 to .27
B	1.095	0.213	1120	1.75 to 5.0	0.7 to 7.2	0 to 0.25
	1.095	.213	2000	1.75 to 6.0	1.0 to 7.2	.02 to .25
	1.095	.213	3200	1.75 to 5.0	1.1 to 6.4	.11 to .26
	1.095	.213	3600	1.75 to 5.0	2.0 to 6.1	.23 to .25
C	1.095	0.408	1120	1.75 to 4.5	0.4 to 7.1	0 to 0.27
	1.095	.408	2100 to 2200	1.75 to 5.0	1.0 to 7.5	.06 to .26
	1.095	.408	3000 to 3200	1.75 to 5.0	1.1 to 6.2	.07 to .25
	1.095	.408	3600	2.5 to 3.0	3.2 to 3.9	.24 only
D	1.095	0.810	1120	1.75 to 5.0	0.4 to 6.7	0 to 0.25
	1.095	.810	3000 to 3100	1.75 to 5.0	1.1 to 6.0	.10 to .29
	1.095	.810	3600 to 3700	1.75 to 5.0	1.5 to 6.5	.17 to .32
E	1.195	0.403	1120	1.75 to 4.5	0.5 to 6.4	0 to 0.24
	1.195	.403	2100 to 2200	1.75 to 6.0	.8 to 6.2	.02 to .25
	1.195	.403	3050 to 3150	1.75 to 5.0	1.3 to 6.0	.13 to .24
	1.195	.403	3600	2.5 to 3.0	2.7 to 3.1	.18 to .22
F	1.60	0.587	1500	2.0 to 10.0	0.6 to 1.5	0 to 0.31
G	1.10	.408	1120	1.75 to 5.0	0.7 to 3.1	0 to 0.28
	1.10	.408	2200	1.75 to 5.0	.8 to 3.1	0 to .28
	1.10	.408	3200 to 3400	1.75 to 5.0	1.0 to 2.4	.12 to .30
	1.10	.408	3750	2.5 to 4.0	1.5 to 2.6	.26 to .28

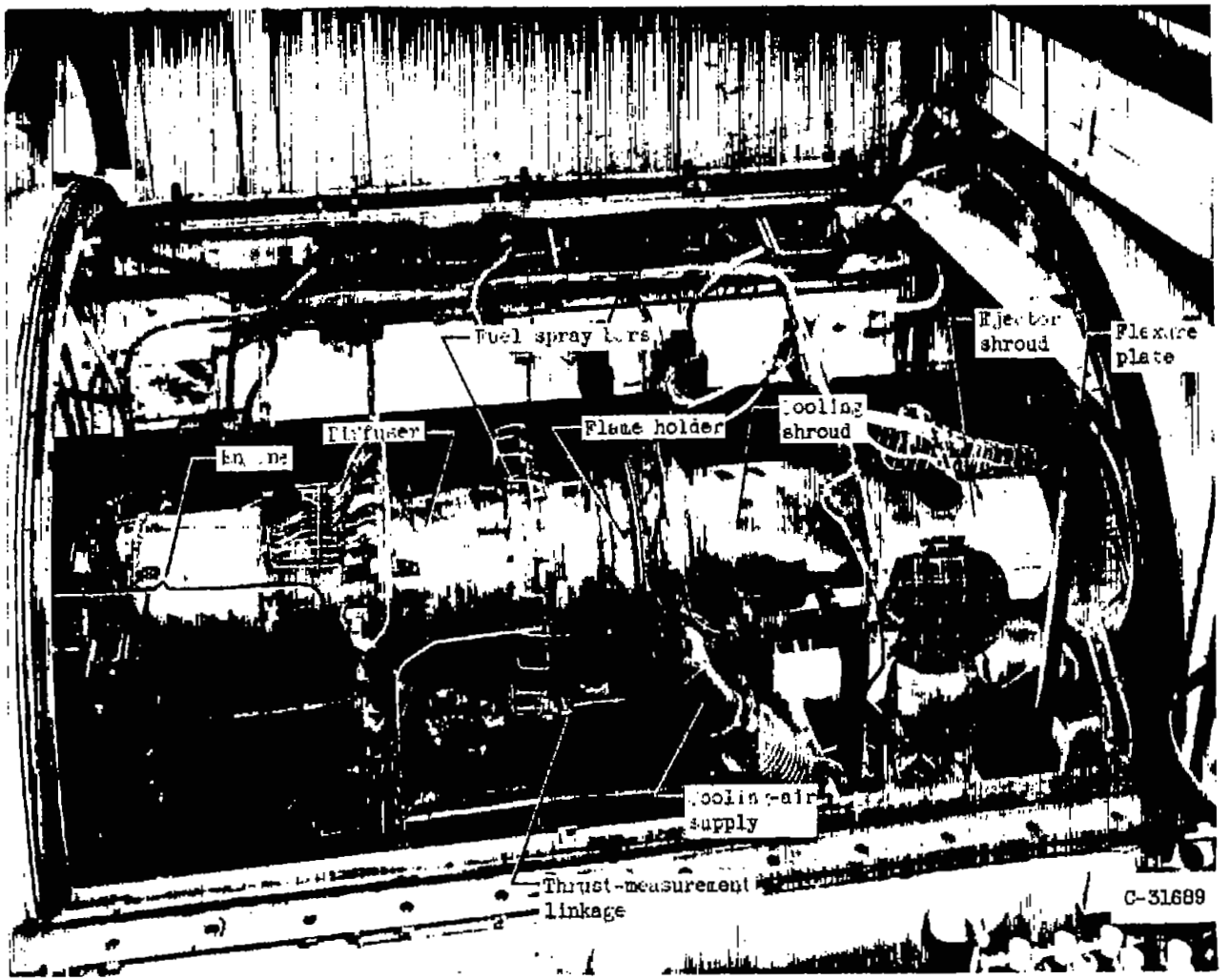

(a) Photograph.

Figure 1. - Full-scale ejector test setup in altitude test chamber.

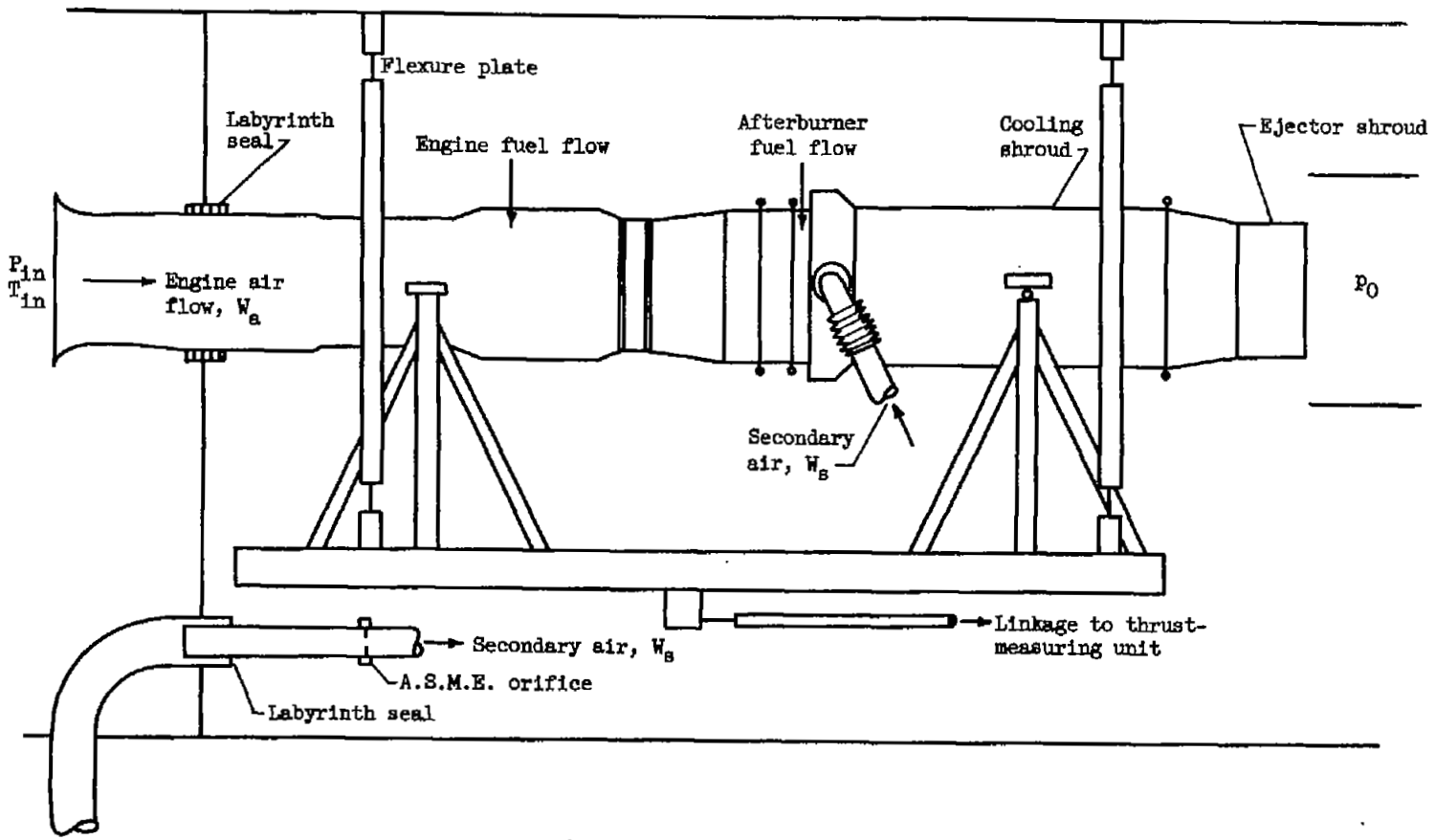

(b) Diagram.

Figure 1. - Concluded. Full-scale ejector test setup in altitude test chamber.

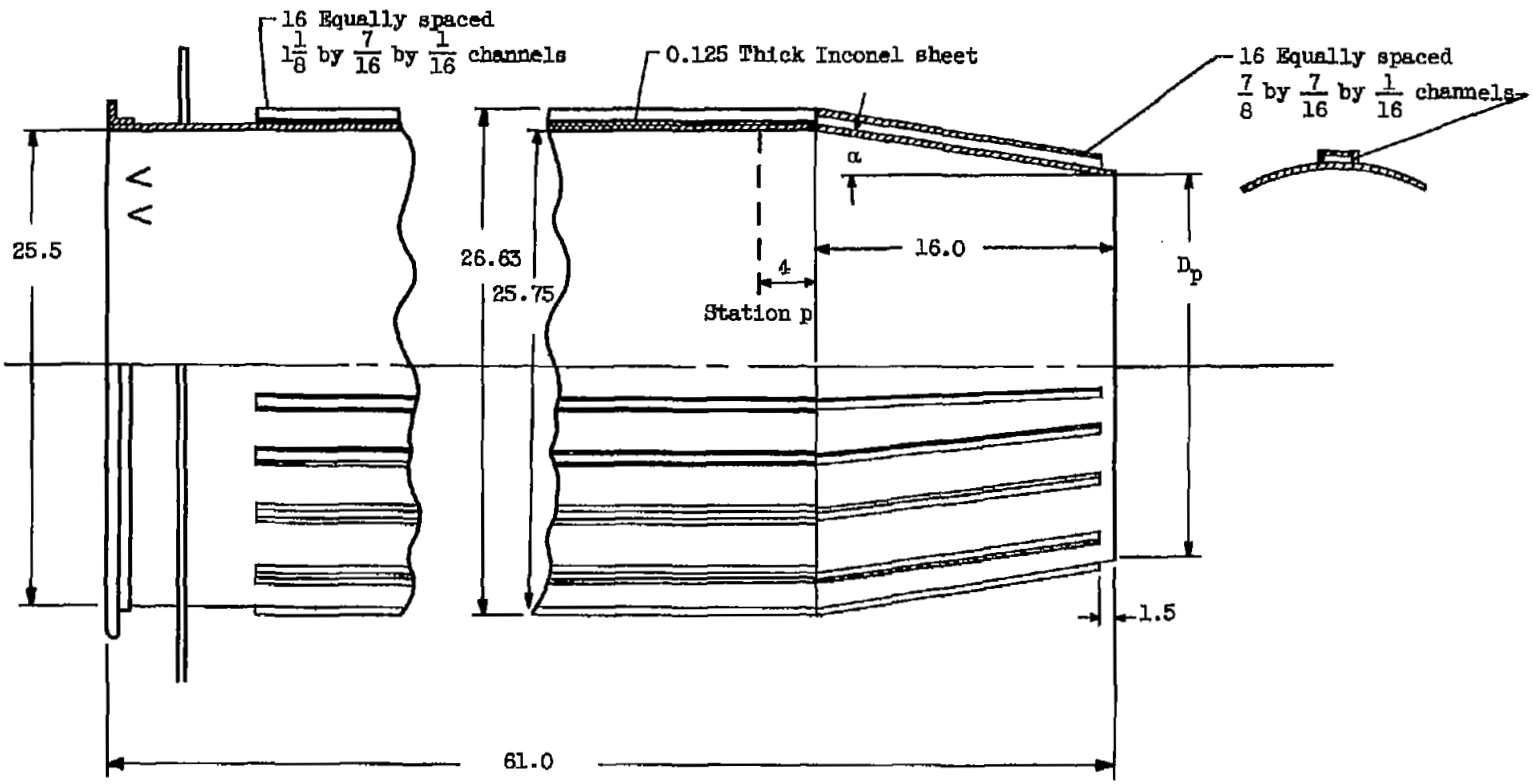

Ejector configuration	Half-cone angle, α	Exit diameter, D_p
A,B,C,D,E,G	8°	21.1
F	17°	15.75

(a) Dimensions used for full-scale ejector investigation. (Dimensions in inches.)

Figure 2. - Afterburner shell.

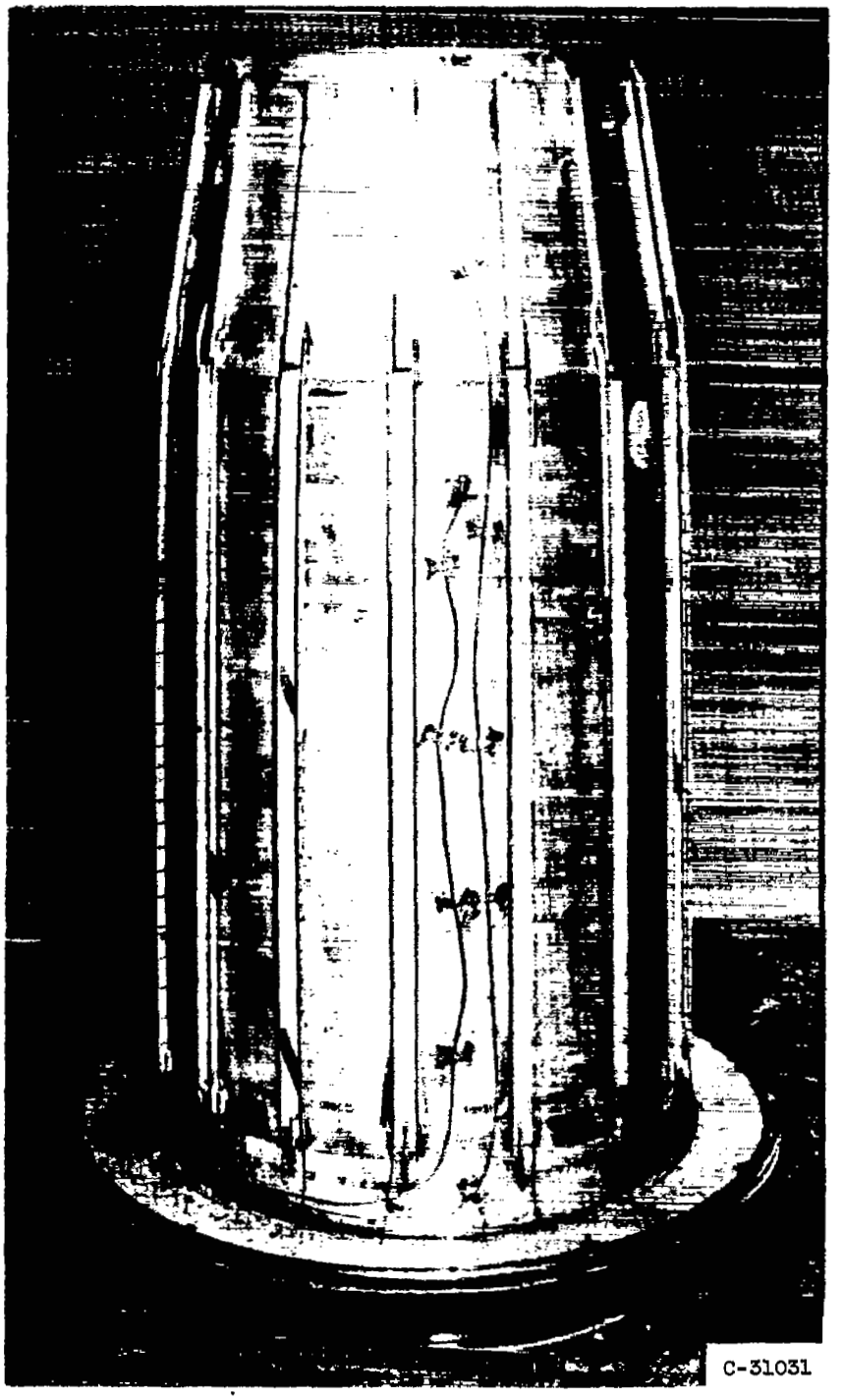

(b) Photograph of shell and primary nozzle.

Figure 2. - Concluded. Afterburner shell.

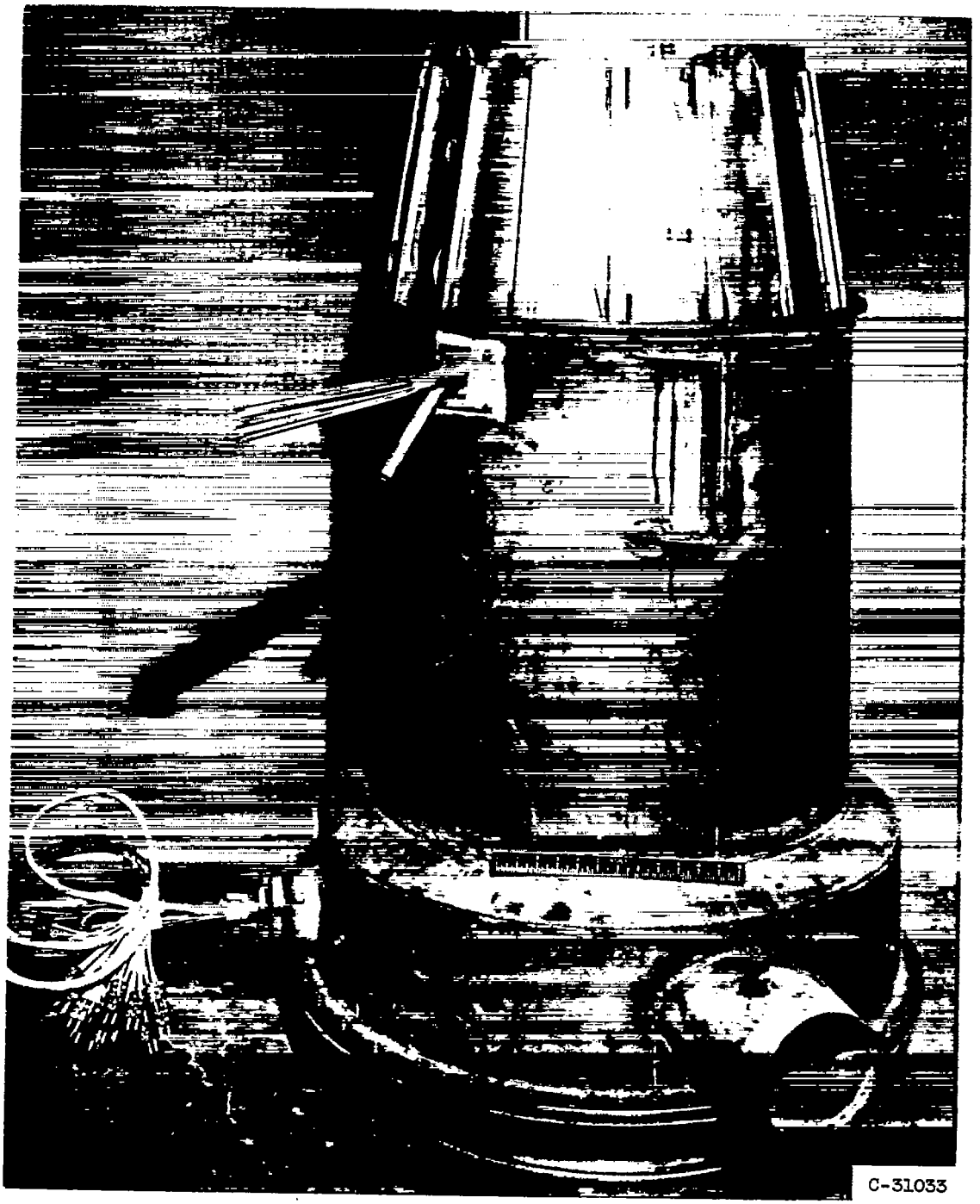

Figure 3. - Afterburner and cooling-shroud assembly.

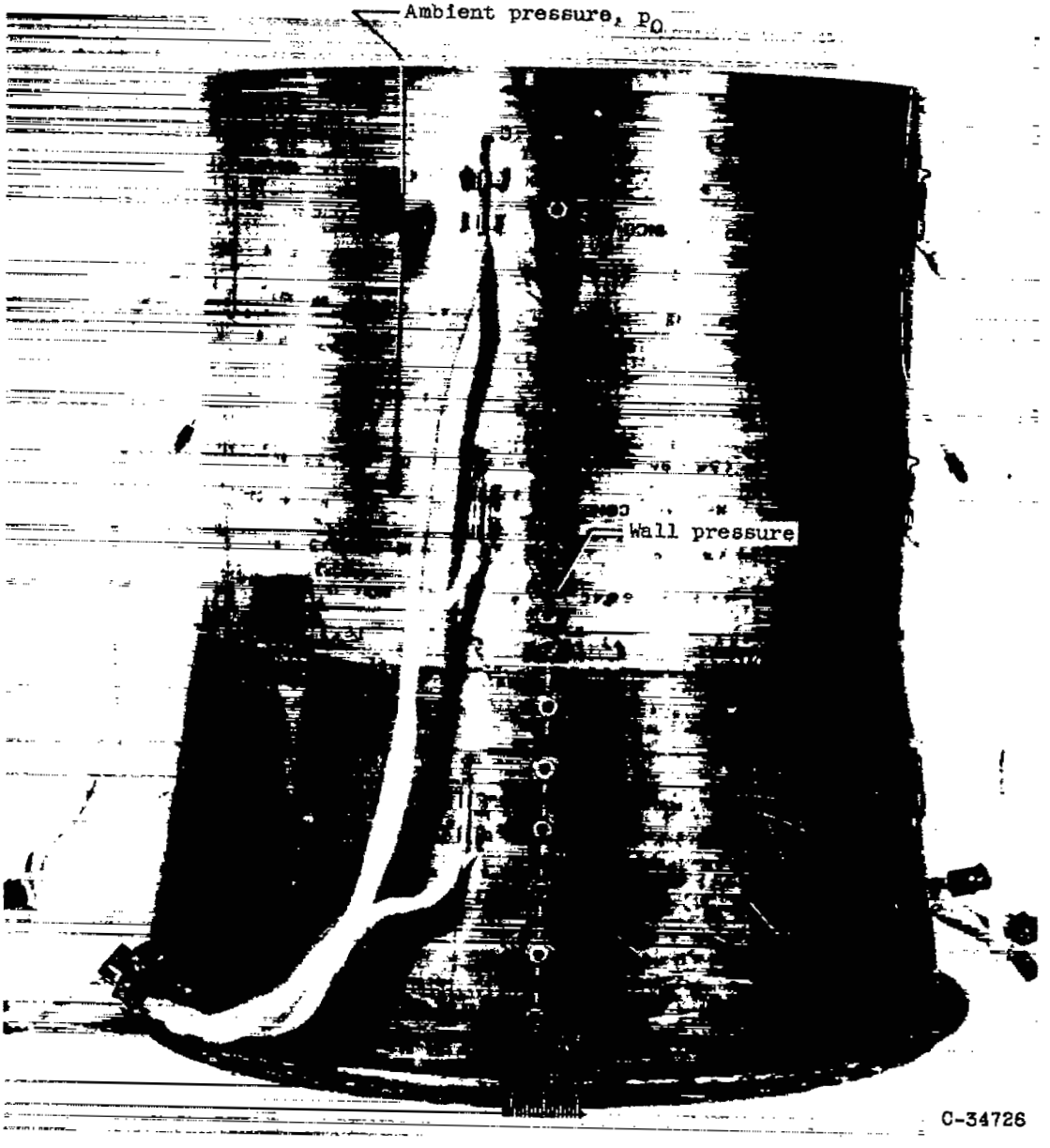

(a) Cylindrical type.

Figure 4. - Ejector shroud.

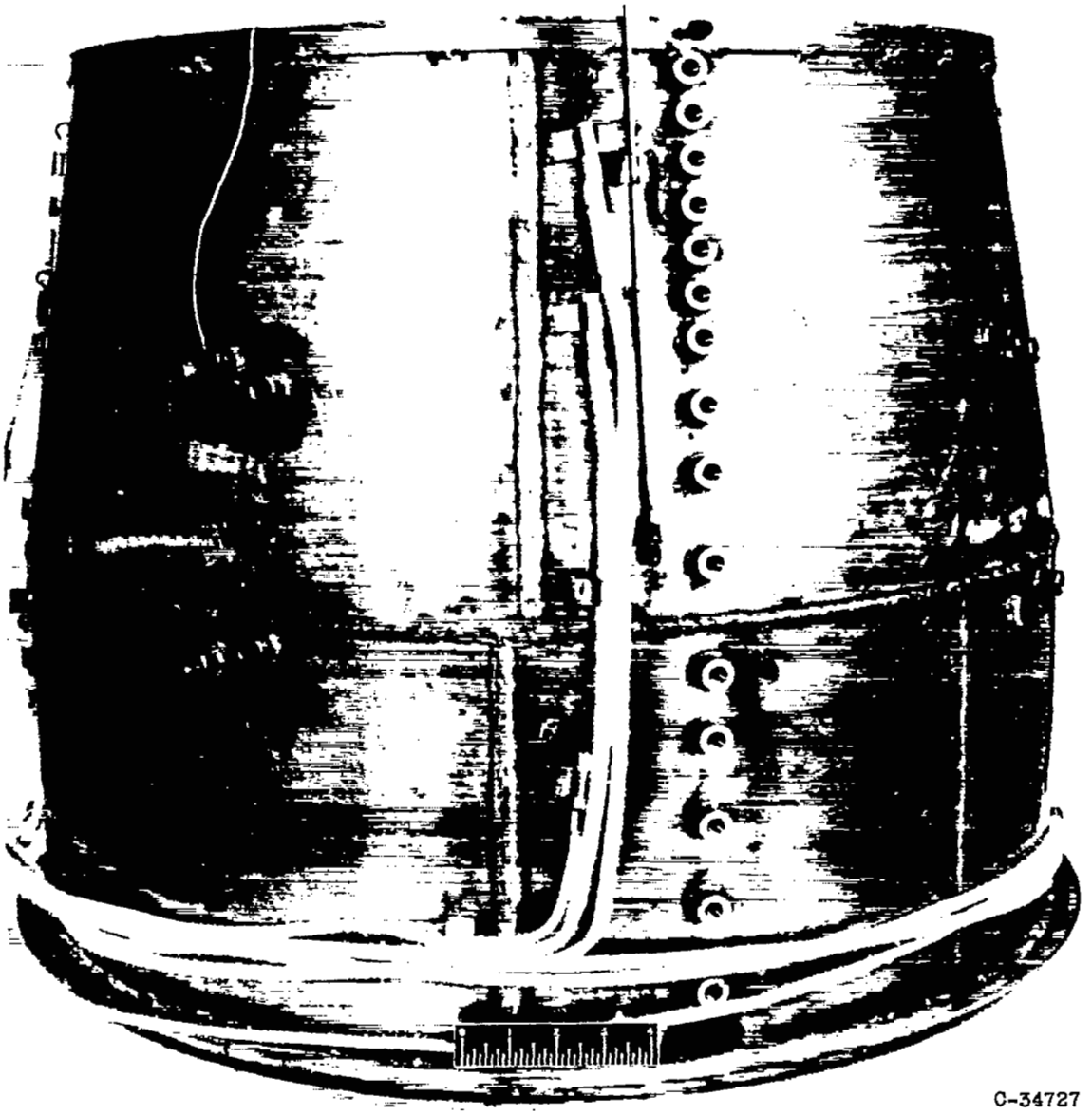

(b) Conical type.

Figure 4. - Concluded. Ejector shroud.

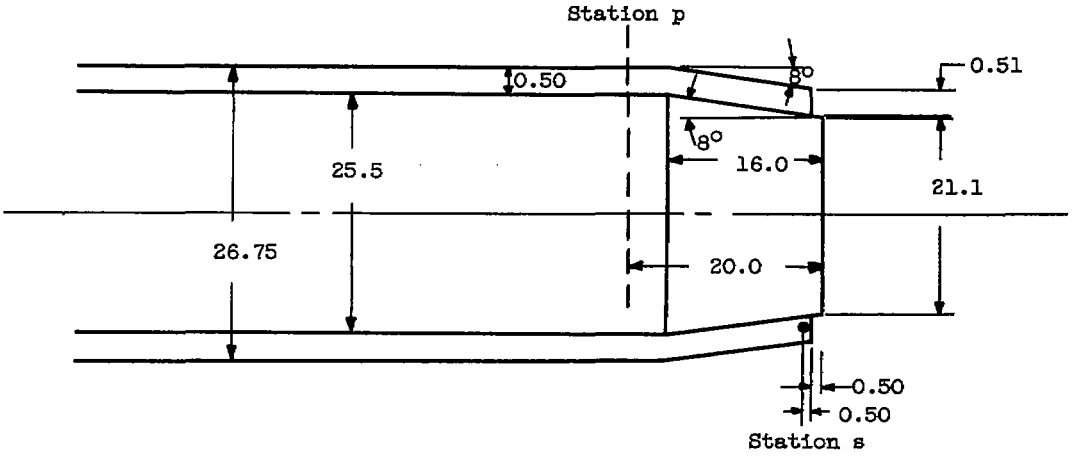

(a) Basic engine configuration.

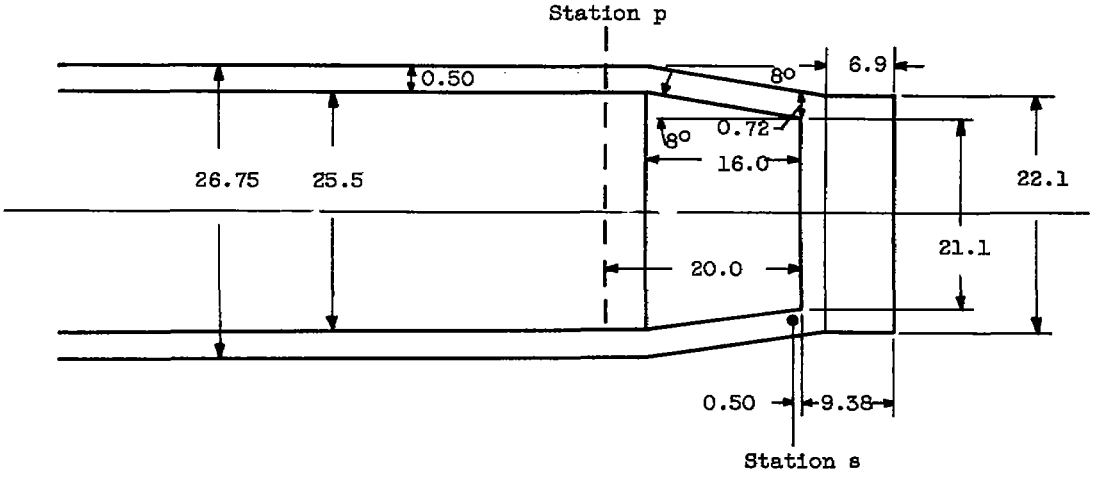

(b) Configuration A; diameter ratio, 1.048; spacing ratio, 0.445.

Figure 5. - Various ejector configurations (dimensions in inches).

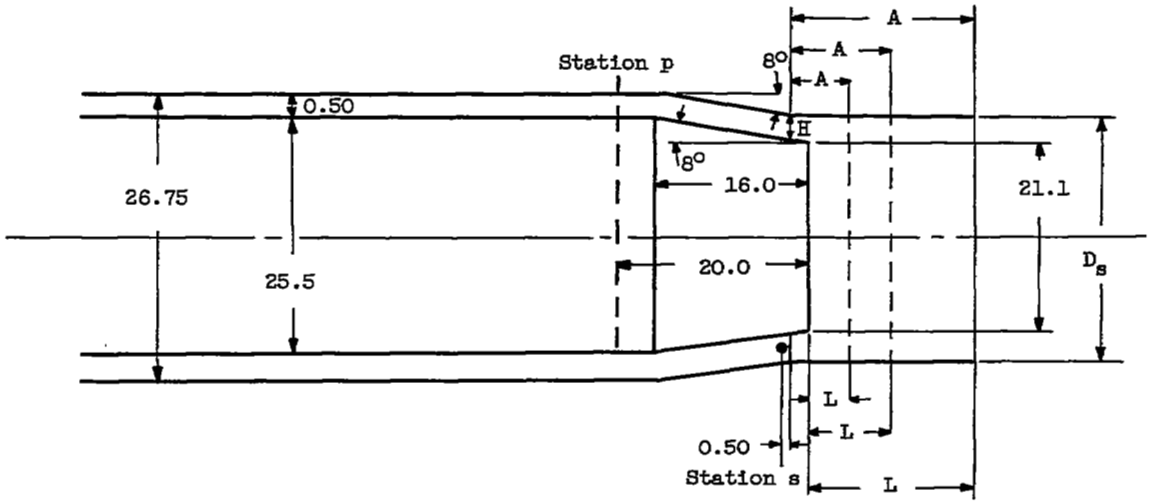

Configuration	Diameter ratio, D_s/D_p	Spacing ratio, L/D_p	D_s	L	A	H
B	1.095	0.213	23.1	4.5	6.62	0.58
C	1.095	.408	23.1	8.6	10.72	.58
D	1.095	.810	23.1	17.1	19.22	.58

(c) Configurations B, C, and D.

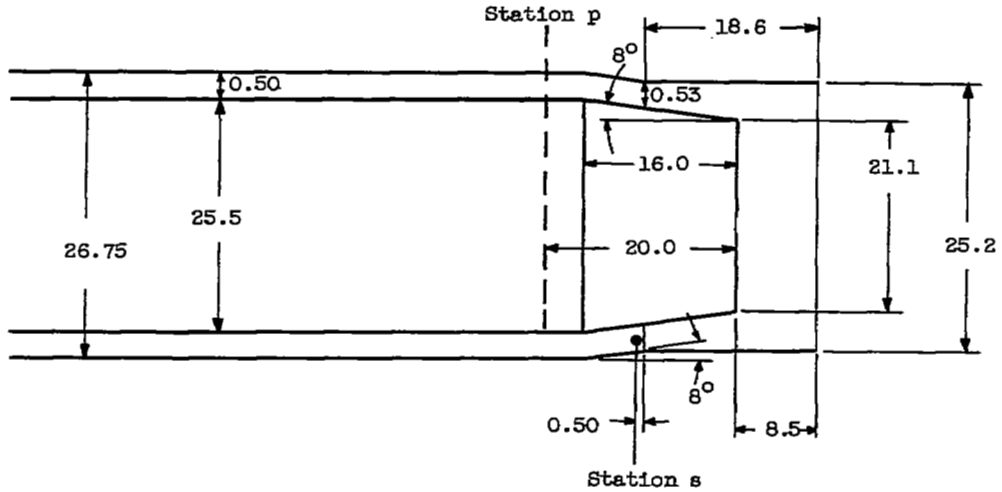

(d) Configuration E; diameter ratio, 1.195; spacing ratio, 0.403.

Figure 5. - Continued. Various ejector configurations (dimensions in inches).

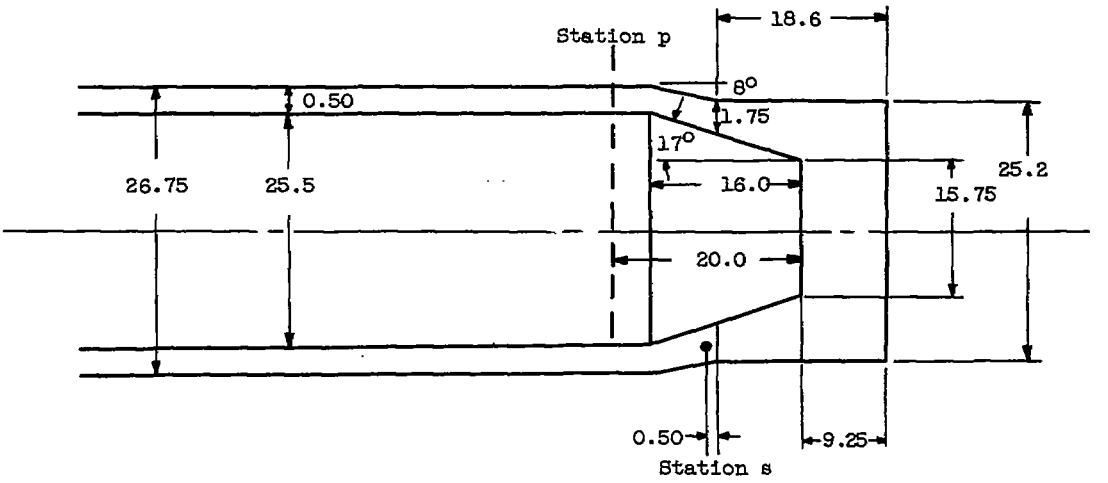

(e) Configuration F; diameter ratio, 1.60; spacing ratio, 0.587.

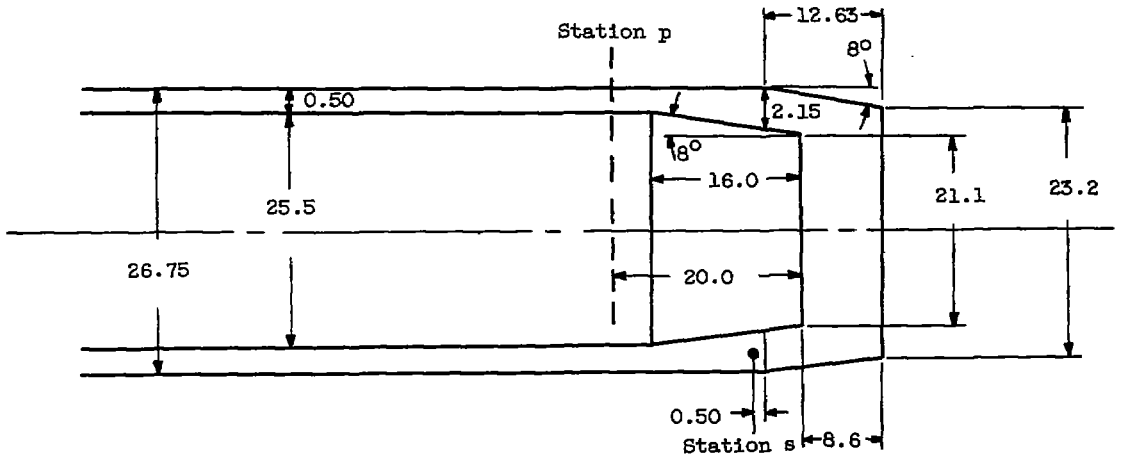

(f) Configuration G; diameter ratio, 1.10; spacing ratio, 0.408.

Figure 5. - Concluded. Various ejector configurations (dimensions in inches).

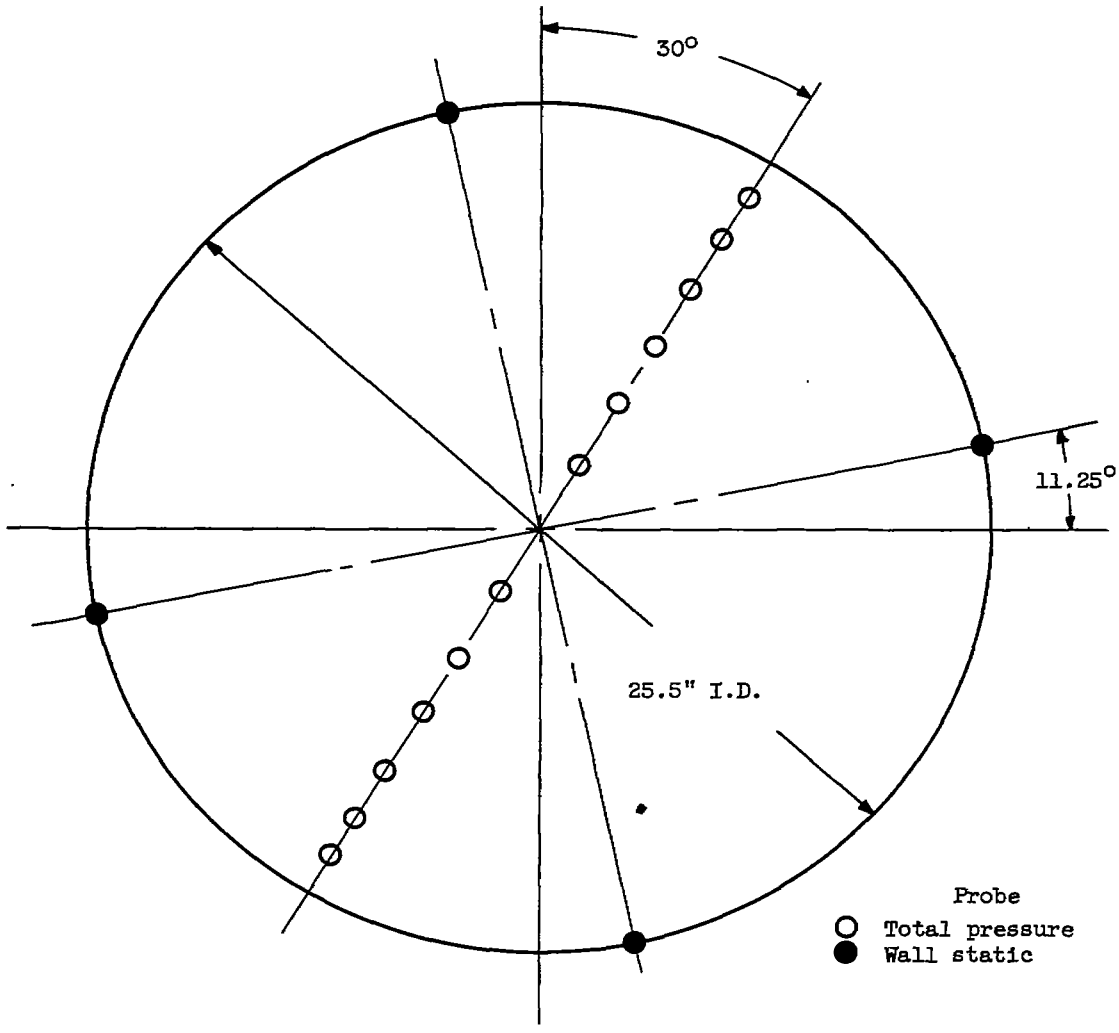

Figure 6. - Primary-stream instrumentation at station p. Water-cooled pressure survey rake located 20 inches upstream of primary nozzle exit (viewed looking upstream). (Total-pressure probes are spaced at equal flow areas.)

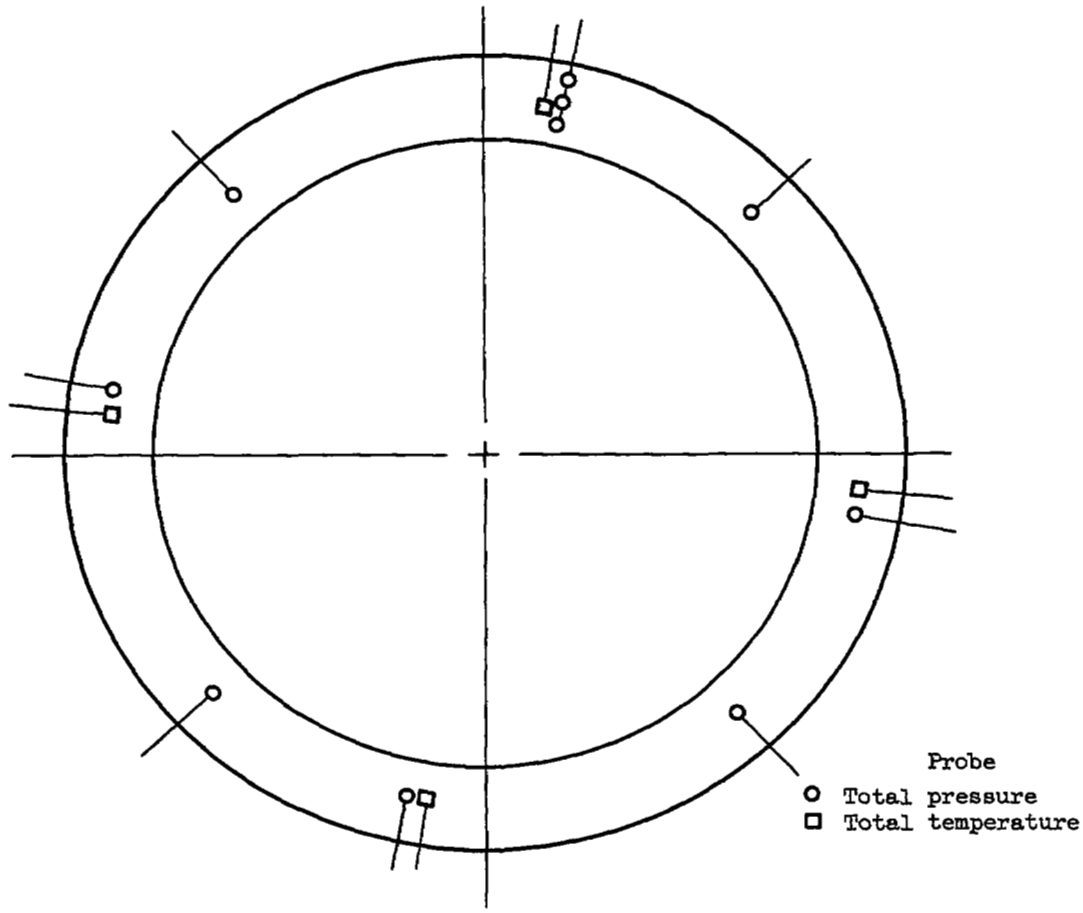

Figure 7. - Secondary-stream instrumentation at station s (viewed looking upstream).

[redacted]

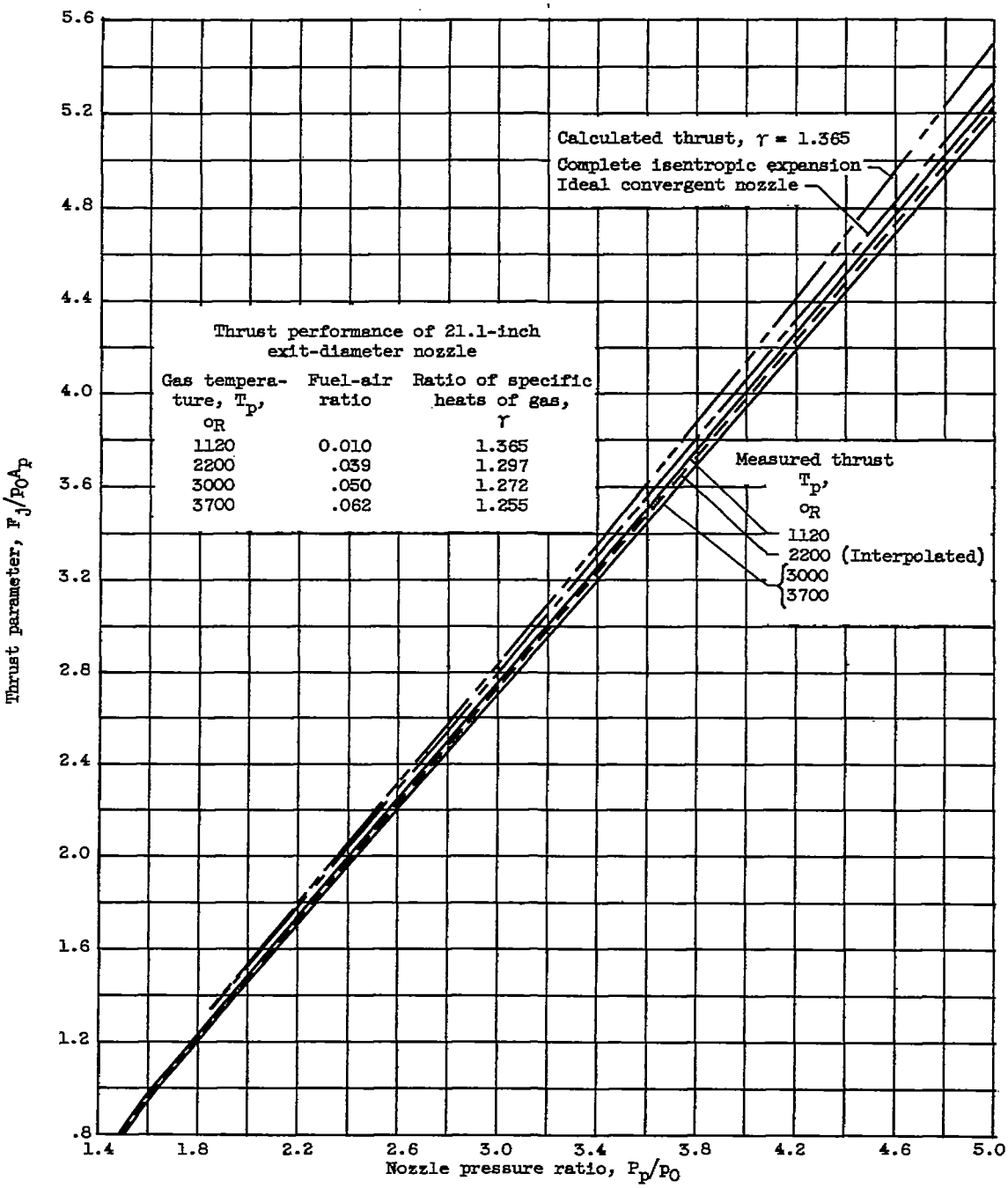

Figure 8. - Thrust performance of 21.1-inch-diameter conical primary nozzle.

[redacted]

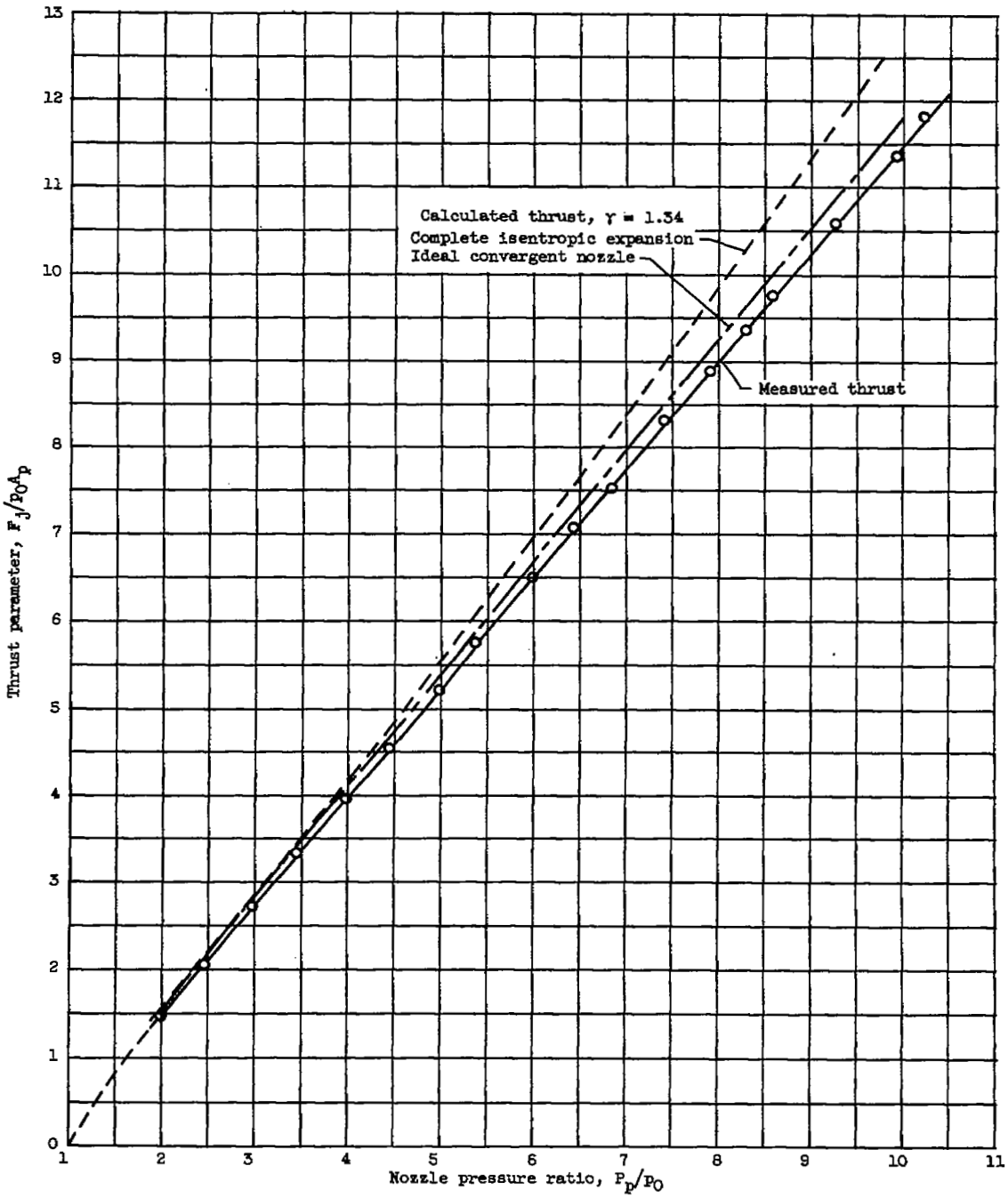

Figure 9. - Thrust performance of 15.75-inch-diameter conical primary nozzle. Gas temperature, 1500° R; fuel-air ratio, 0.015; ratio of specific heats of gas, 1.337.

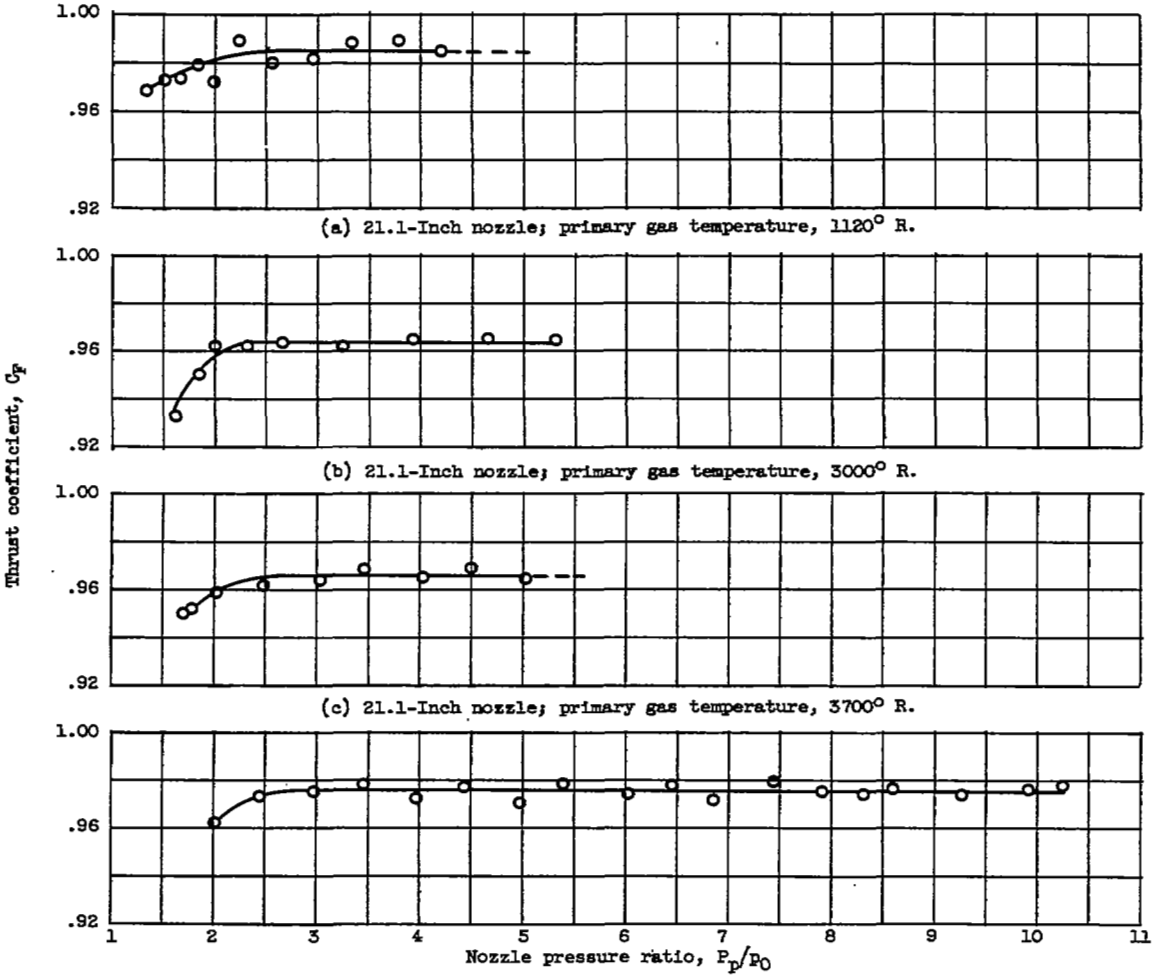

(a) 21.1-Inch nozzle; primary gas temperature, 1120° R.

(b) 21.1-Inch nozzle; primary gas temperature, 3000° R.

(c) 21.1-Inch nozzle; primary gas temperature, 3700° R.

(d) 15.75-Inch nozzle; primary gas temperature, 1500° R.

Figure 10. - Thrust coefficient of conical primary nozzles.

[redacted]

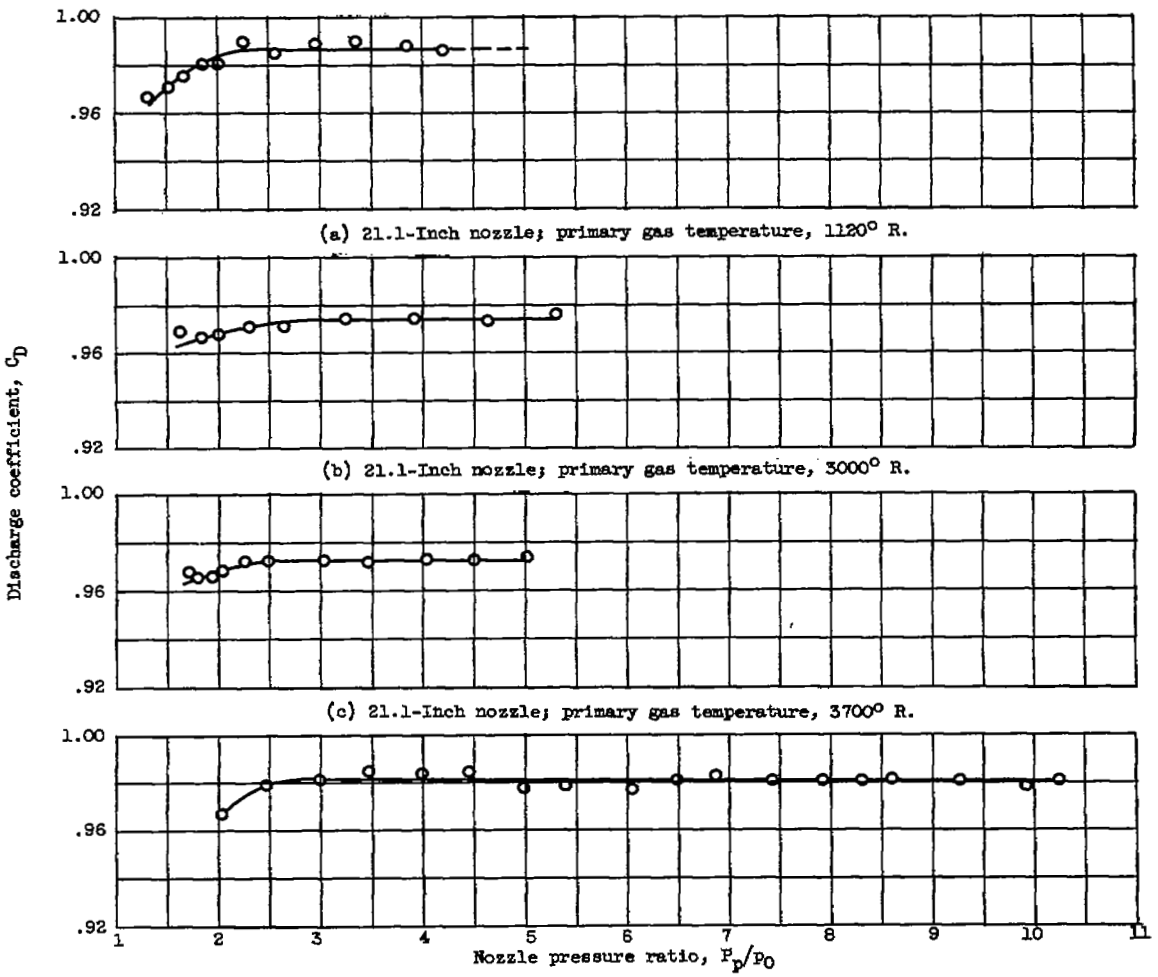

(a) 21.1-Inch nozzle; primary gas temperature, 1120° R.

(b) 21.1-Inch nozzle; primary gas temperature, 3000° R.

(c) 21.1-Inch nozzle; primary gas temperature, 3700° R.

(d) 15.75-Inch nozzle; primary gas temperature, 1500° R.

Figure 11. - Discharge coefficient of conical primary nozzles.

[redacted]

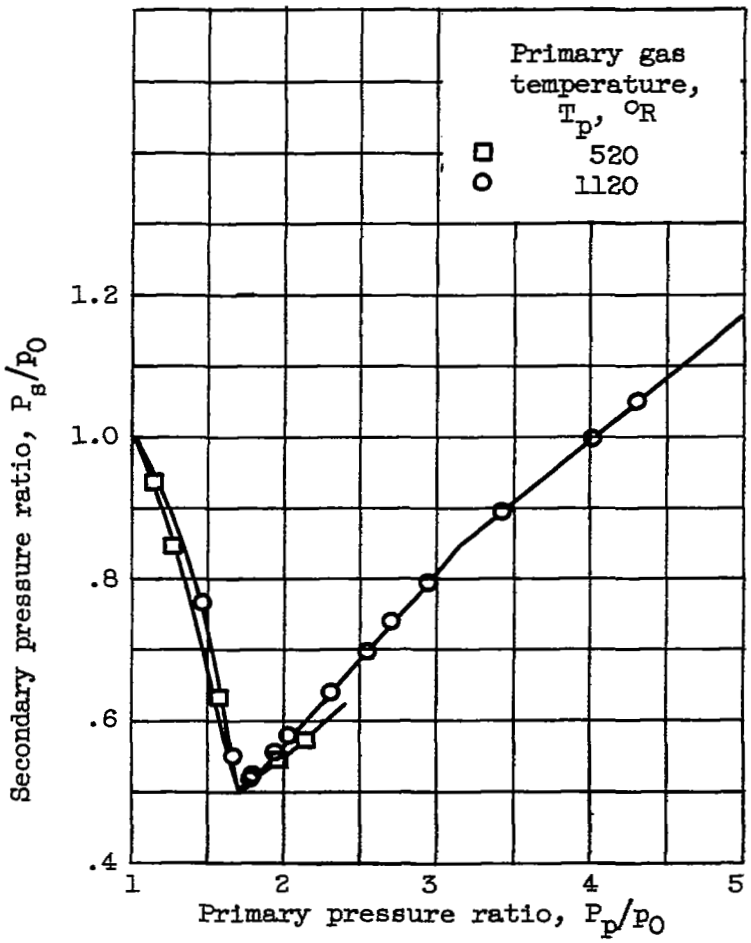

Figure 12. - Ejector pumping characteristics of configuration A at zero secondary flow. Diameter ratio, 1.048; spacing ratio, 0.445.

[redacted]

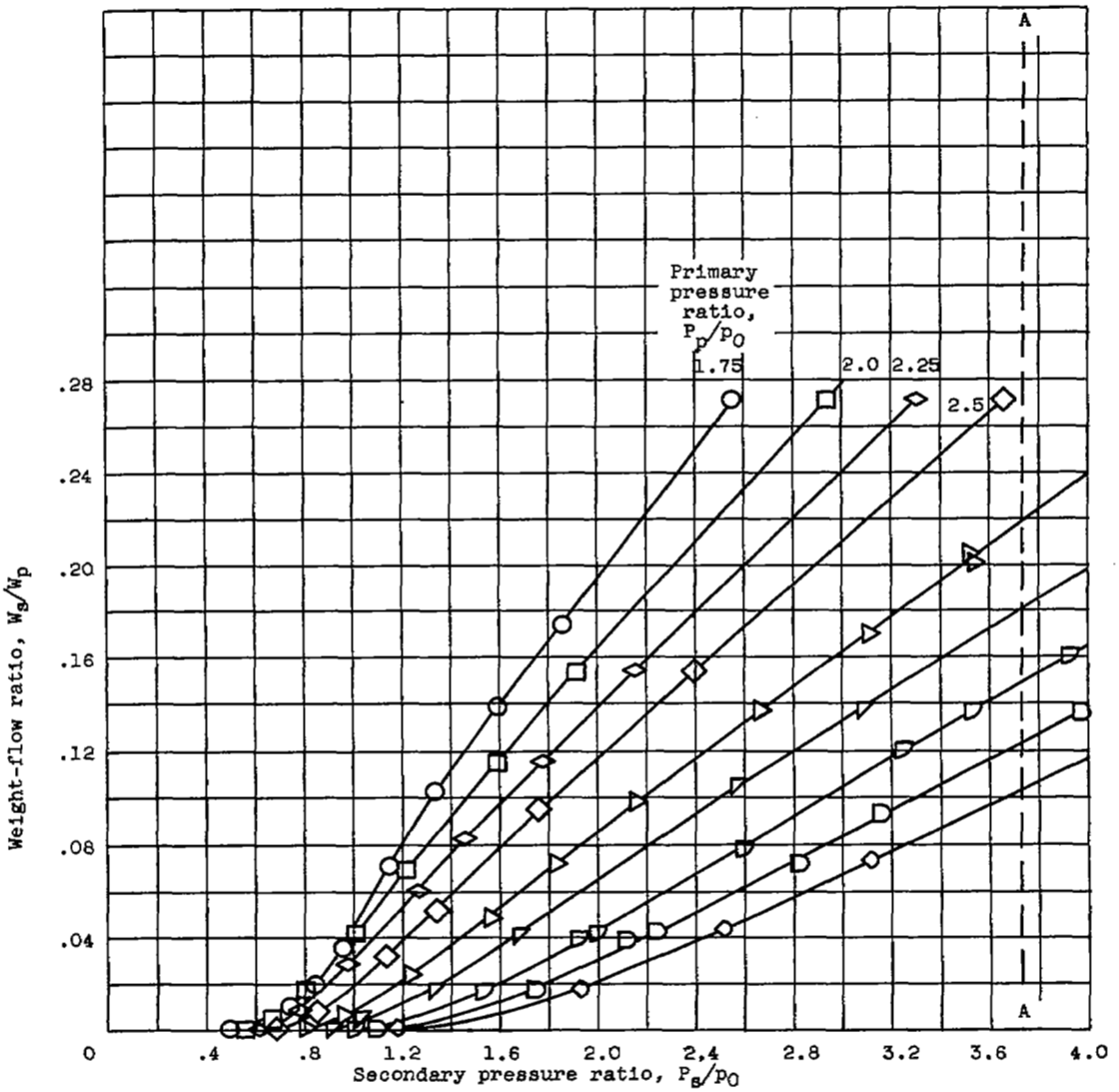

(a) Primary gas temperature, 1120° R.

Figure 13. - Effect of primary and secondary pressure ratio on ejector weight-flow ratio for configuration A. Diameter ratio, 1.048; spacing ratio, 0.445.

[redacted]

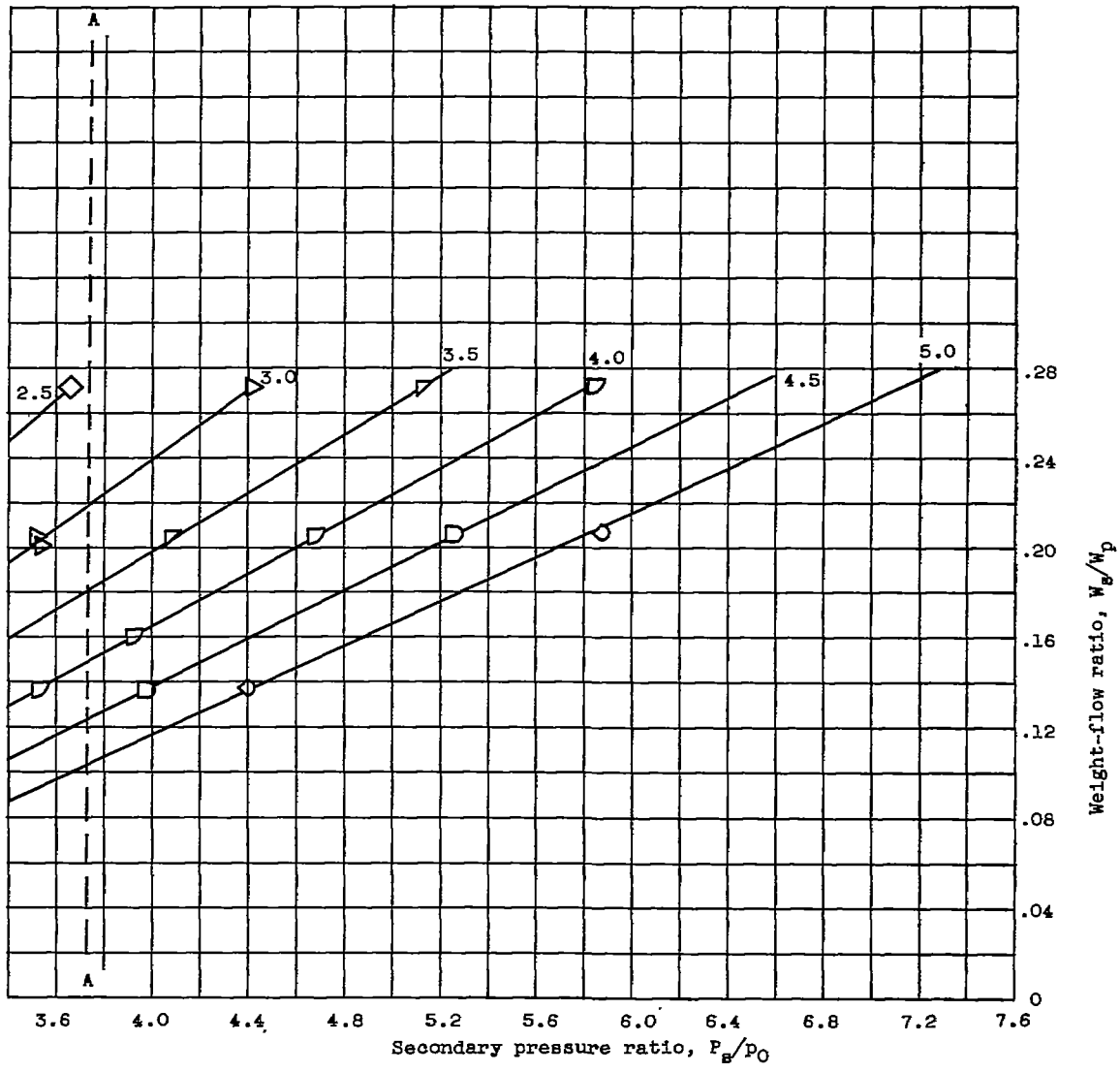

[redacted]

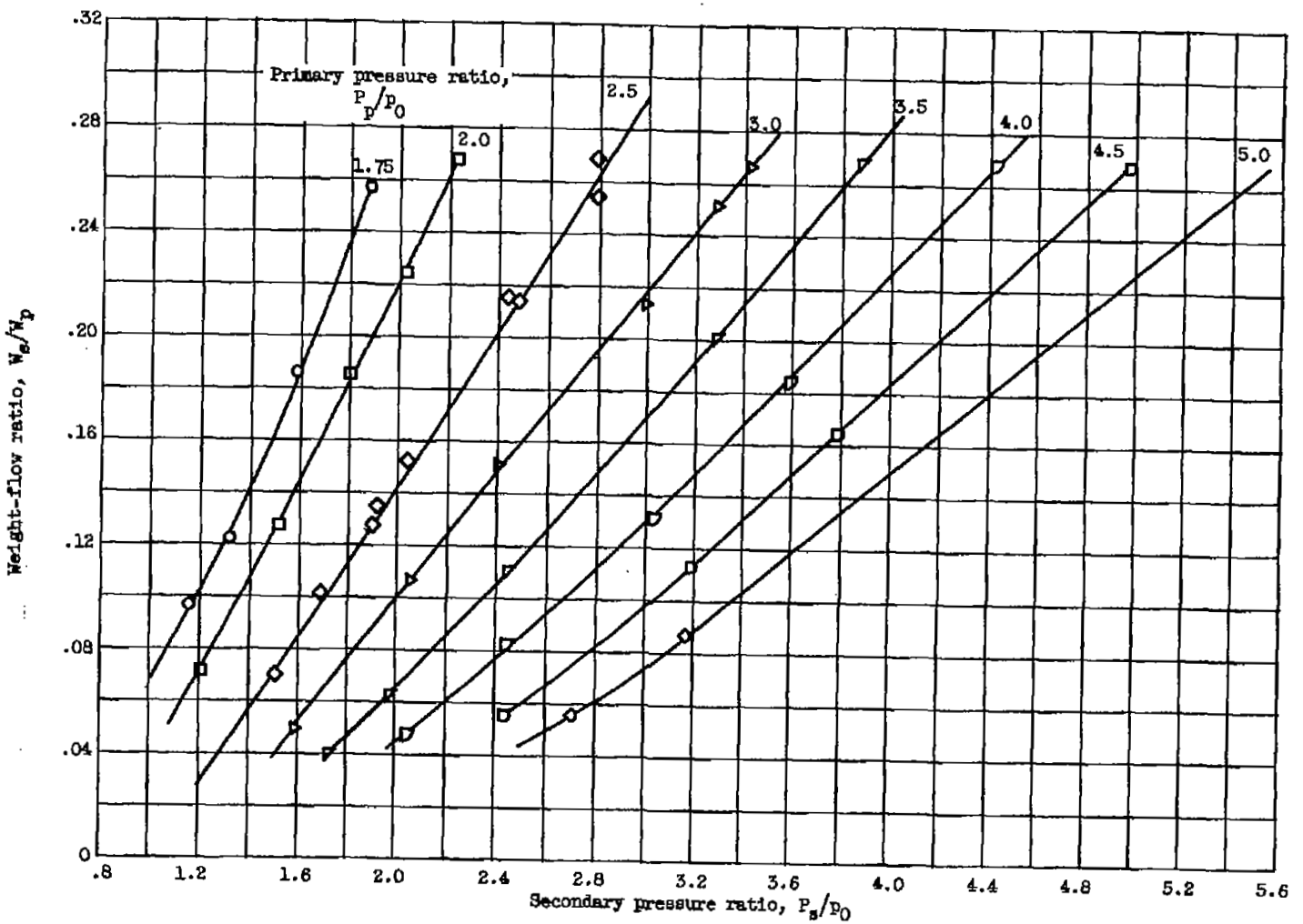

(b) Primary gas temperature, 3000° to 3200° R.

Figure 13. - Continued. Effect of primary and secondary pressure ratio on ejector weight-flow ratio for configuration A. Diameter ratio, 1.048; spacing ratio, 0.445.

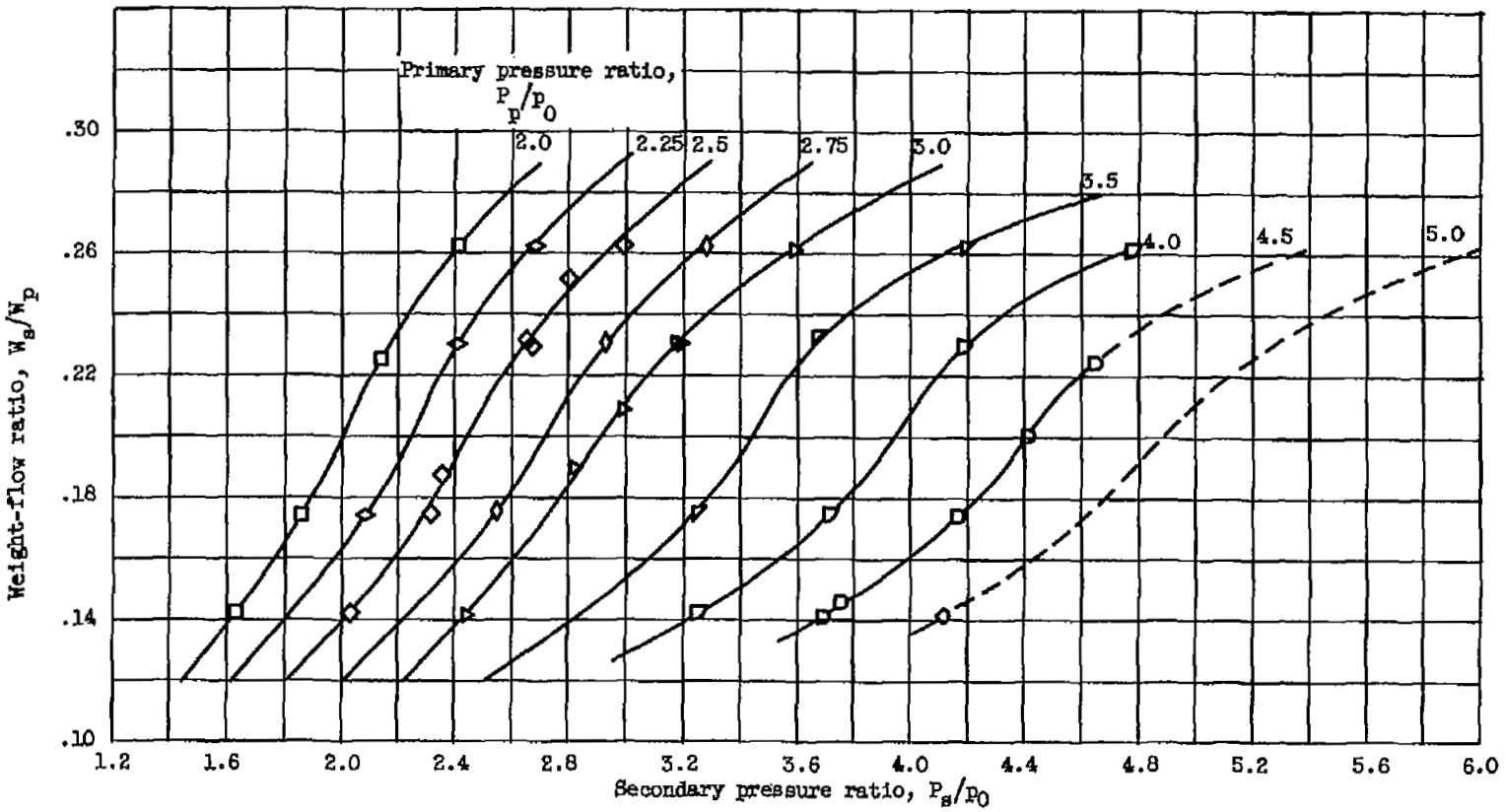

(c) Primary gas temperature, 3600° to 3700° R.

Figure 13. - Concluded. Effect of primary and secondary pressure ratio on ejector weight-flow ratio for configuration A. Diameter ratio, 1.048; spacing ratio, 0.445.

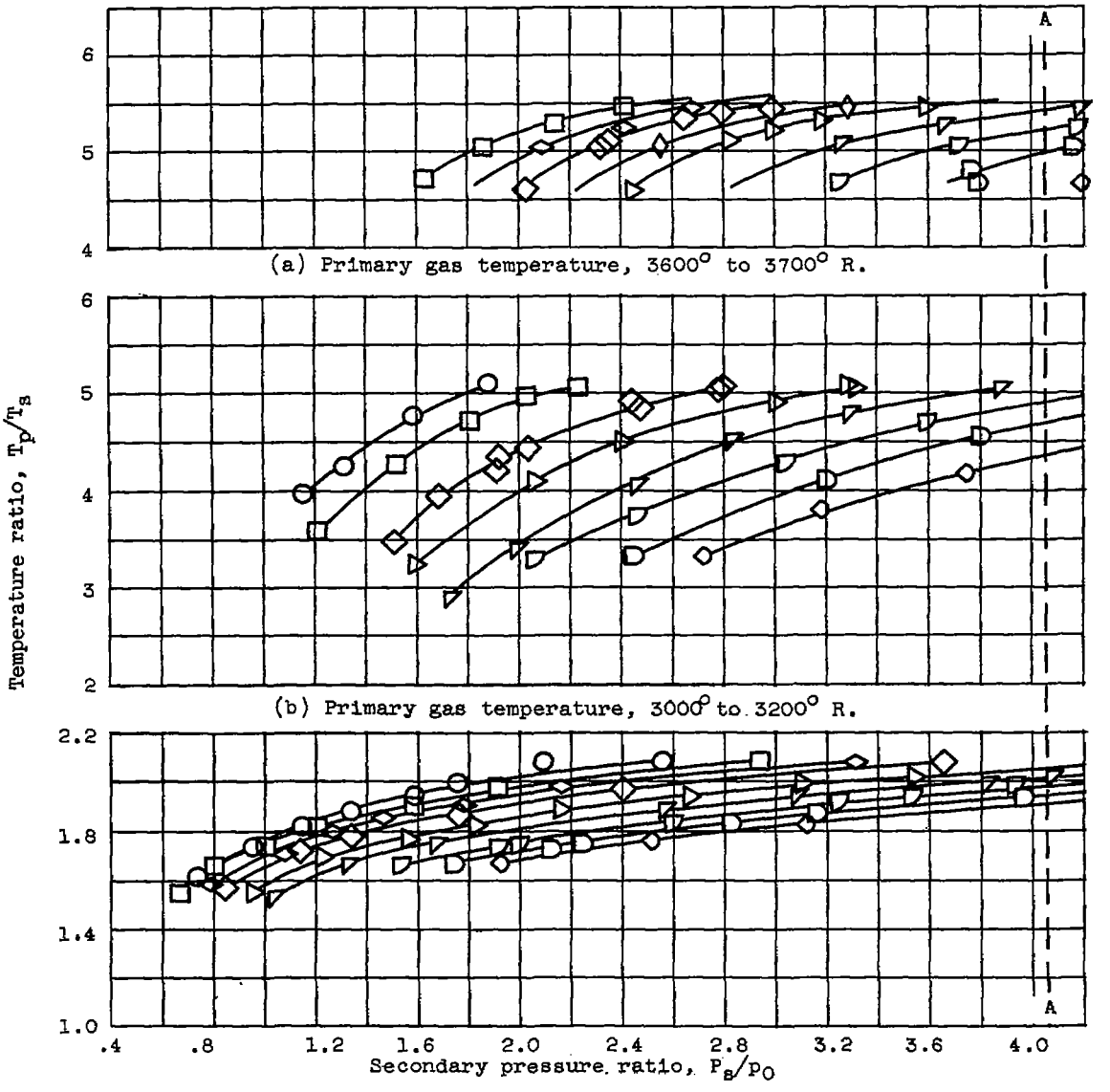

Figure 14. - Ratio of primary gas temperature to secondary air temperature as a function of operating condition for ejector configuration A. Diameter ratio, 1.048; spacing ratio, 0.445.

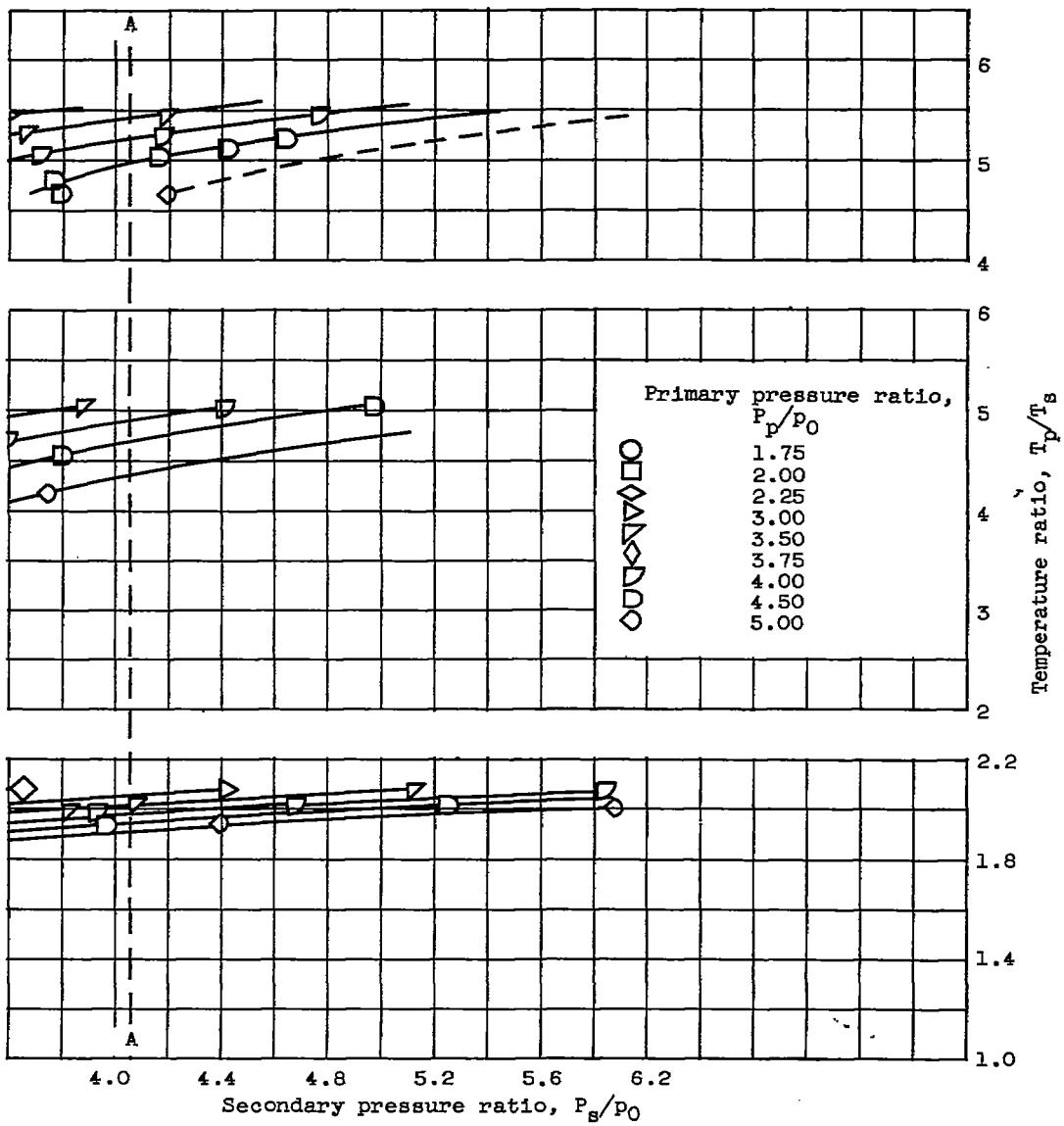
A
A
6
5
4
6
5
4
3
2
2.2
1.8
1.4
1.0
Primary pressure ratio, P_p/p_0
1.75
2.00
2.25
3.00
3.50
3.75
4.00
4.50
5.00
Temperature ratio, T_p/T_s
4.0
4.4
4.8
5.2
5.6
6.2
Secondary pressure ratio, P_s/p_0

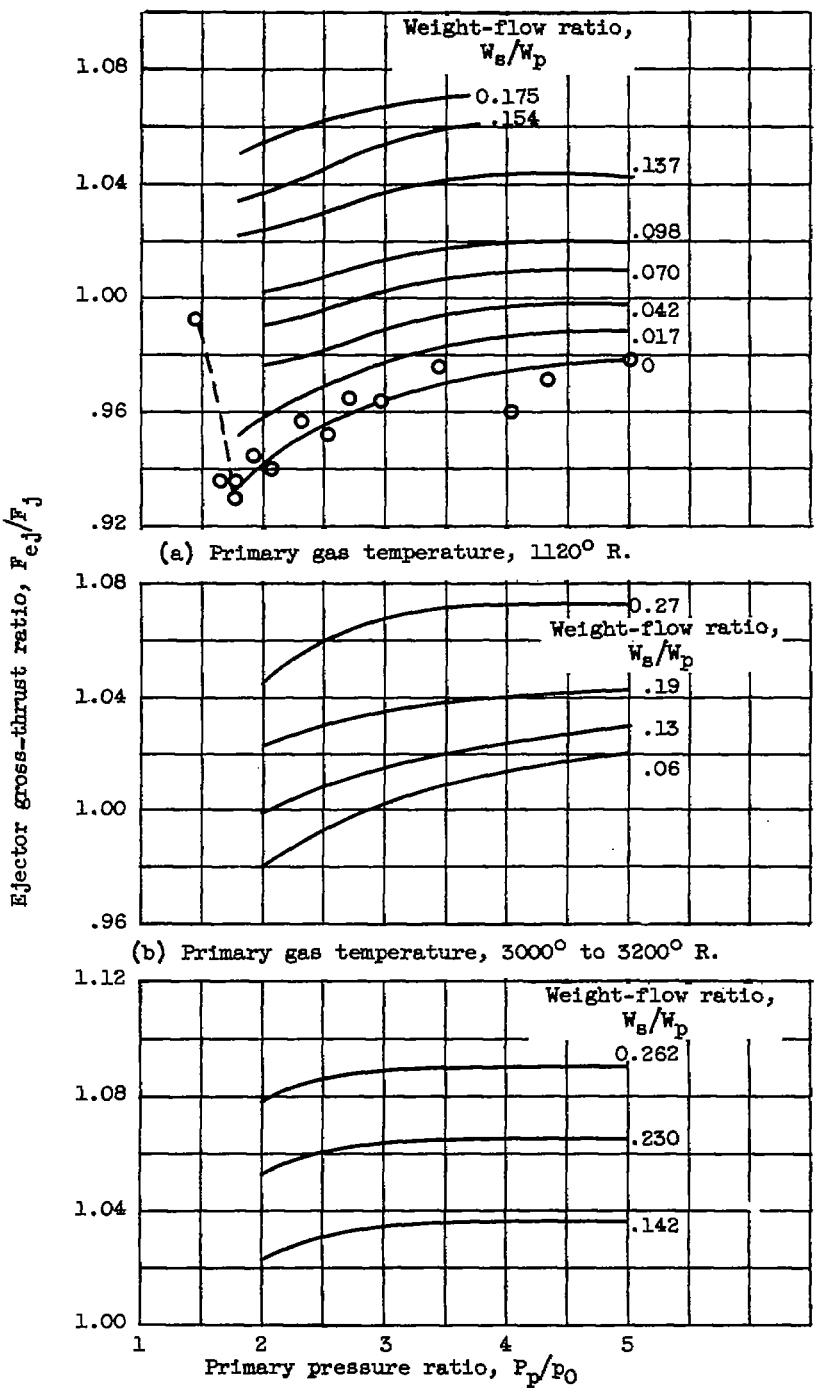

Figure 15. - Ejector gross-thrust ratio at constant values of weight-flow ratio for configuration A. Diameter ratio, 1.048; spacing ratio, 0.445.

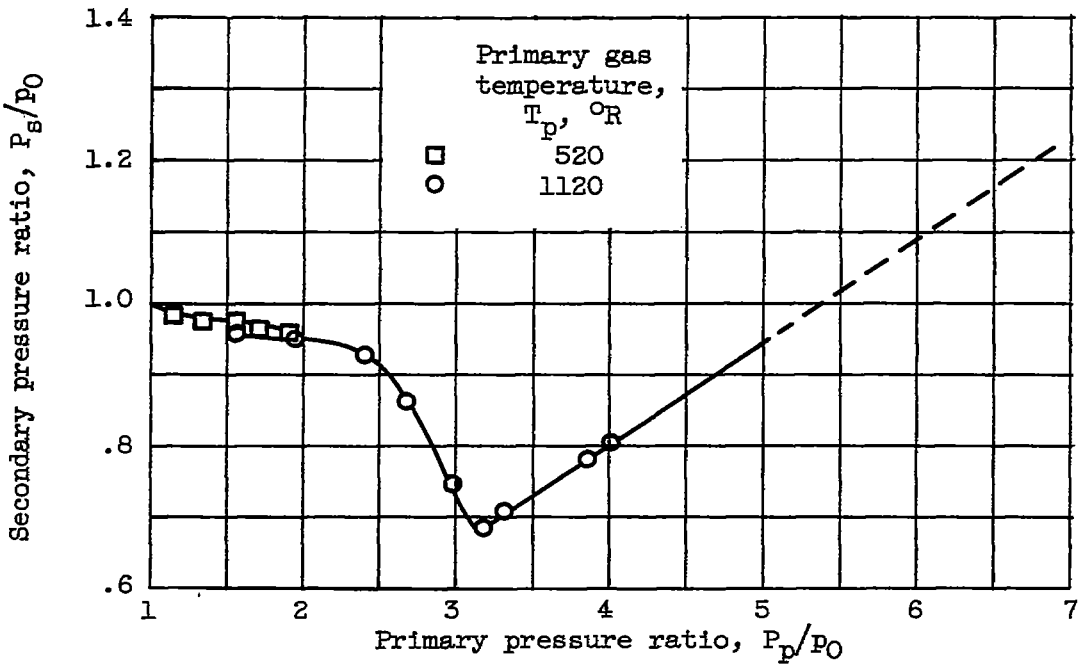

Figure 16. - Ejector pumping characteristics of configuration B at zero secondary flow. Diameter ratio, 1.095; spacing ratio, 0.213.

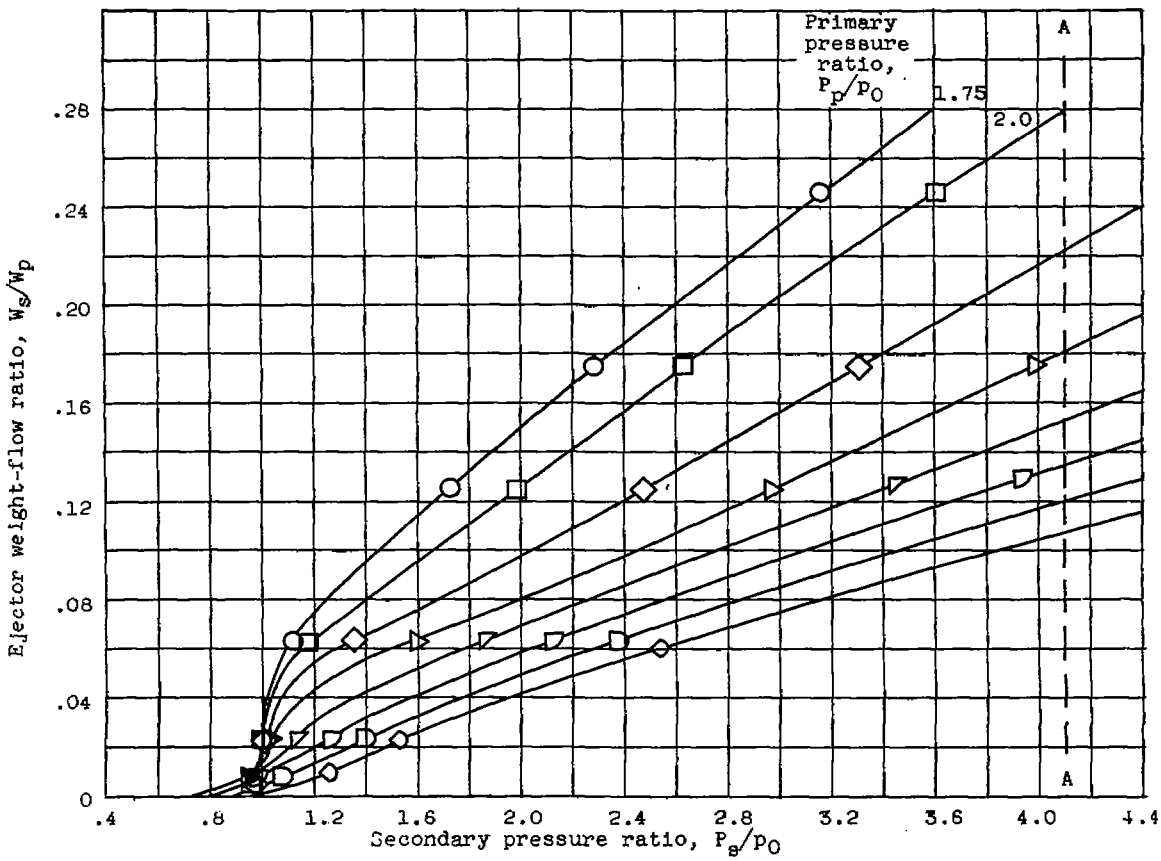

(a) Primary gas temperature, 1120° R.

Figure 17. - Effect of primary and secondary pressure ratio on ejector weight-flow ratio for configuration B. Diameter ratio, 1.095; spacing ratio, 0.213.

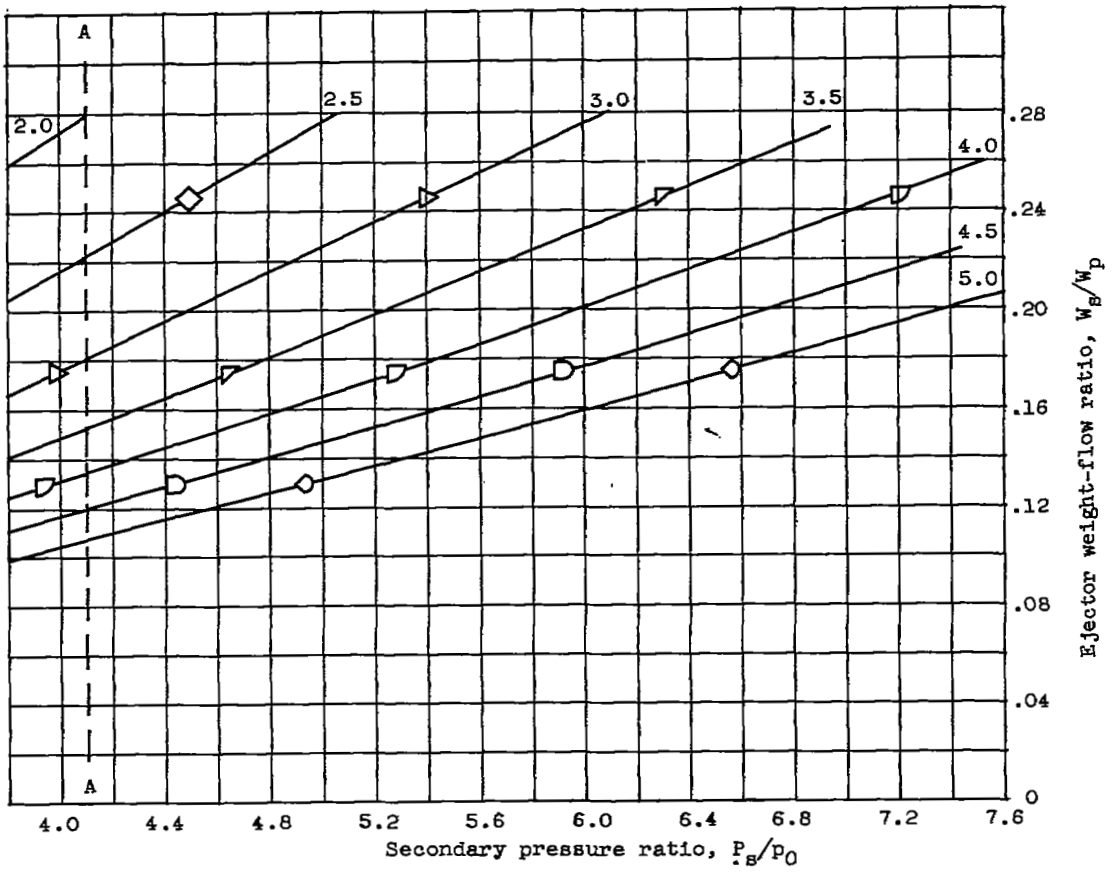

[redacted]

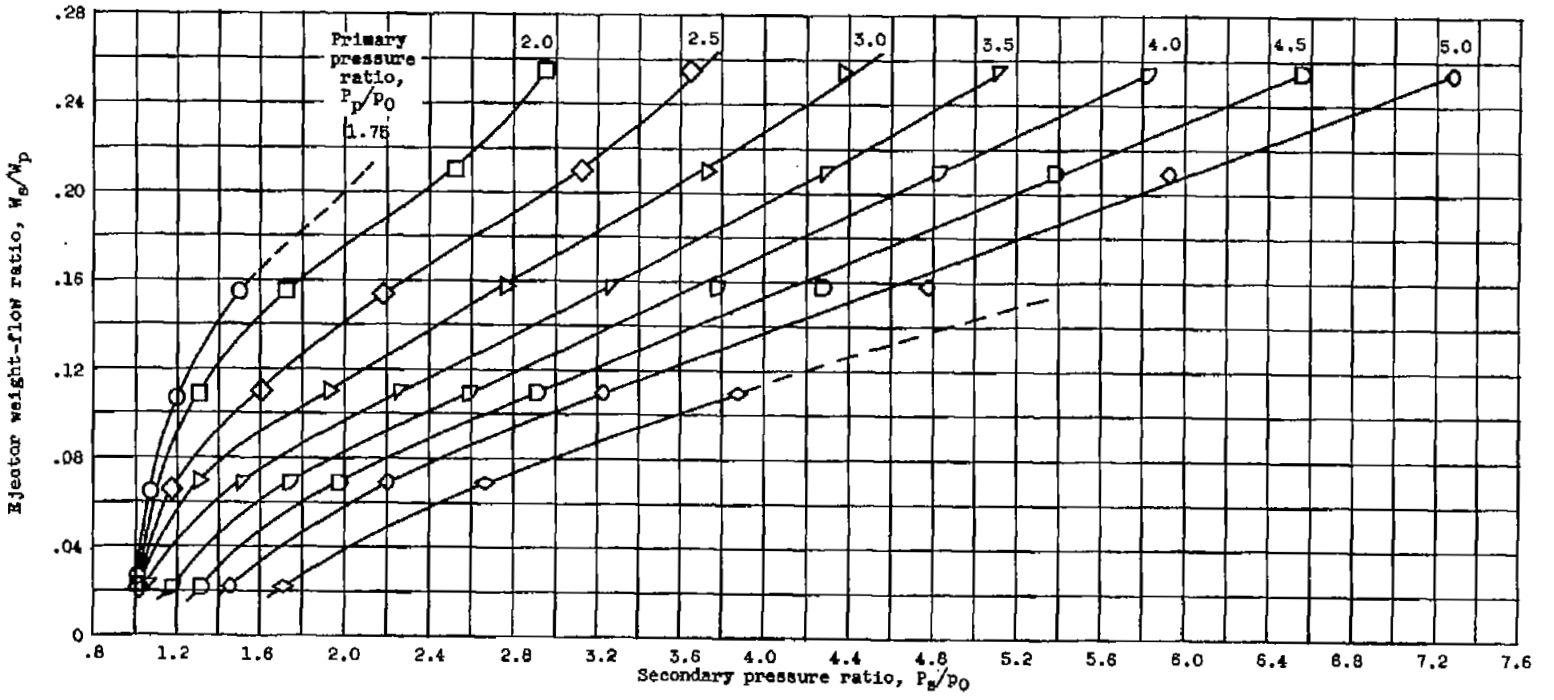

(b) Primary gas temperature, 2000° R.

Figure 17. - Continued. Effect of primary and secondary pressure ratio on ejector weight-flow ratio for configuration B. Diameter ratio, 1.095; spacing ratio, 0.213.

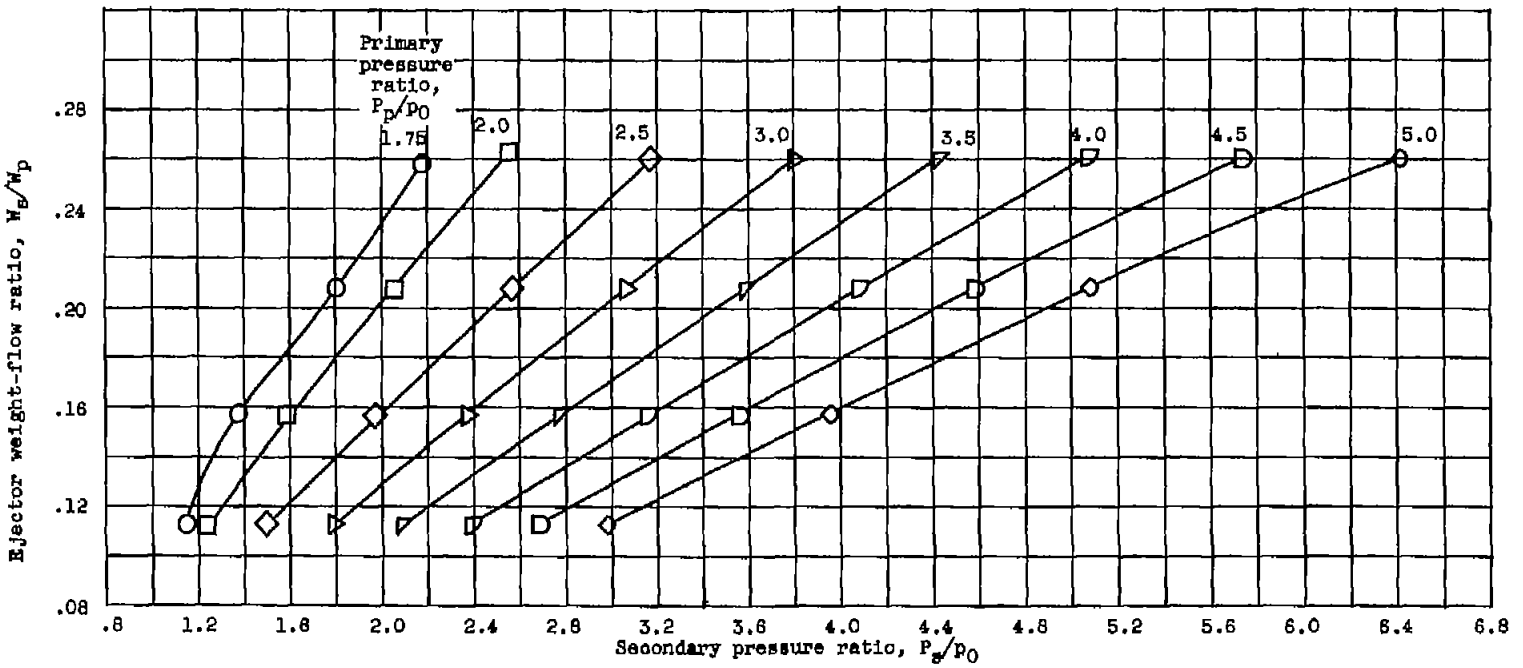

(c) Primary gas temperature, 3200° R.

Figure 17. - Continued. Effect of primary and secondary pressure ratio on ejector weight-flow ratio for configuration B. Diameter ratio, 1.095; spacing ratio, 0.213.

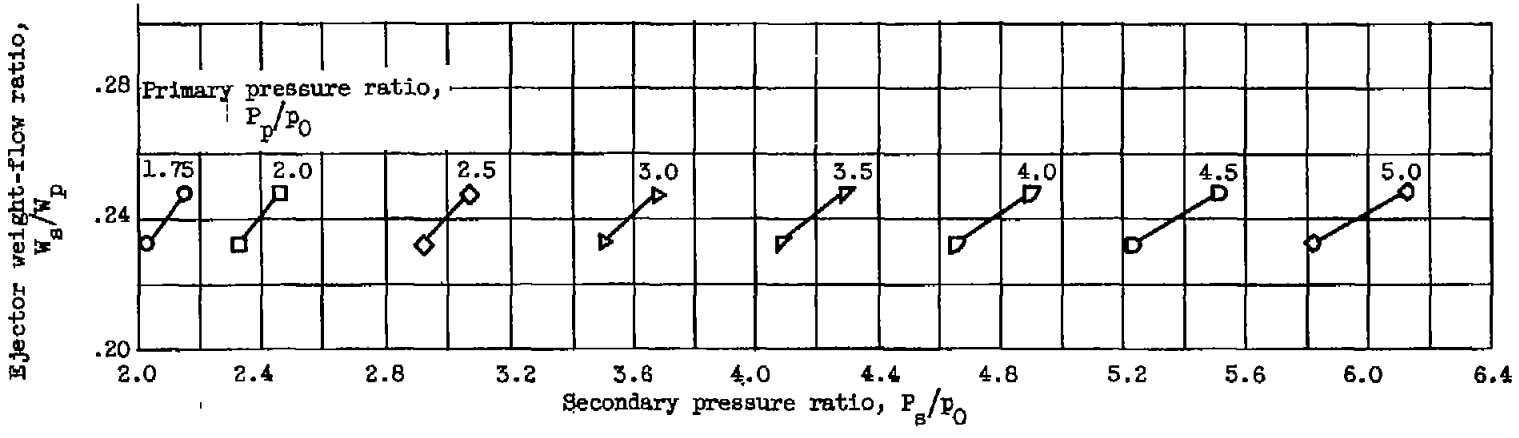

(d) Primary gas temperature, 3600° R.

Figure 17. - Concluded. Effect of primary and secondary pressure ratio on ejector weight-flow ratio for configuration B. Diameter ratio, 1.095; spacing ratio, 0.213.

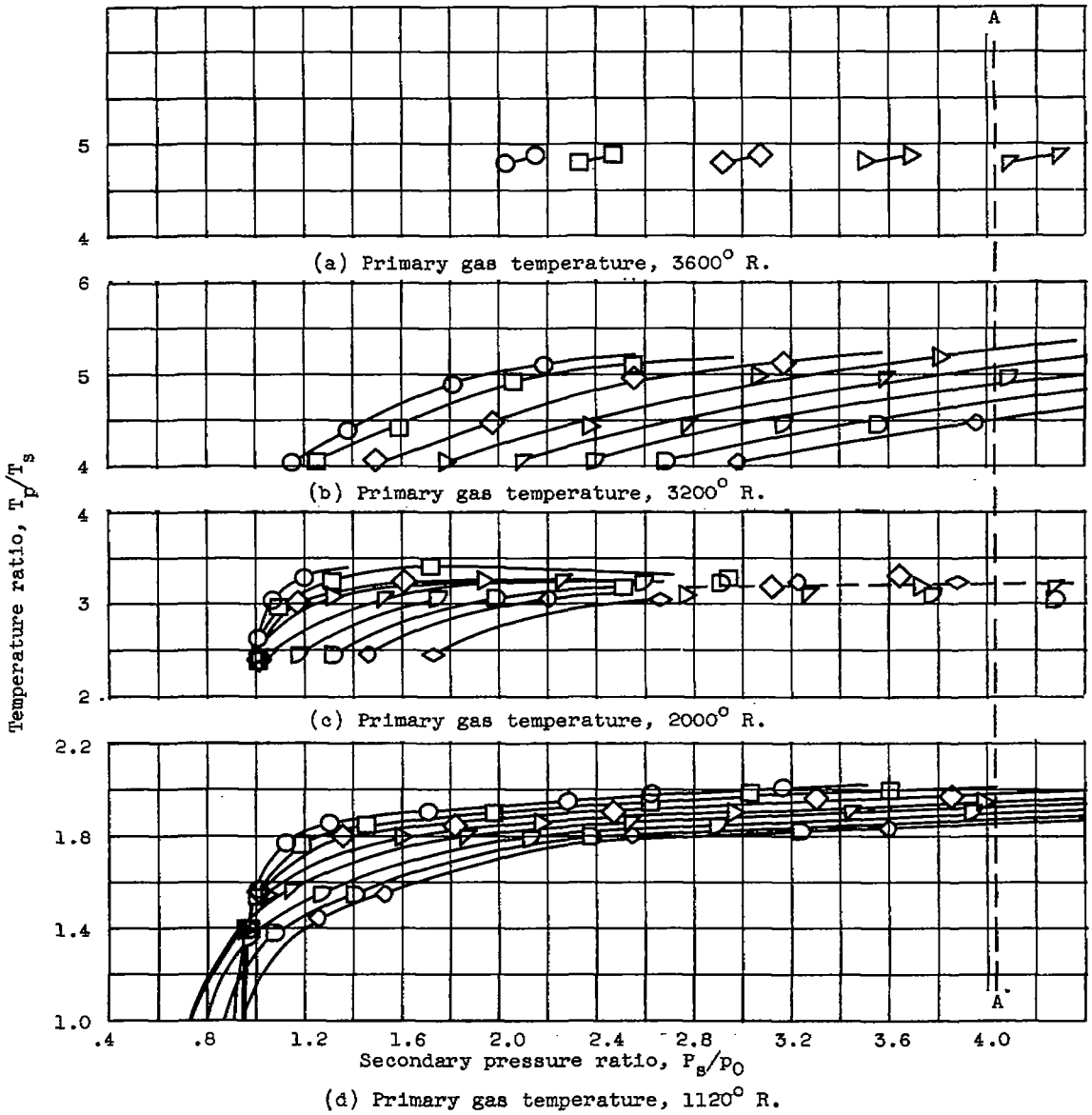

Figure 18. - Ratio of primary gas temperature to secondary air temperature as a function of operating condition for ejector configuration B. Diameter ratio, 1.095; spacing ratio, 0.213.

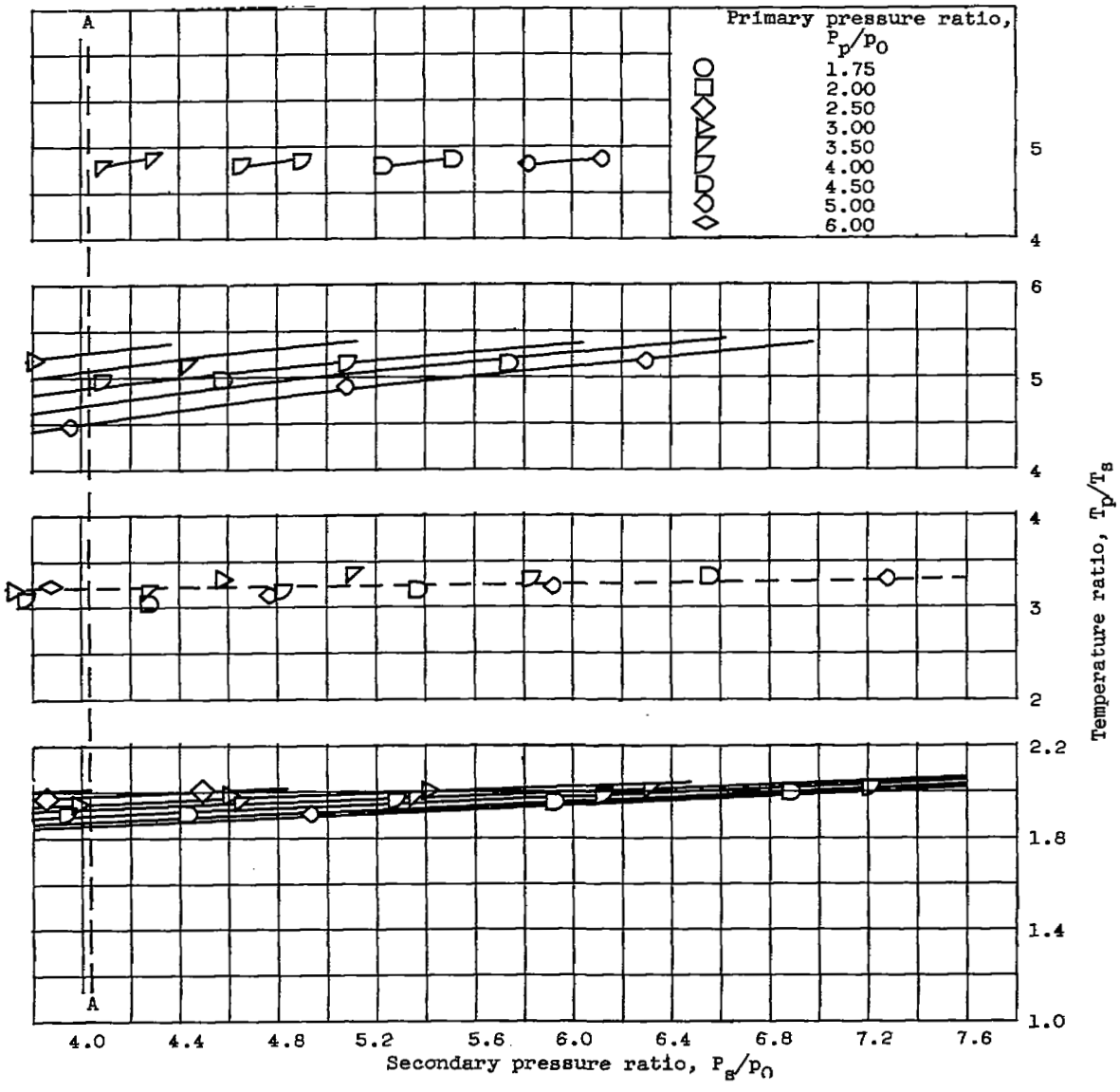
Primary pressure ratio, P_p/p_0
1.75
2.00
2.50
3.00
3.50
4.00
4.50
5.00
6.00
A
A
5
4
6
5
4
4
3
2
2.2
1.8
1.4
1.0
4.0
4.4
4.8
5.2
5.6
6.0
6.4
6.8
7.2
7.6
Secondary pressure ratio, P_s/p_0
Temperature ratio, T_p/T_s

[redacted]

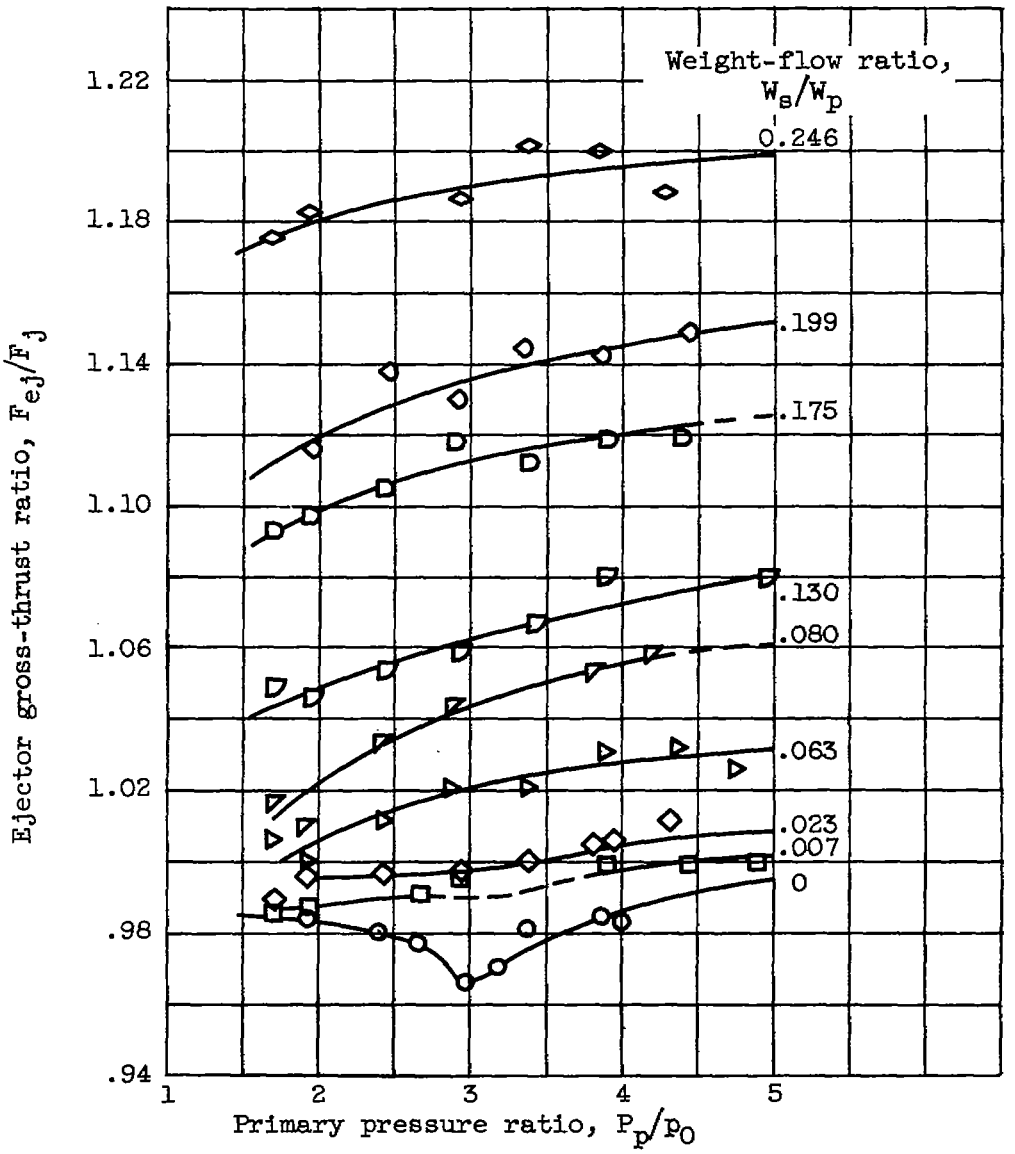

(a) Primary gas temperature, 1120° R.

Figure 19. - Ejector gross-thrust ratio at constant values of weight-flow ratio for configuration B. Diameter ratio, 1.095; spacing ratio, 0.213.

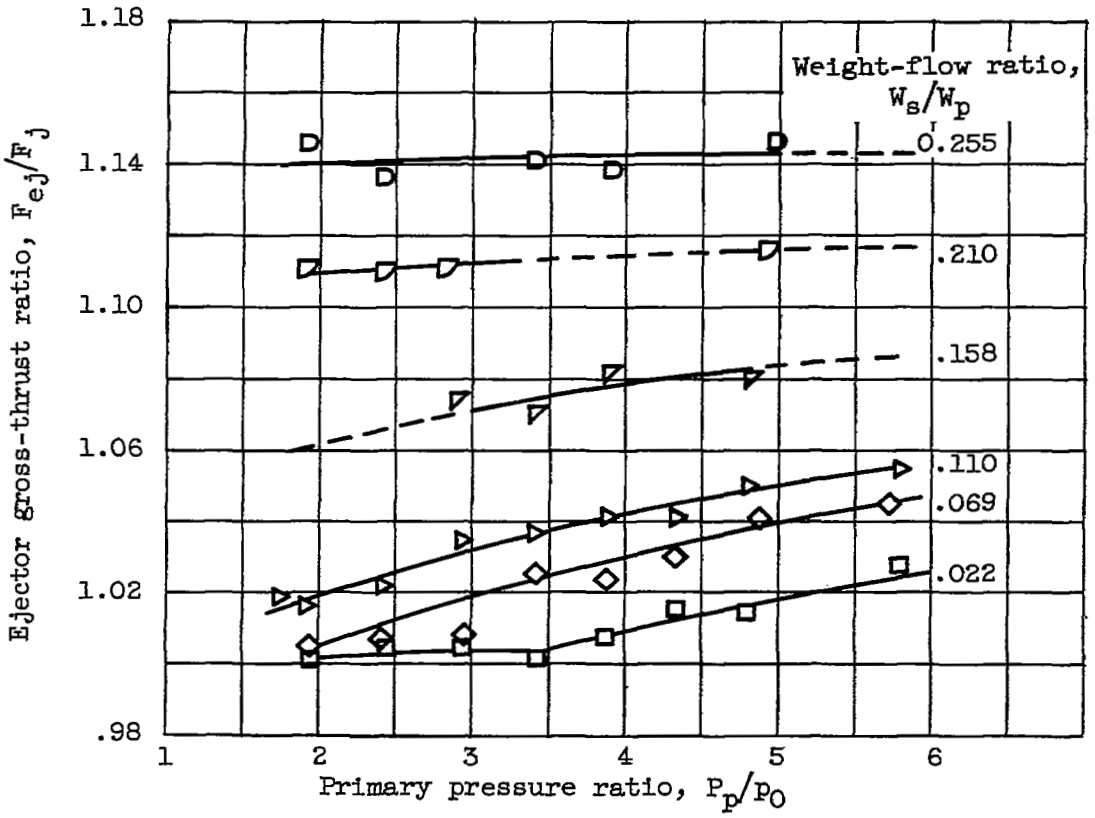

(b) Primary gas temperature, 2000° R.

Figure 19. - Continued. Ejector gross-thrust ratio at constant values of weight-flow ratio for configuration B. Diameter ratio, 1.095; spacing ratio, 0.213.

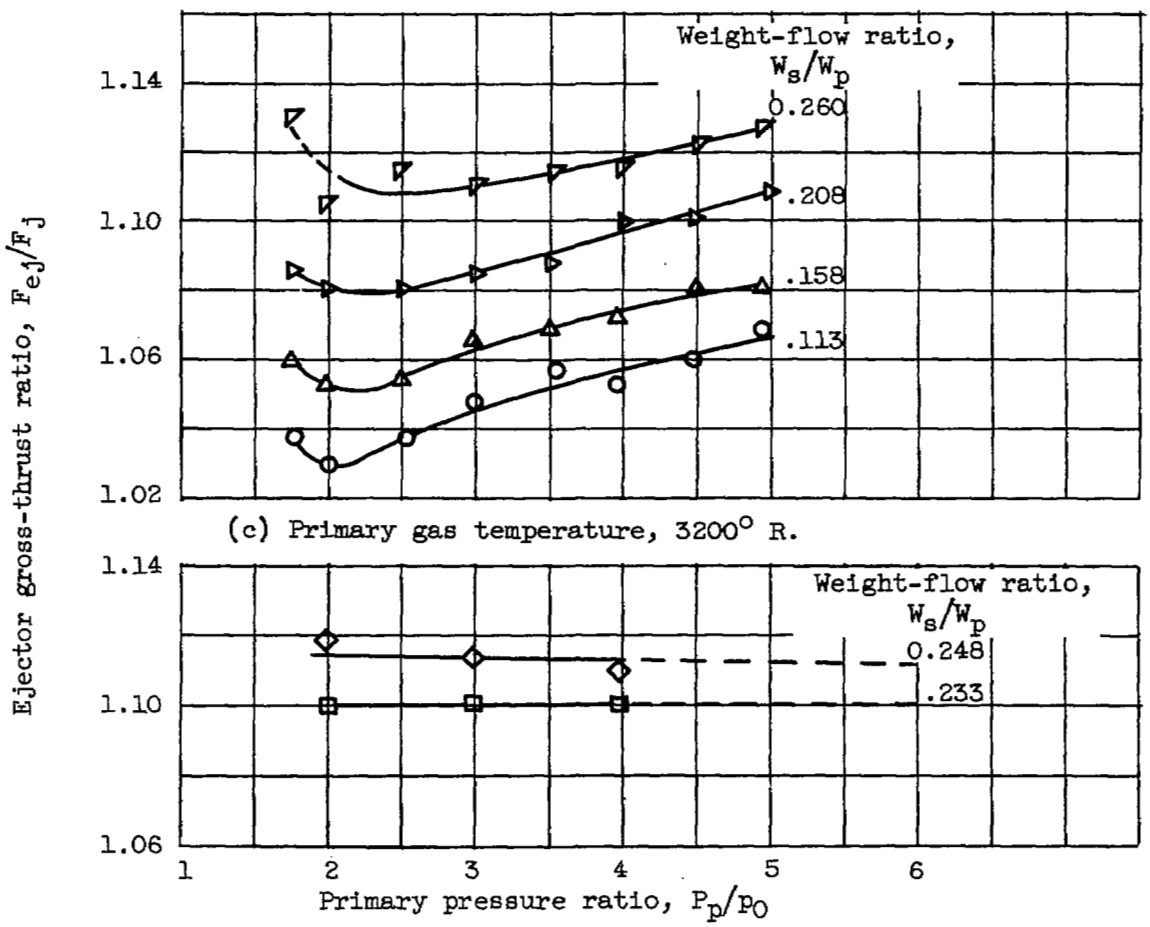

(c) Primary gas temperature, 3200° R.

(d) Constant primary gas temperature, 3600° R.

Figure 19. - Concluded. Ejector gross-thrust ratio at constant values of weight-flow ratio for configuration B. Diameter ratio, 1.095; spacing ratio, 0.213.

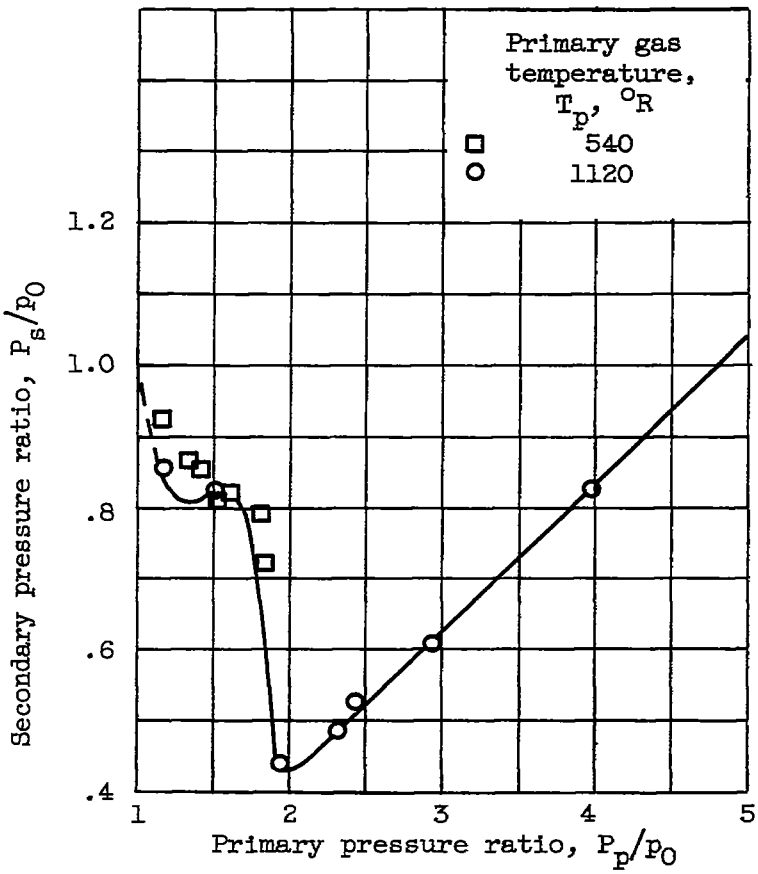

Figure 20. - Ejector pumping characteristics of configuration C at zero secondary flow. Diameter ratio, 1.095; spacing ratio, 0.408.

[redacted]

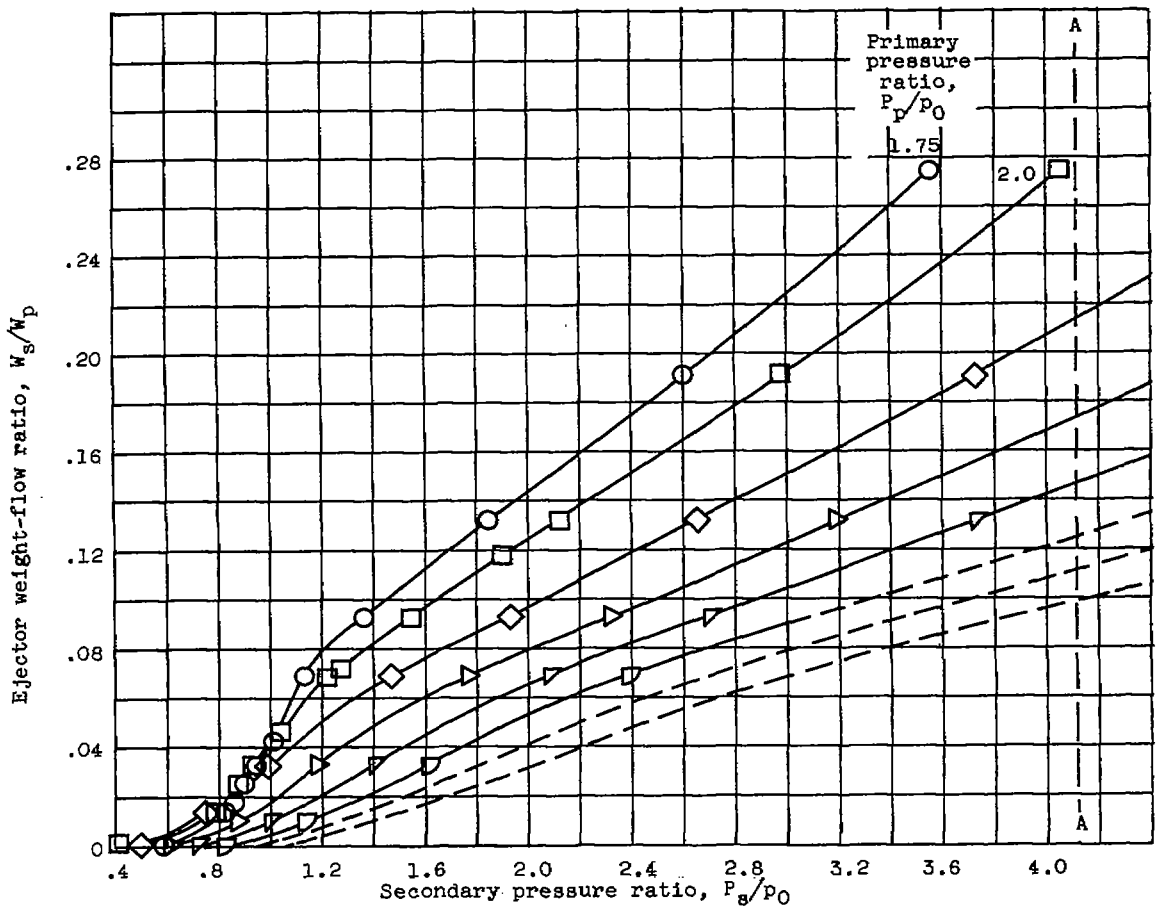

(a) Primary gas temperature, 1120° R.

Figure 21. - Effect of primary and secondary pressure ratio on ejector weight-flow ratio for configuration C. Diameter ratio, 1.095; spacing ratio, 0.408.

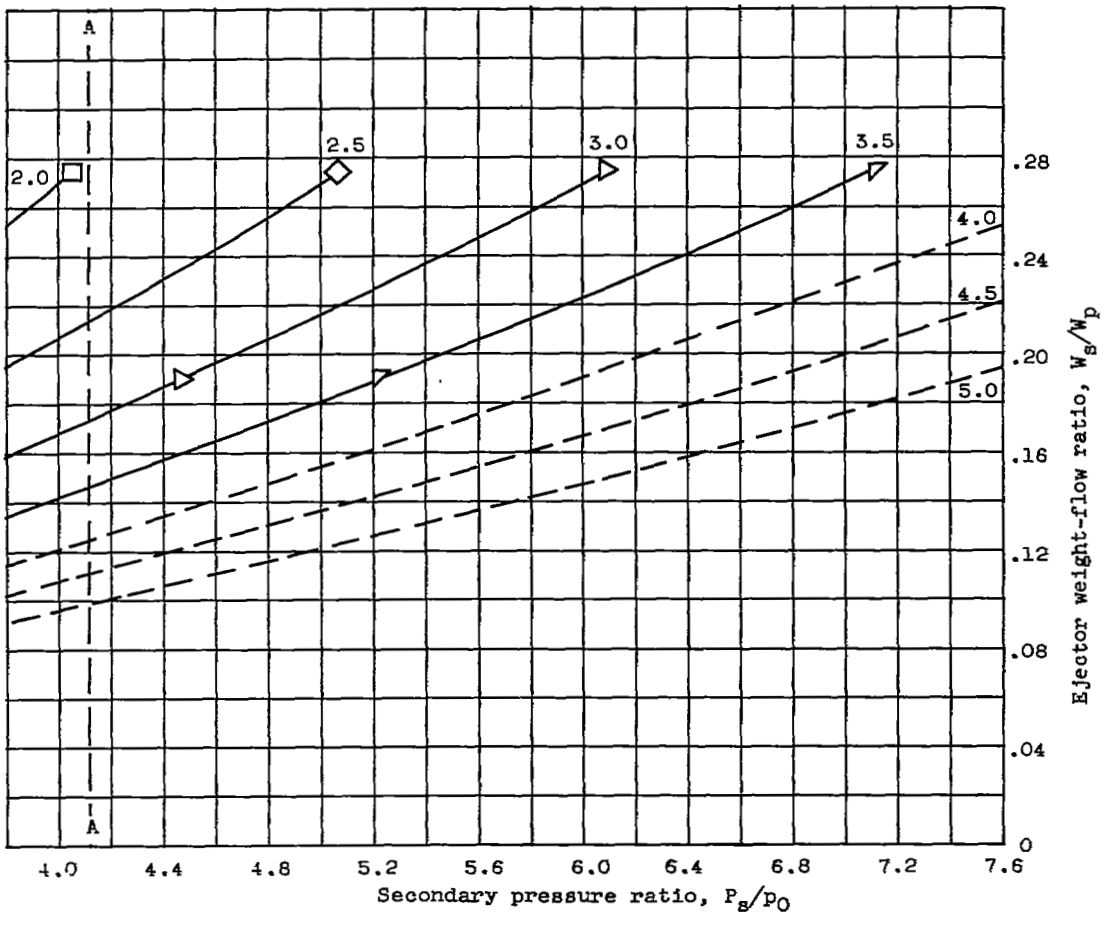
A
2.0
2.5
3.0
3.5
4.0
4.5
5.0
A
.28
.24
.20
.16
.12
.08
.04
0
4.0
4.4
4.8
5.2
5.6
6.0
6.4
6.8
7.2
7.6
Secondary pressure ratio, P_s/p_0
Ejector weight-flow ratio, W_s/W_p

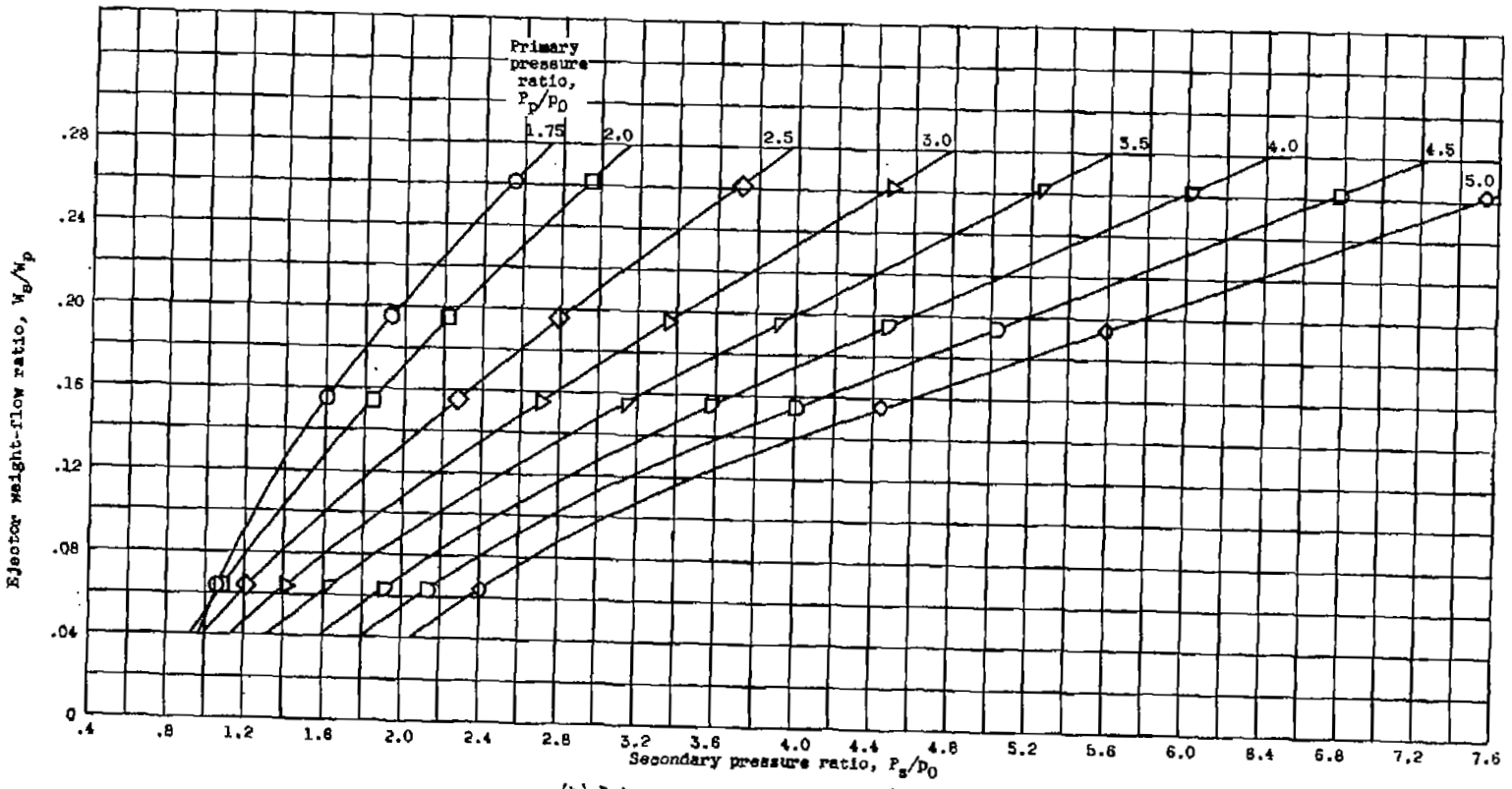

(b) Primary gas temperature, 2100° to 2200° R.

Figure 21. - Continued. Effect of primary and secondary pressure ratio on ejector weight-flow ratio for configuration C. Diameter ratio, 1.095; spacing ratio, 0.406.

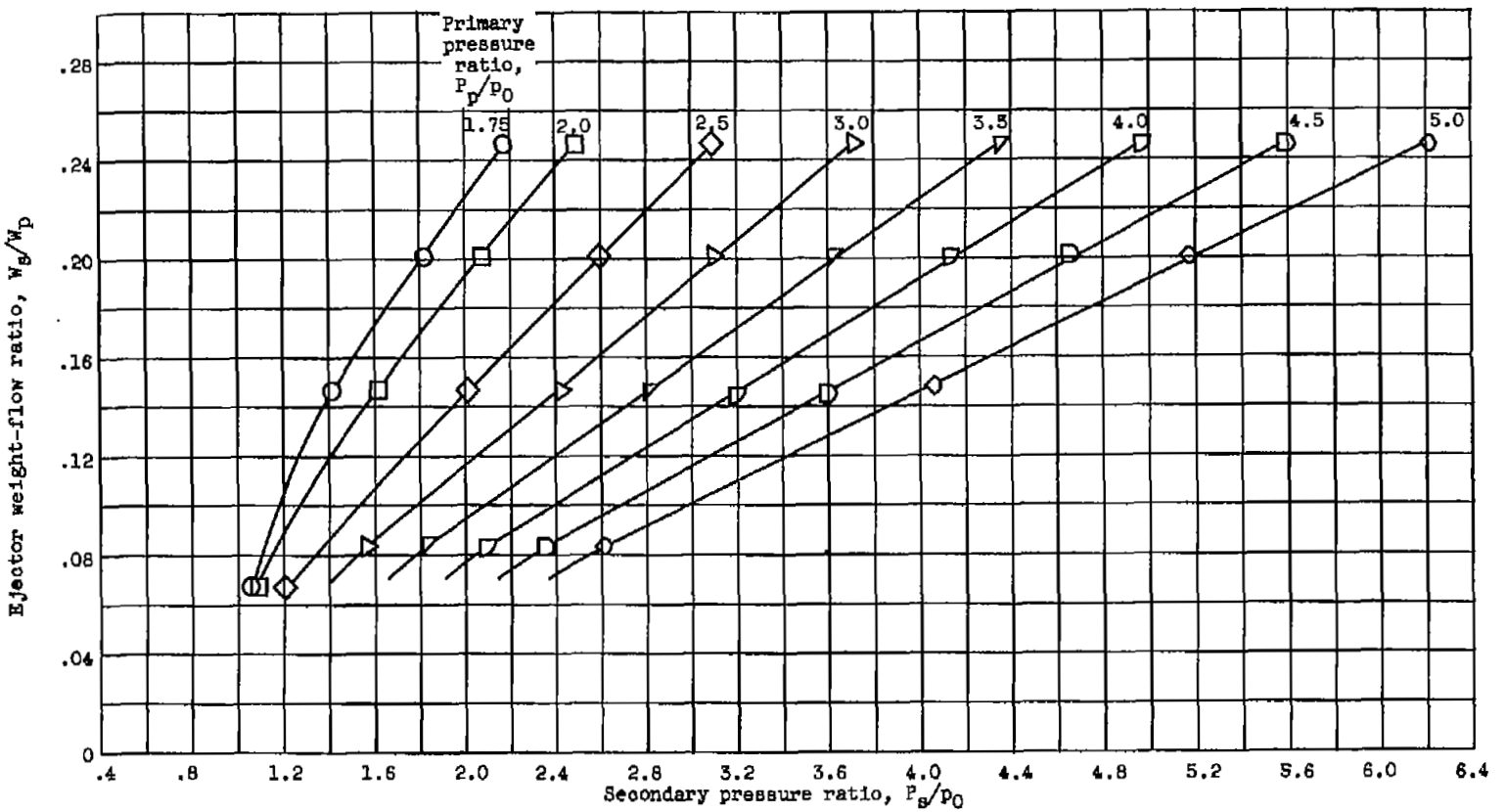

(c) Primary gas temperature, 3000° to 5200° R.

Figure 21. - Concluded. Effect of primary and secondary pressure ratio on ejector weight-flow ratio for configuration C. Diameter ratio, 1.095; spacing ratio, 0.408.

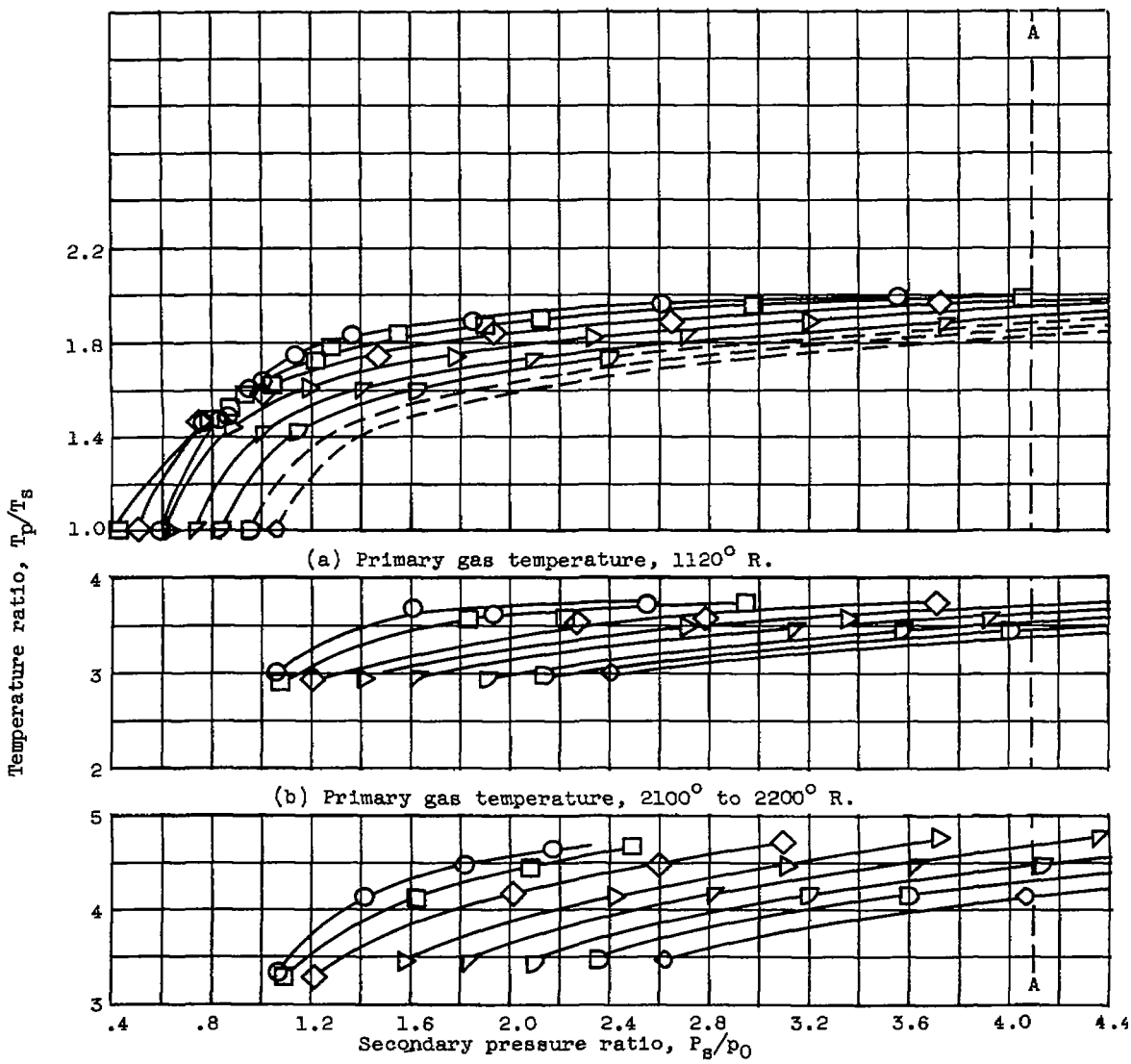

Figure 22. - Ratio of primary gas temperature to secondary air temperature as a function of operating conditions for ejector configuration C.

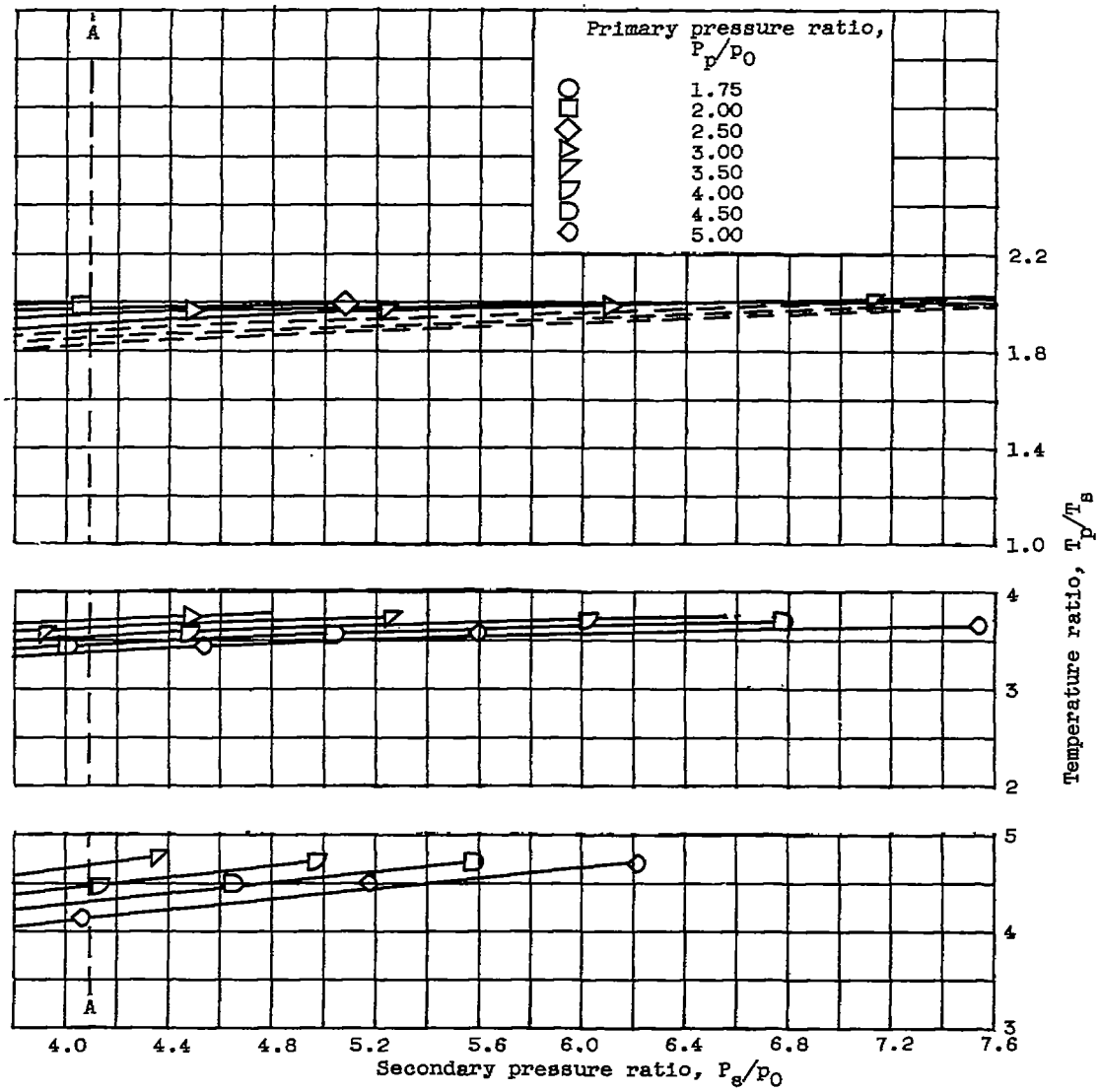

[redacted]

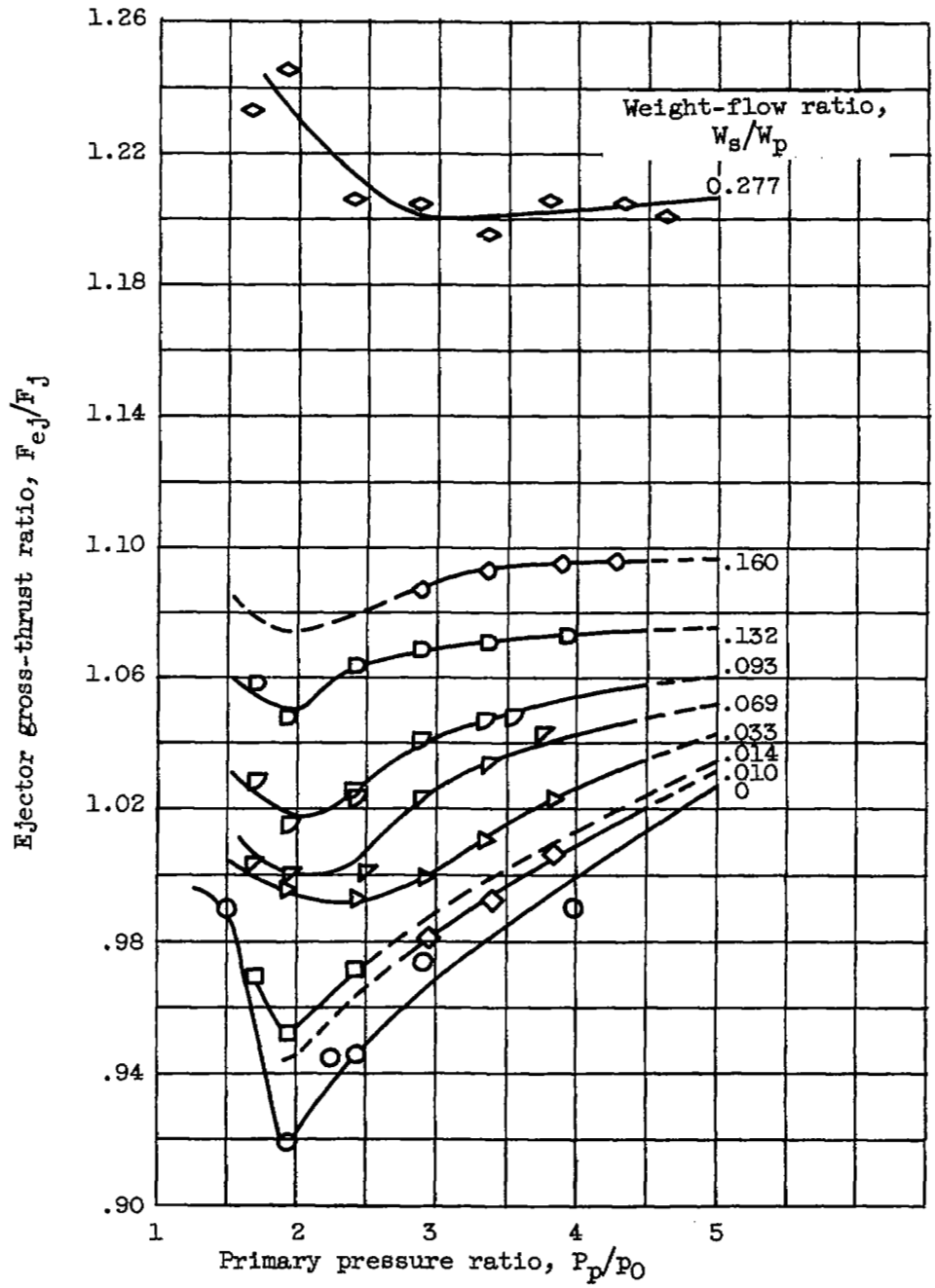

(a) Primary gas temperature, 1120° R.

Figure 23. - Ejector gross-thrust ratio at constant values of weight-flow ratio for configuration C. Diameter ratio, 1.095; spacing ratio, 0.408.

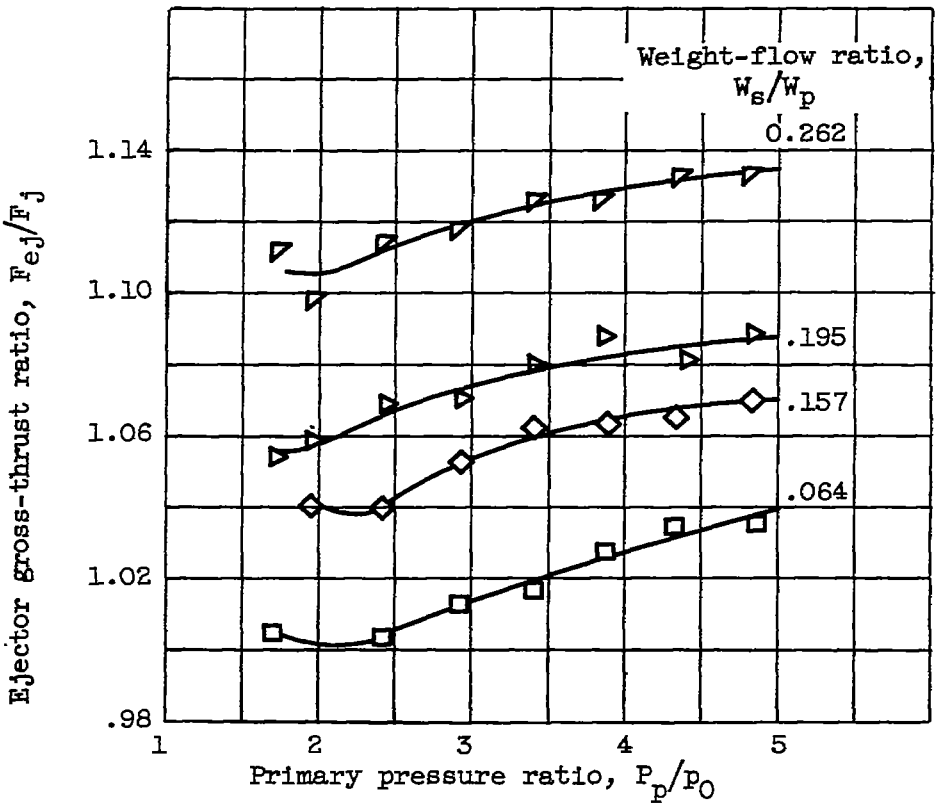

(b) Primary gas temperature, 2100° to 2200° R.

Figure 23. - Continued. Ejector gross-thrust ratio at constant values of weight-flow ratio for configuration C. Diameter ratio, 1.095; spacing ratio, 0.408.

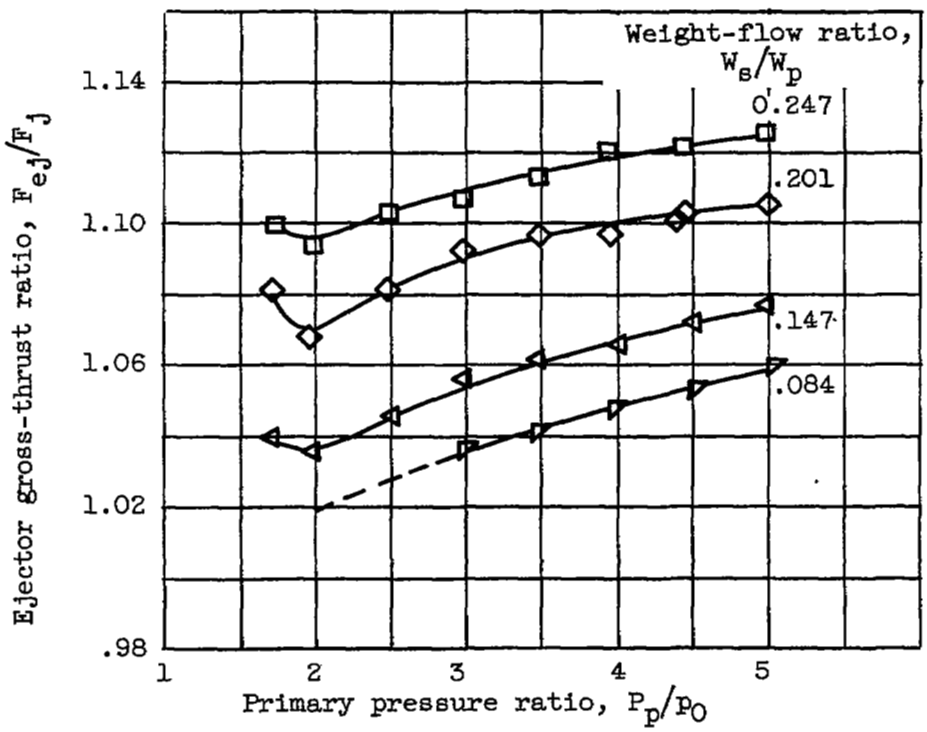

(c) Primary gas temperature, 3000° to 3200° R.

Figure 23. - Concluded. Ejector gross-thrust ratio at constant values of weight-flow ratio for configuration C. Diameter ratio, 1.095; spacing ratio, 0.408.

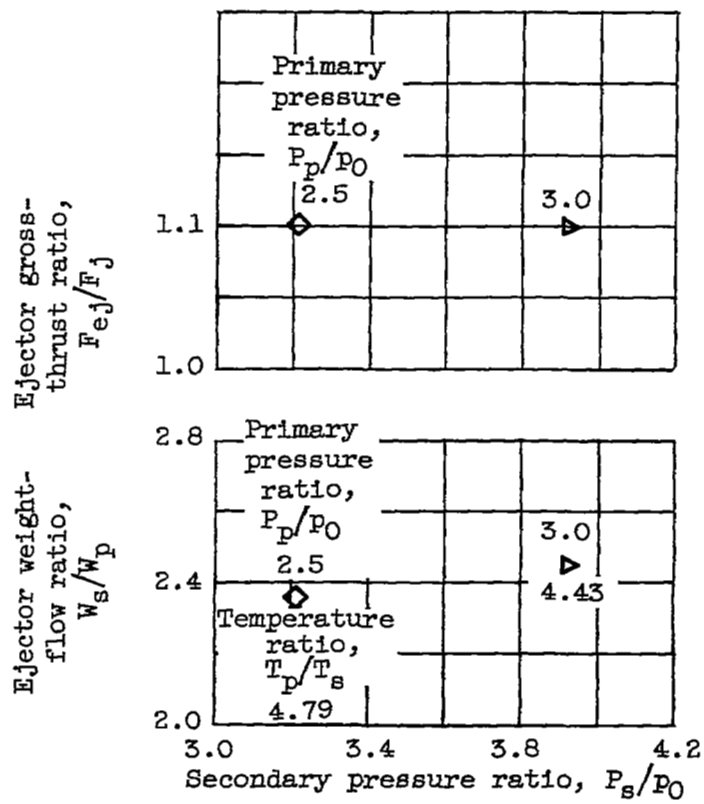

Figure 24. - Limited data for configuration C at a primary gas temperature of 3600° R. Diameter ratio, 1.095; spacing ratio, 0.408.

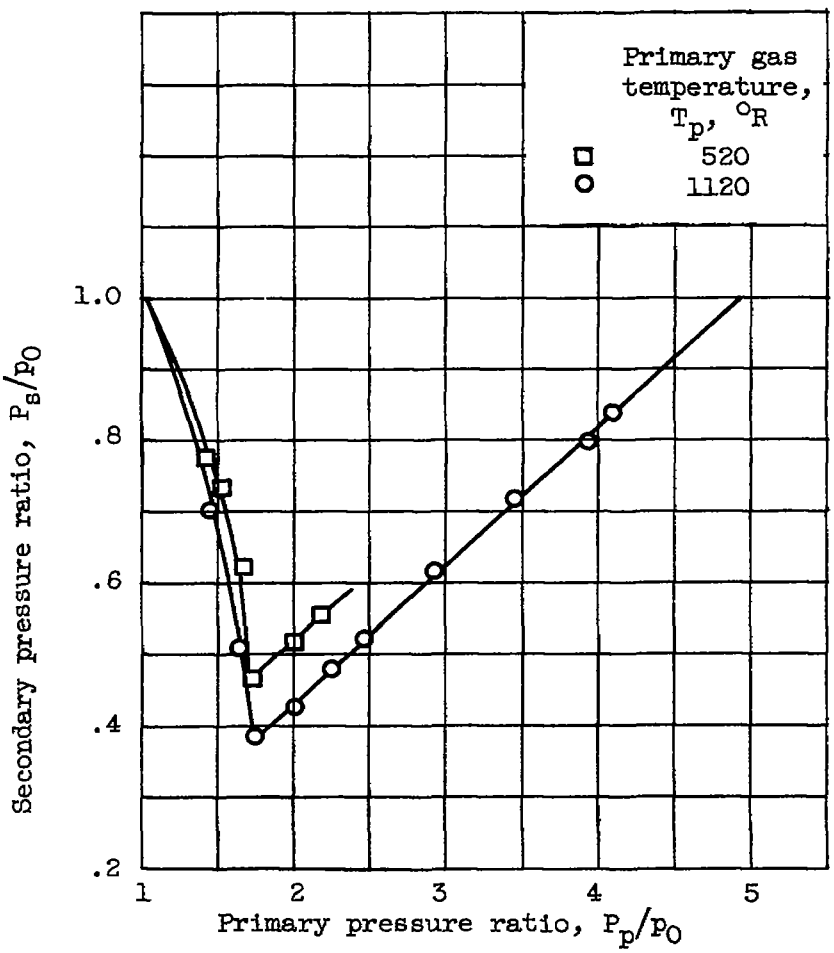

Figure 25. - Ejector pumping characteristics for configuration D at zero secondary flow. Diameter ratio, 1.095; spacing ratio, 0.810.

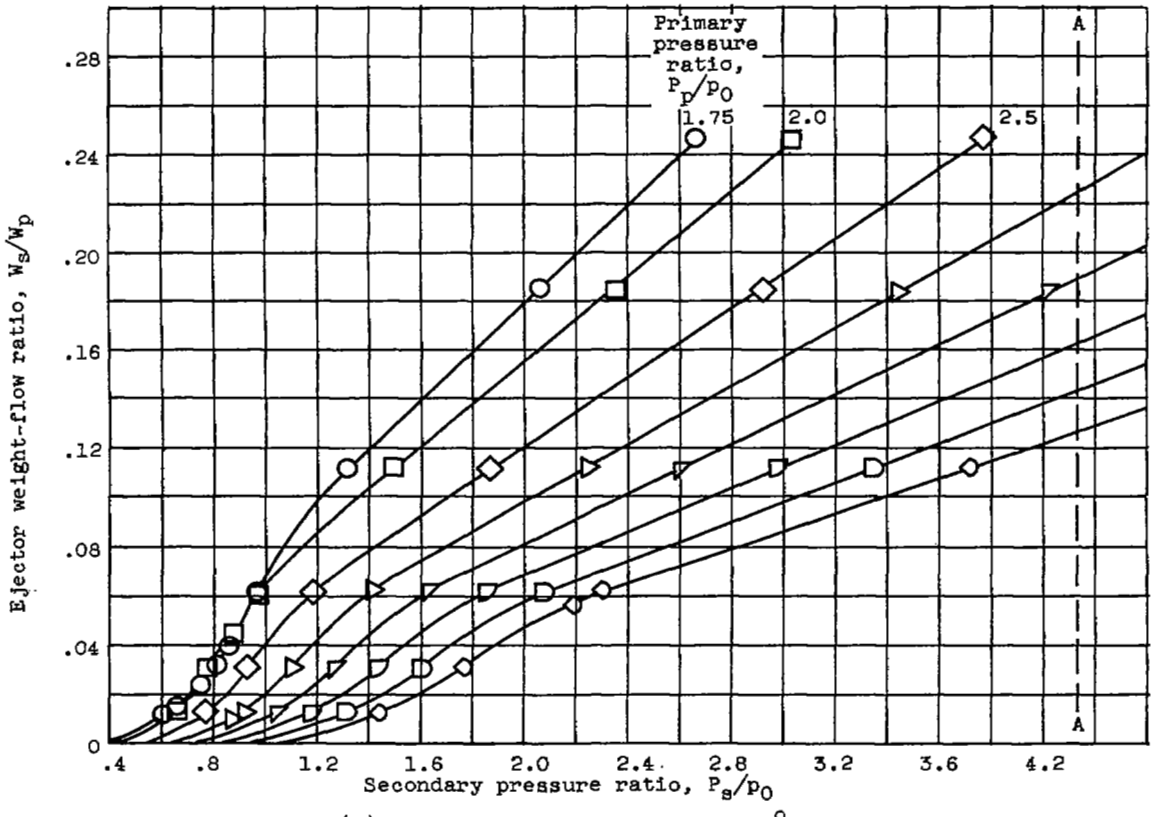

(a) Primary gas temperature, 1120° R.

Figure 26. - Effect of primary and secondary pressure ratio on ejector weight-flow ratio for configuration D. Diameter ratio, 1.095; spacing ratio, 0.810.

[redacted]

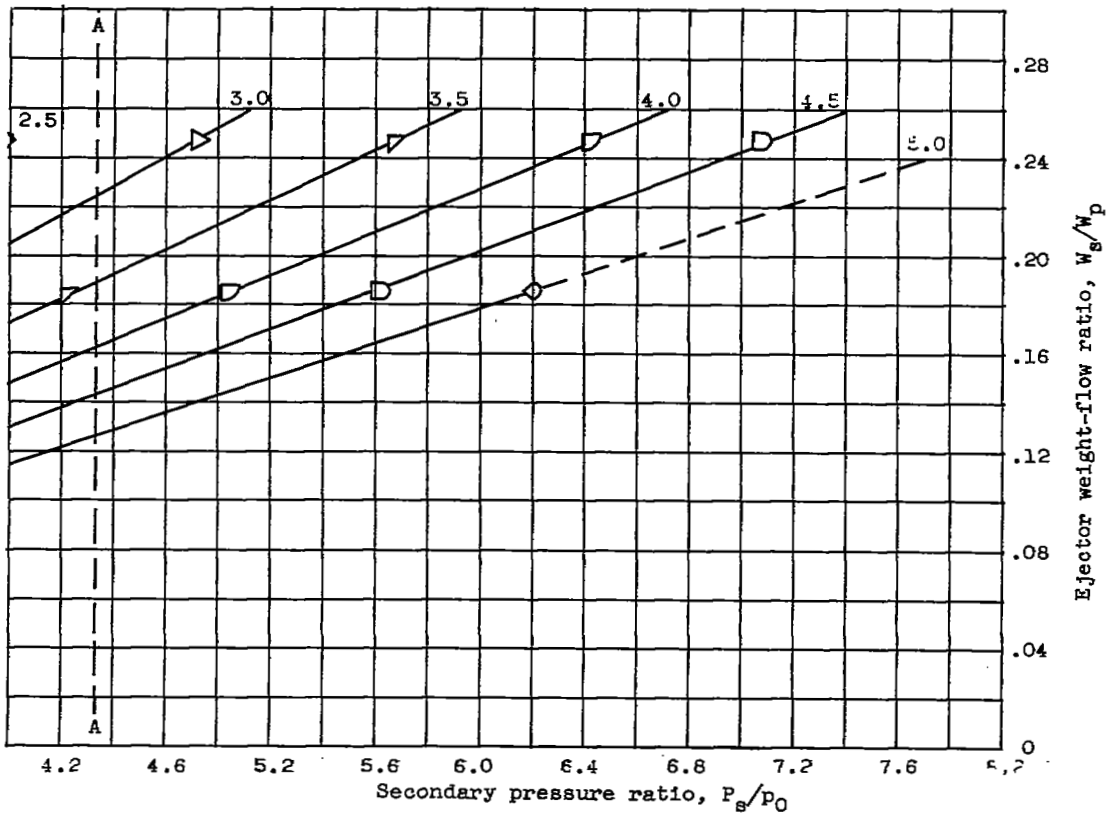

[redacted]

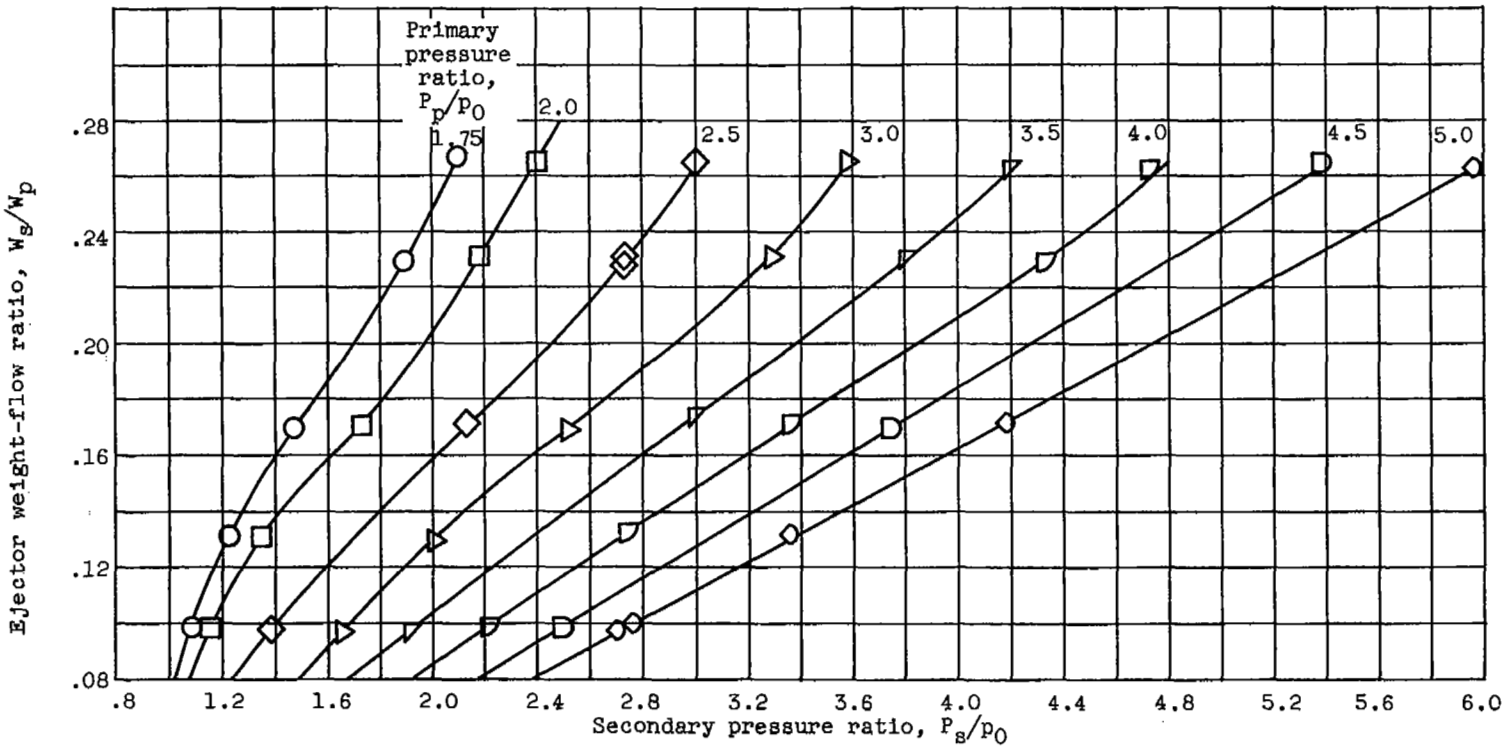

(b) Primary gas temperature, 3000° to 3100° R.

Figure 26. - Continued. Effect of primary and secondary pressure ratio on ejector weight-flow ratio for configuration D. Diameter ratio, 1.095; spacing ratio, 0.810.

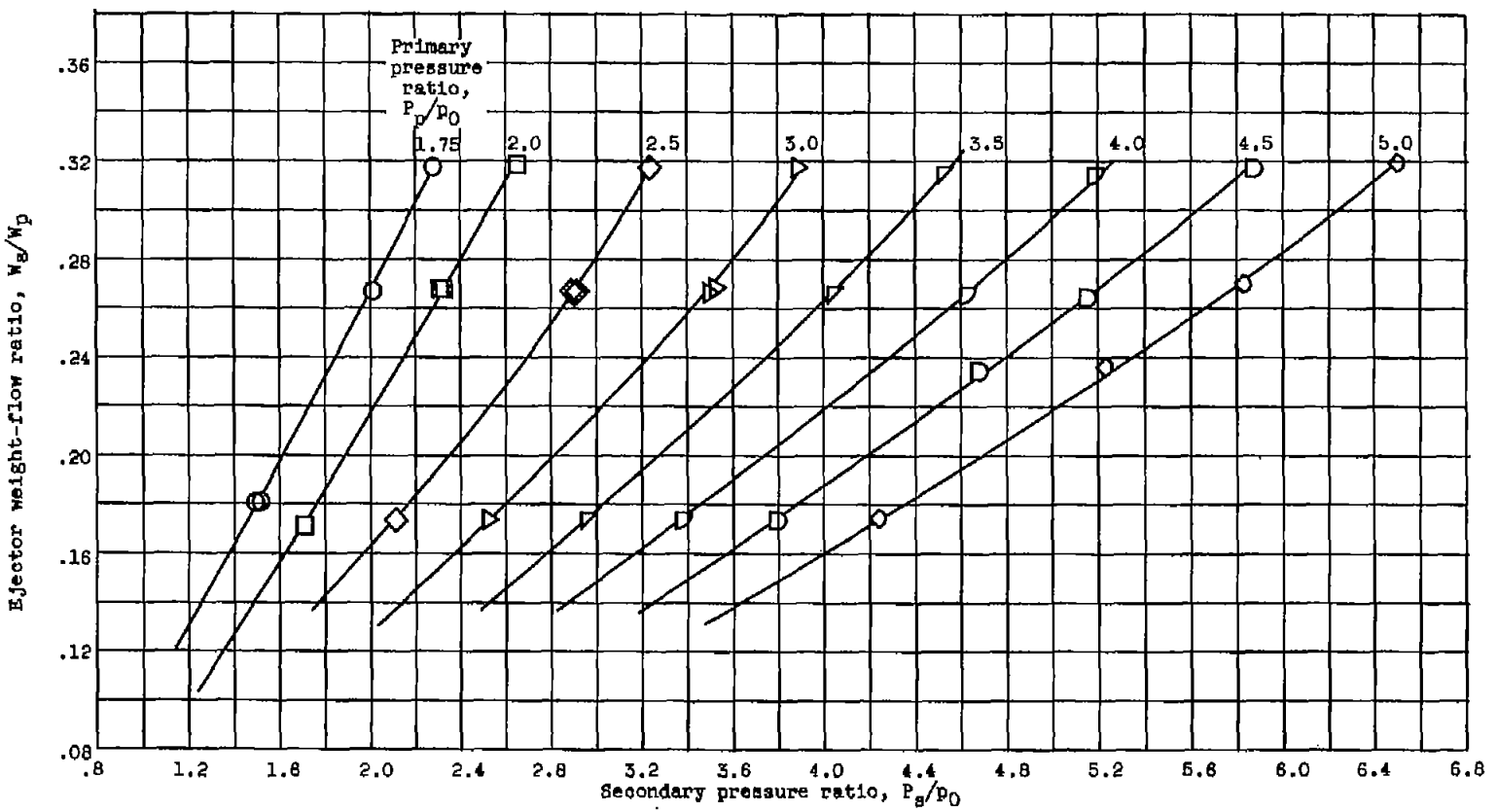

(c) Primary gas temperature, 3600° to 3700° R.

Figure 26. - Concluded. Effect of primary and secondary pressure ratio on ejector weight-flow ratio for configuration D. Diameter ratio, 1.095; spacing ratio, 0.810.

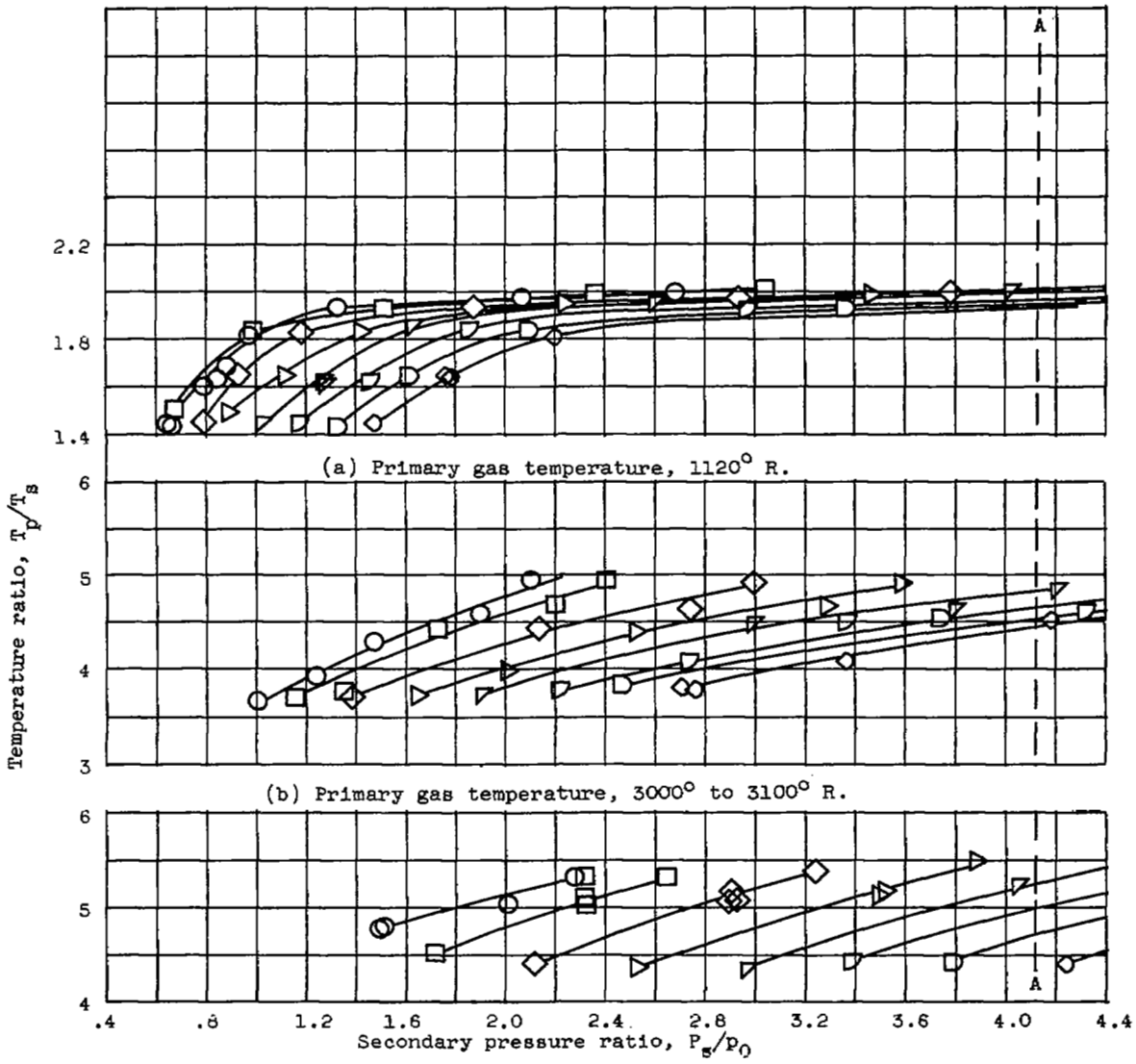

(a) Primary gas temperature, 1120° R.

(b) Primary gas temperature, 3000° to 3100° R.

(c) Primary gas temperature, 3600° to 3700° R.

Figure 27. - Ratio of primary gas temperature to secondary air temperature as a function of operating conditions for ejector configuration D. Diameter ratio, 1.095; spacing ratio, 0.810.

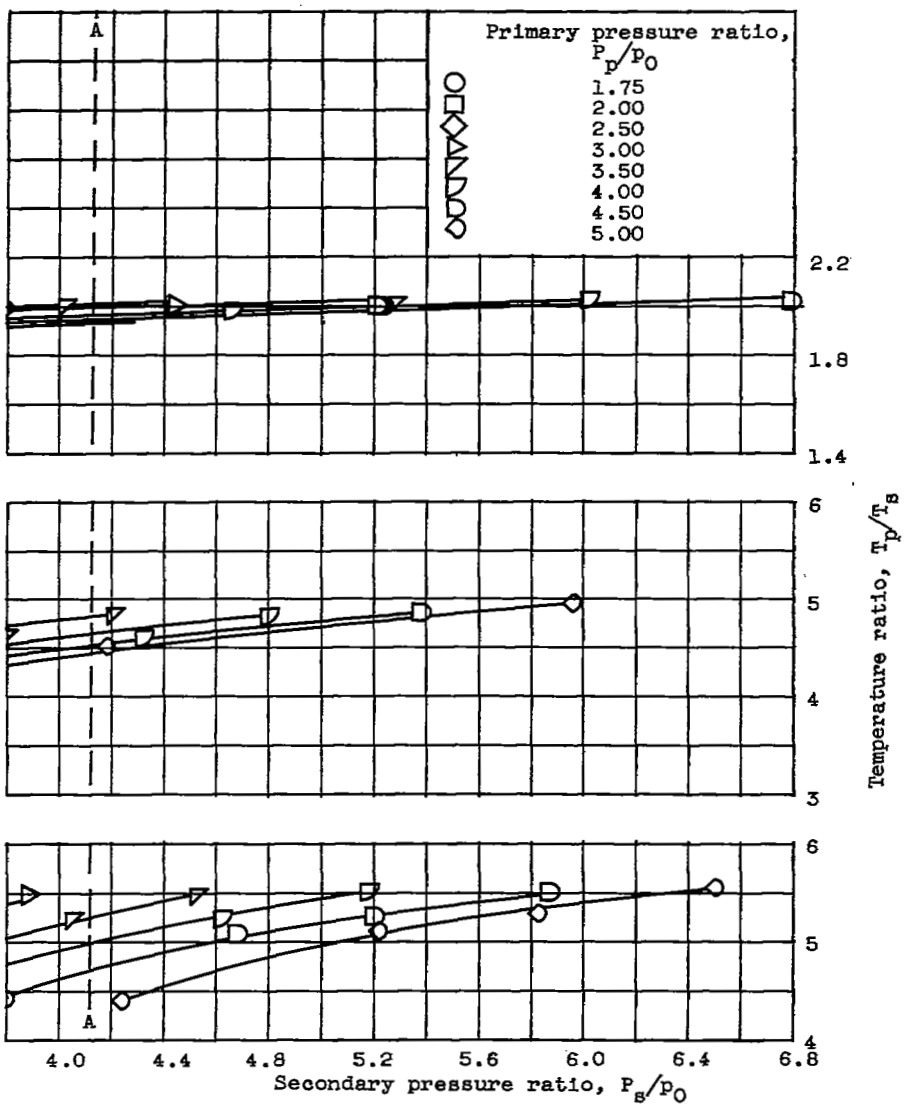
Primary pressure ratio, P_p/p_0
1.75
2.00
2.50
3.00
3.50
4.00
4.50
5.00
A
2.2
1.8
1.4
6
5
4
3
6
5
4
A
4.0
4.4
4.8
5.2
5.6
6.0
6.4
6.8
Secondary pressure ratio, P_s/p_0
Temperature ratio, T_p/T_s

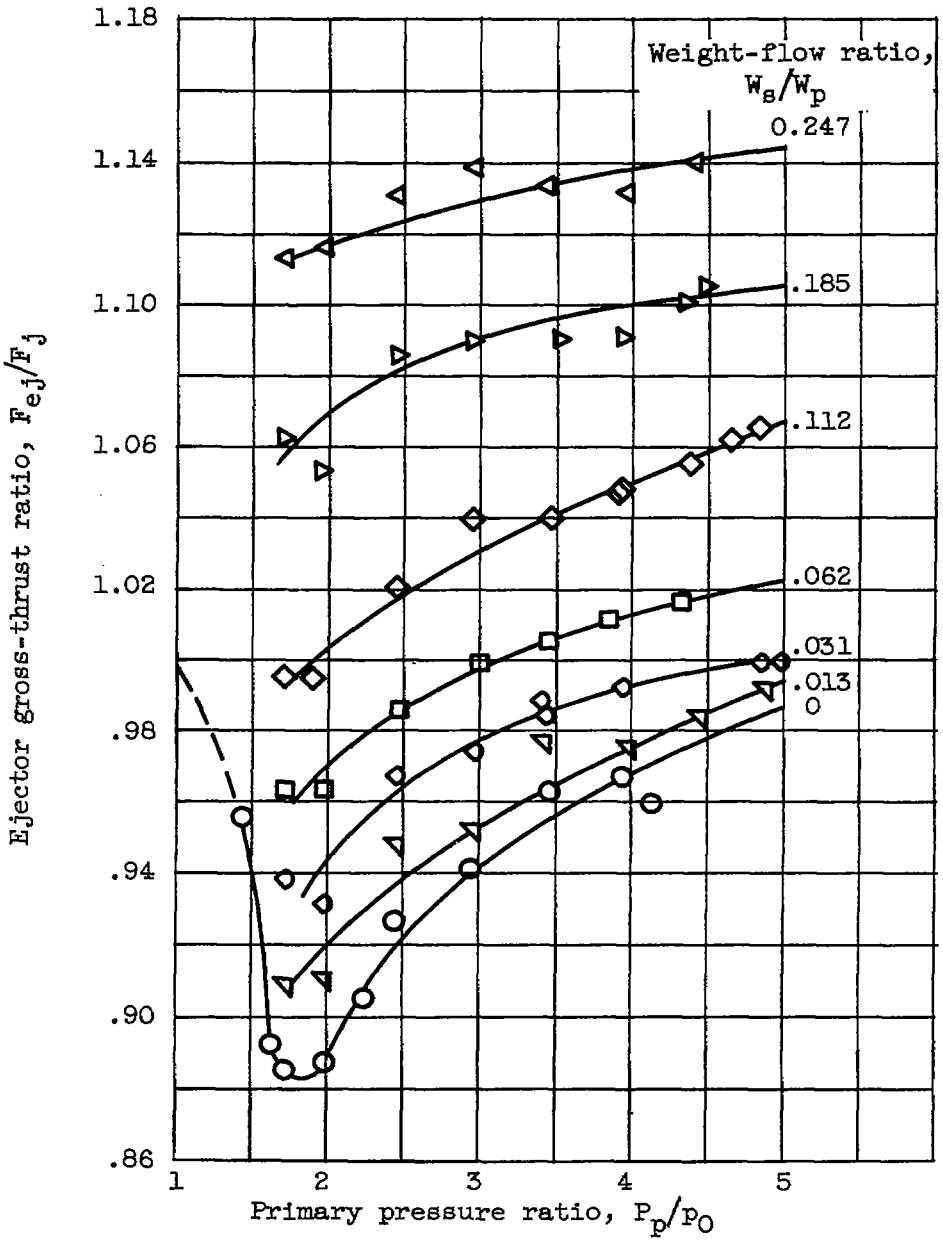

(a) Primary gas temperature, 1120° R.

Figure 28. - Ejector gross-thrust ratio at constant values of weight-flow ratio for configuration D. Diameter ratio, 1.095; spacing ratio, 0.810.

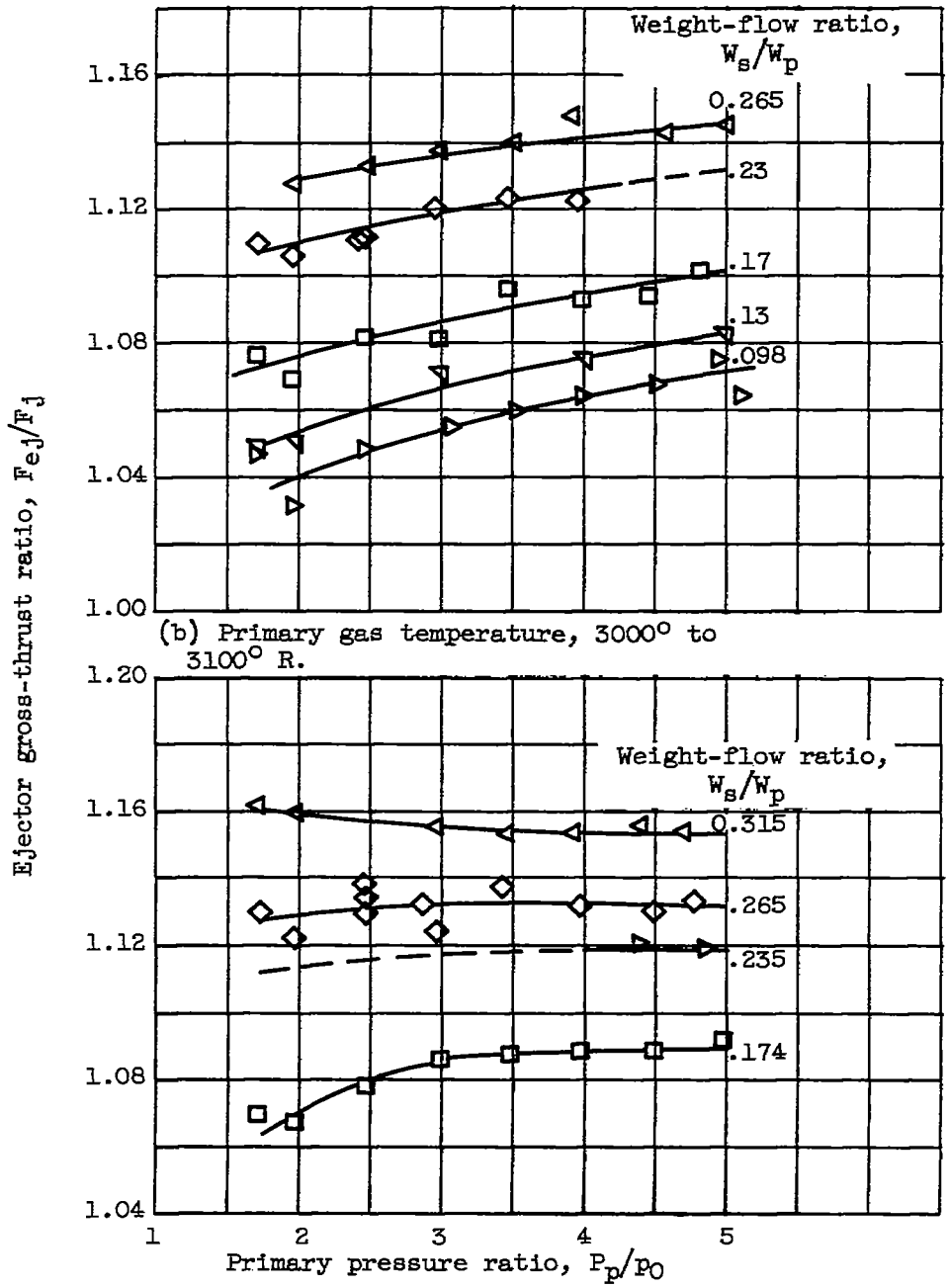

(b) Primary gas temperature, 3000° to 3100° R.

(c) Primary gas temperature, 3600° to 3700° R.

Figure 28. - Concluded. Ejector gross-thrust ratio at constant values of weight-flow ratio for configuration D. Diameter ratio, 1.095; spacing ratio, 0.810.

[redacted]

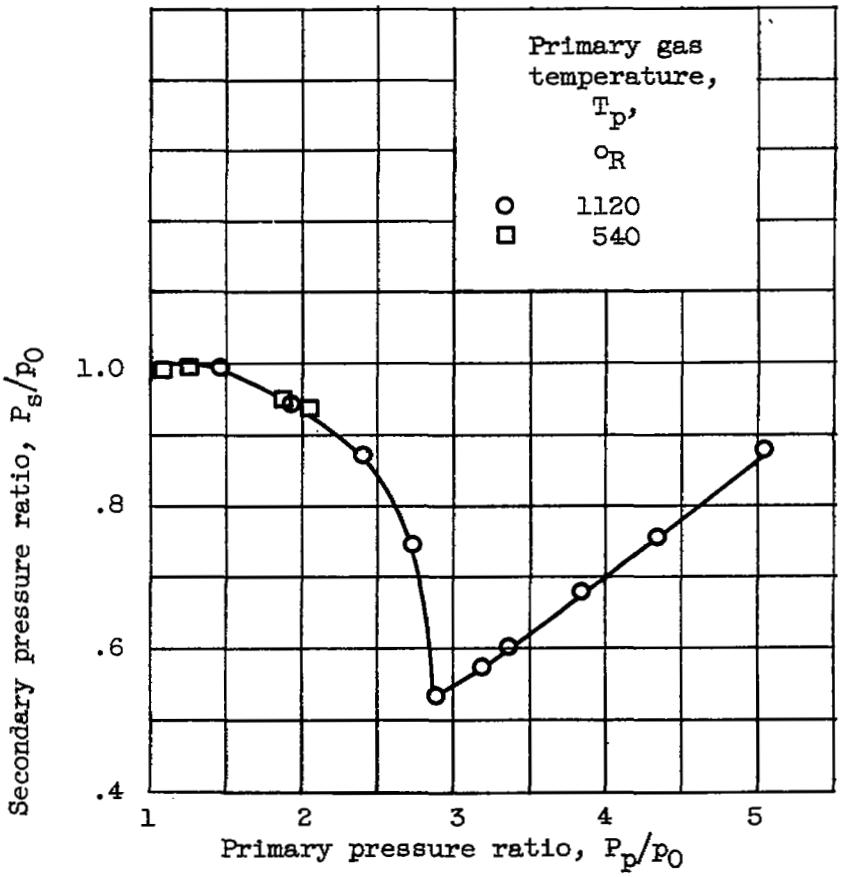

Figure 29. - Ejector pumping characteristics of configuration E at zero secondary flow. Diameter ratio, 1.195; spacing ratio, 0.403.

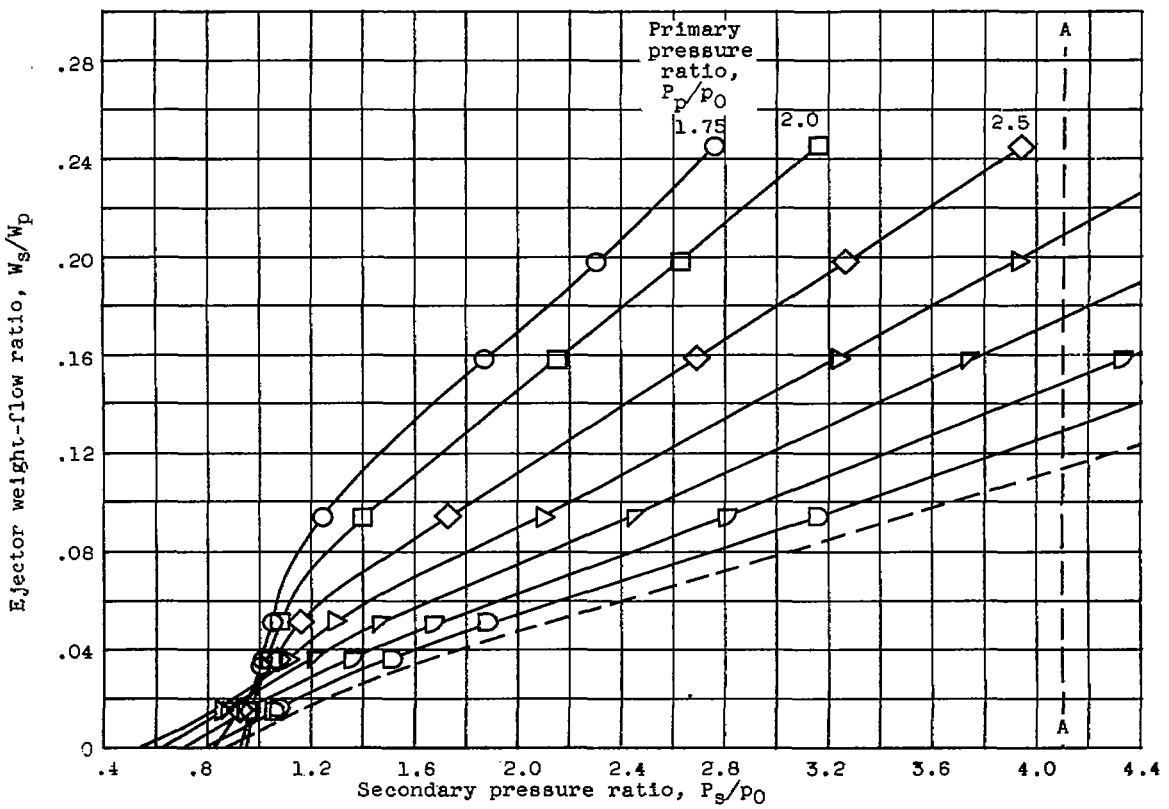

(a) Primary gas temperature, 1120° R.

Figure 30. - Effect of primary and secondary pressure ratio on ejector weight-flow ratio for configuration E. Diameter ratio, 1.195; spacing ratio, 0.403.

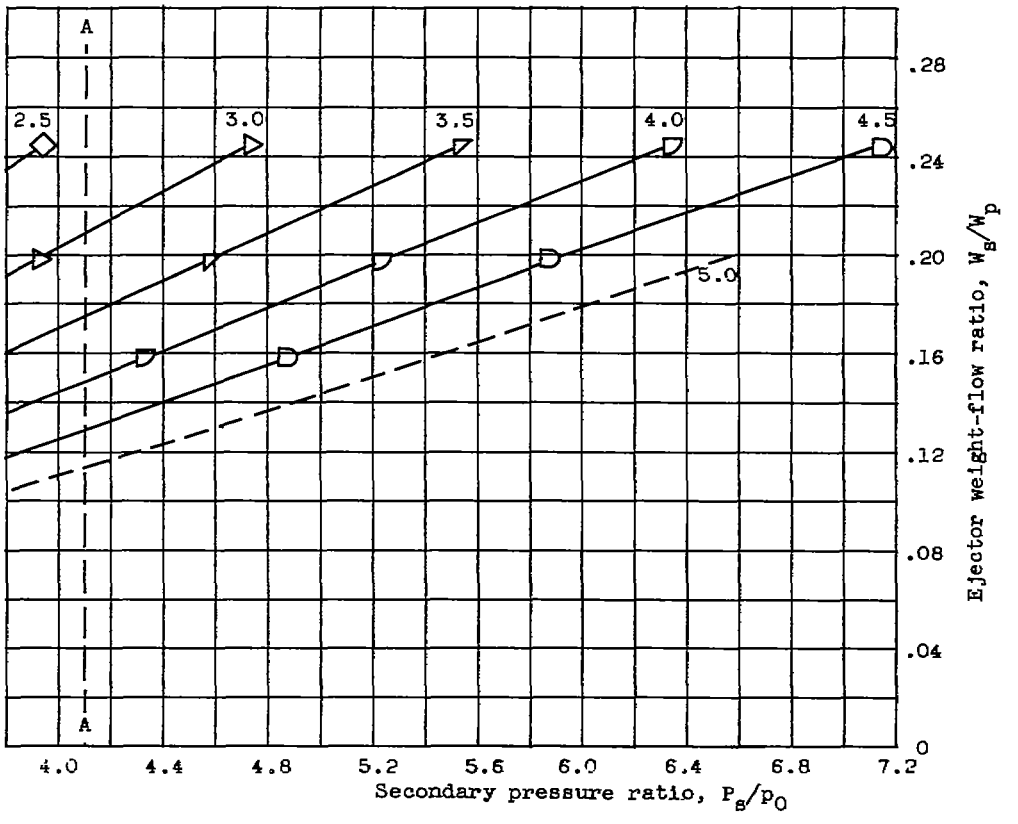

[redacted]

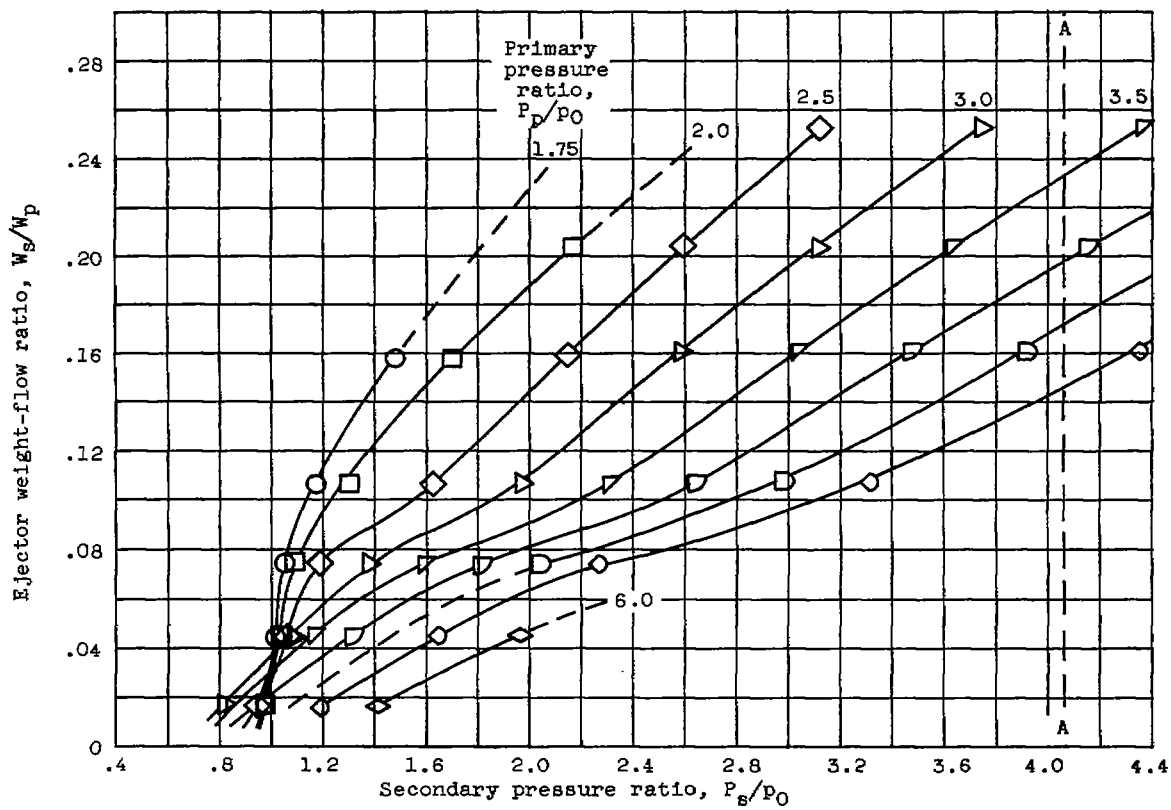

(b) Primary gas temperature, 2100° to 2200° R.

Figure 30. - Continued. Effect of primary and secondary pressure ratio on ejector weight-flow ratio for configuration E. Diameter ratio, 1.195; spacing ratio, 0.403.

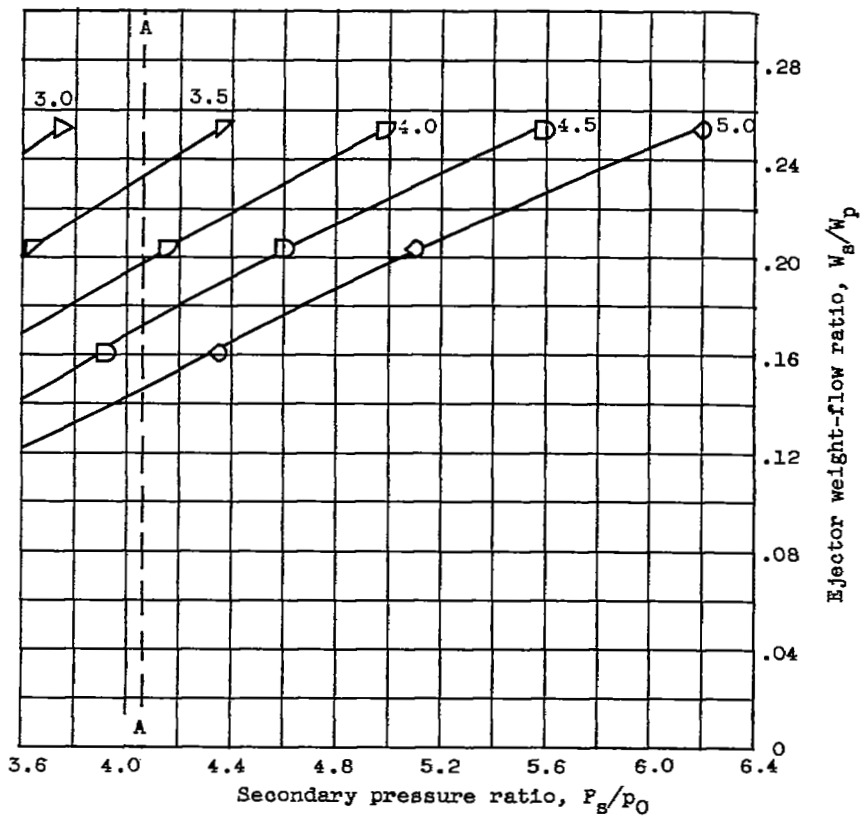
A
3.0
3.5
4.0
4.5
5.0
A
.28
.24
.20
.16
.12
.08
.04
0
3.6
4.0
4.4
4.8
5.2
5.6
6.0
6.4
Secondary pressure ratio, P_s/p_0
Ejector weight-flow ratio, W_s/W_p

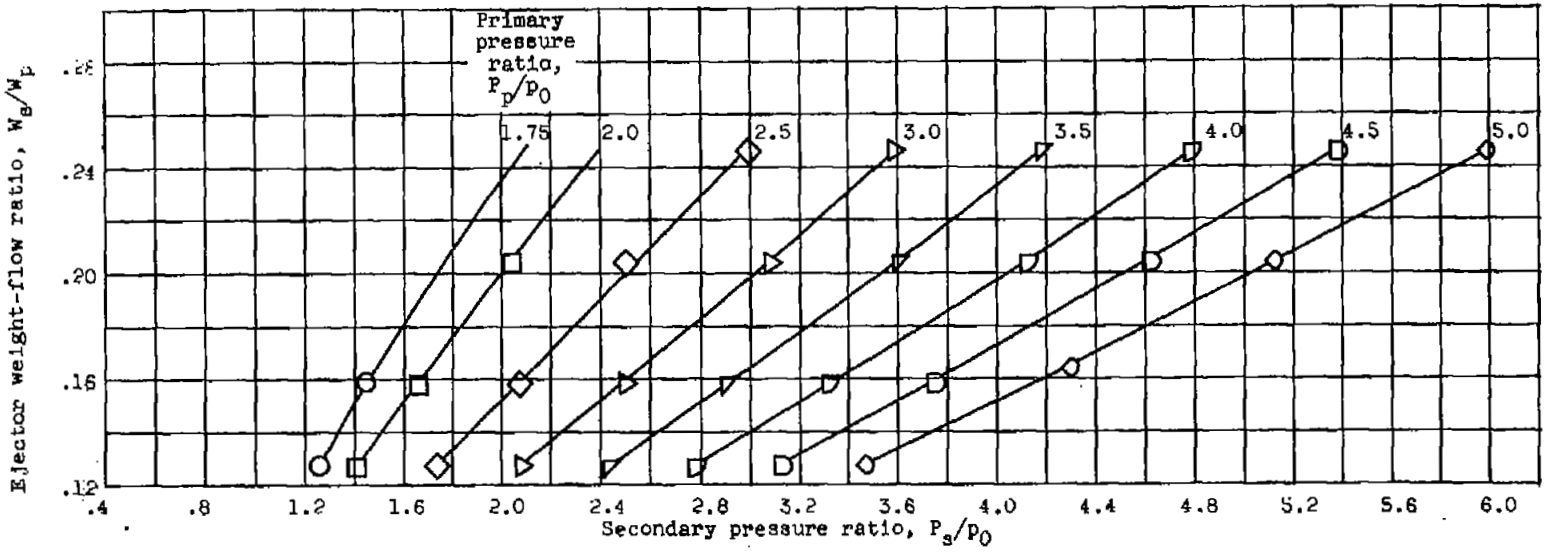

(c) Primary gas temperature, 3050° to 3150° R.

Figure 30. - Concluded. Effect of primary and secondary pressure ratio on ejector weight-flow ratio for configuration E. Diameter ratio, 1.195; spacing ratio, 0.403.

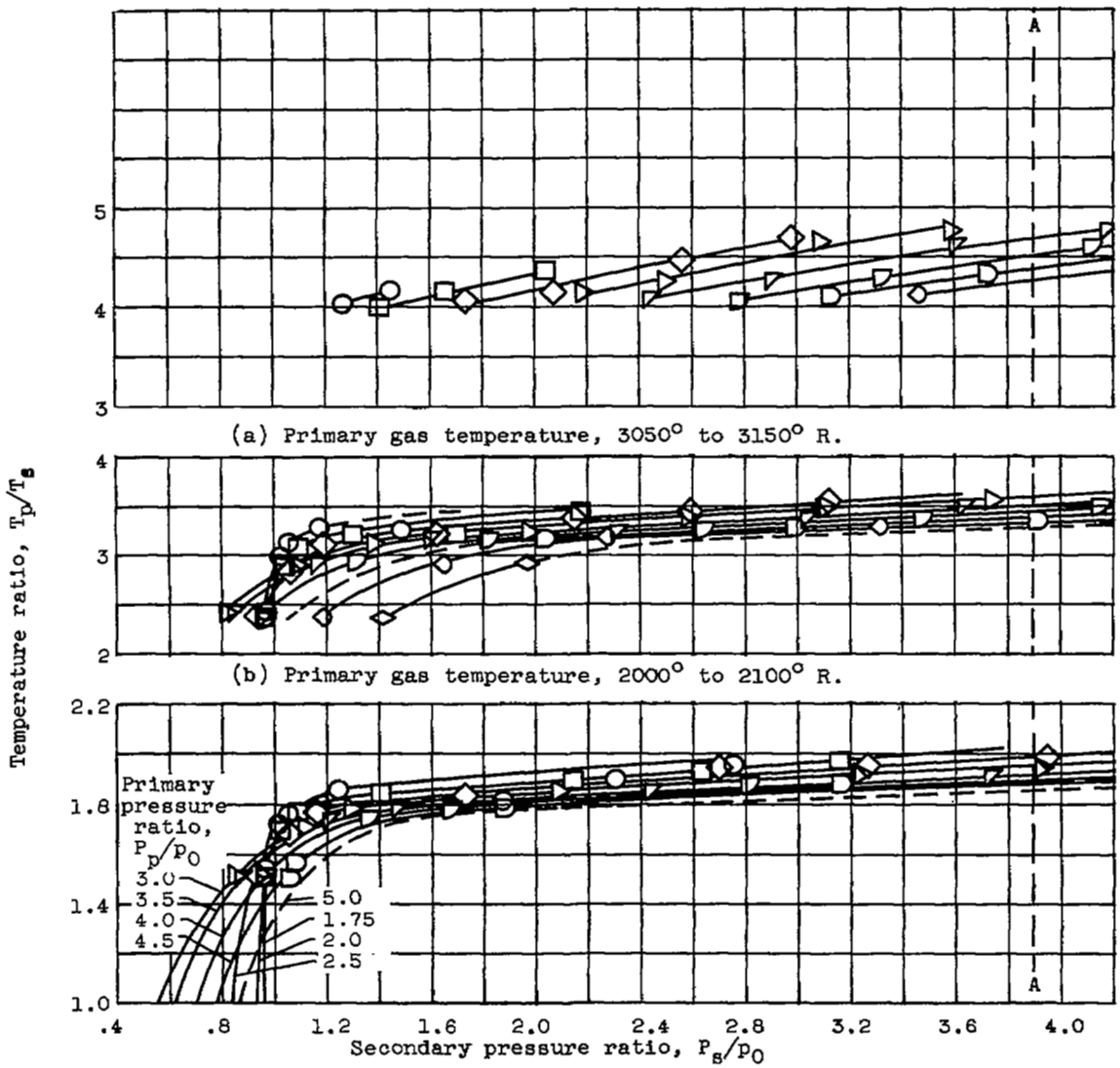

Figure 31. - Ratio of primary gas temperature to secondary air temperature as a function of operating conditions for ejector configuration E. Diameter ratio, 1.195; spacing ratio, 0.403.

[redacted]

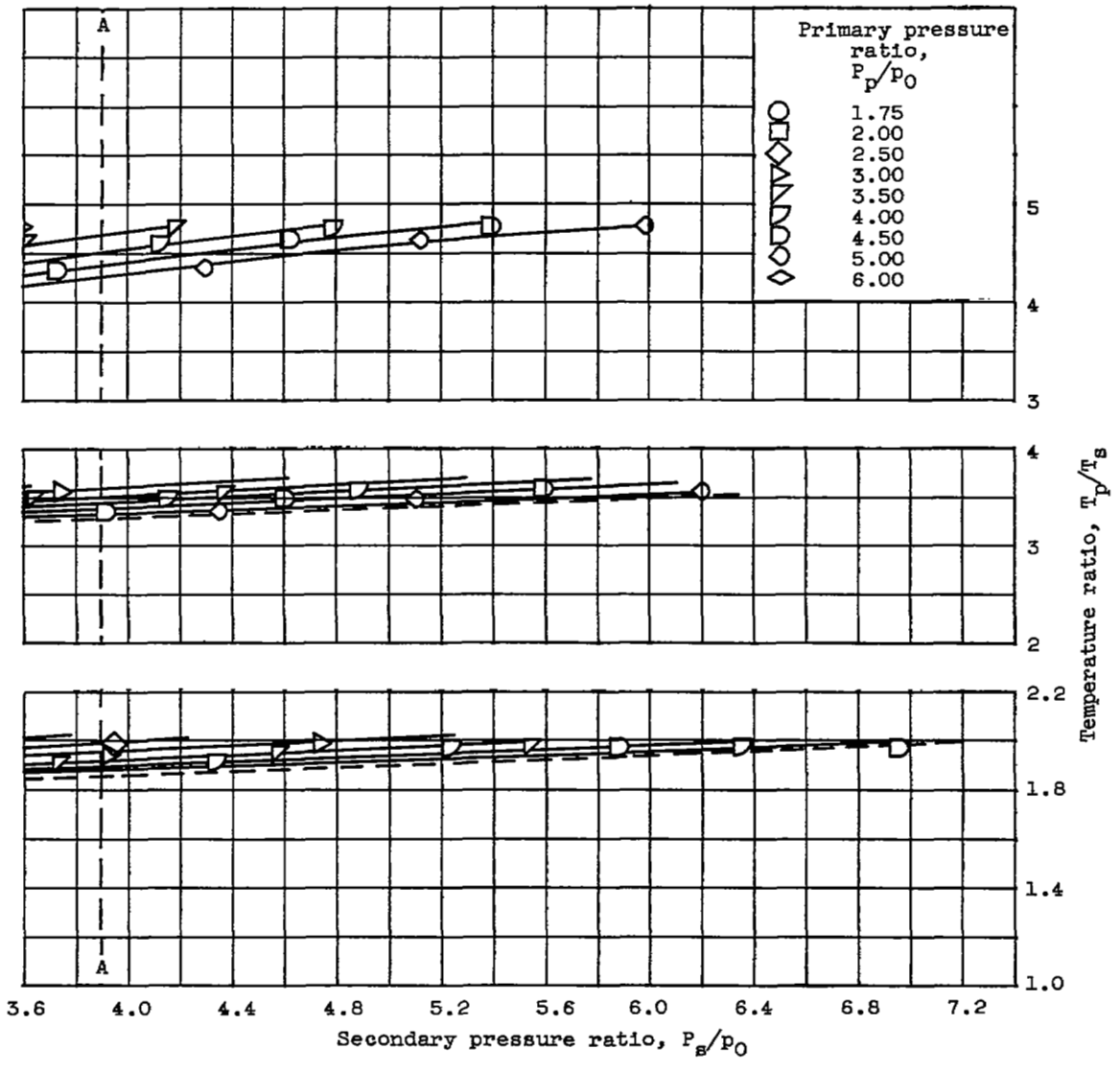
Primary pressure ratio, P_p/p_0
1.75
2.00
2.50
3.00
3.50
4.00
4.50
5.00
6.00
A
A
5
4
3
4
3
2
2.2
1.8
1.4
1.0
Temperature ratio, T_p/T_s
3.6
4.0
4.4
4.8
5.2
5.6
6.0
6.4
6.8
7.2
Secondary pressure ratio, P_s/p_0

CX-12

7a1c

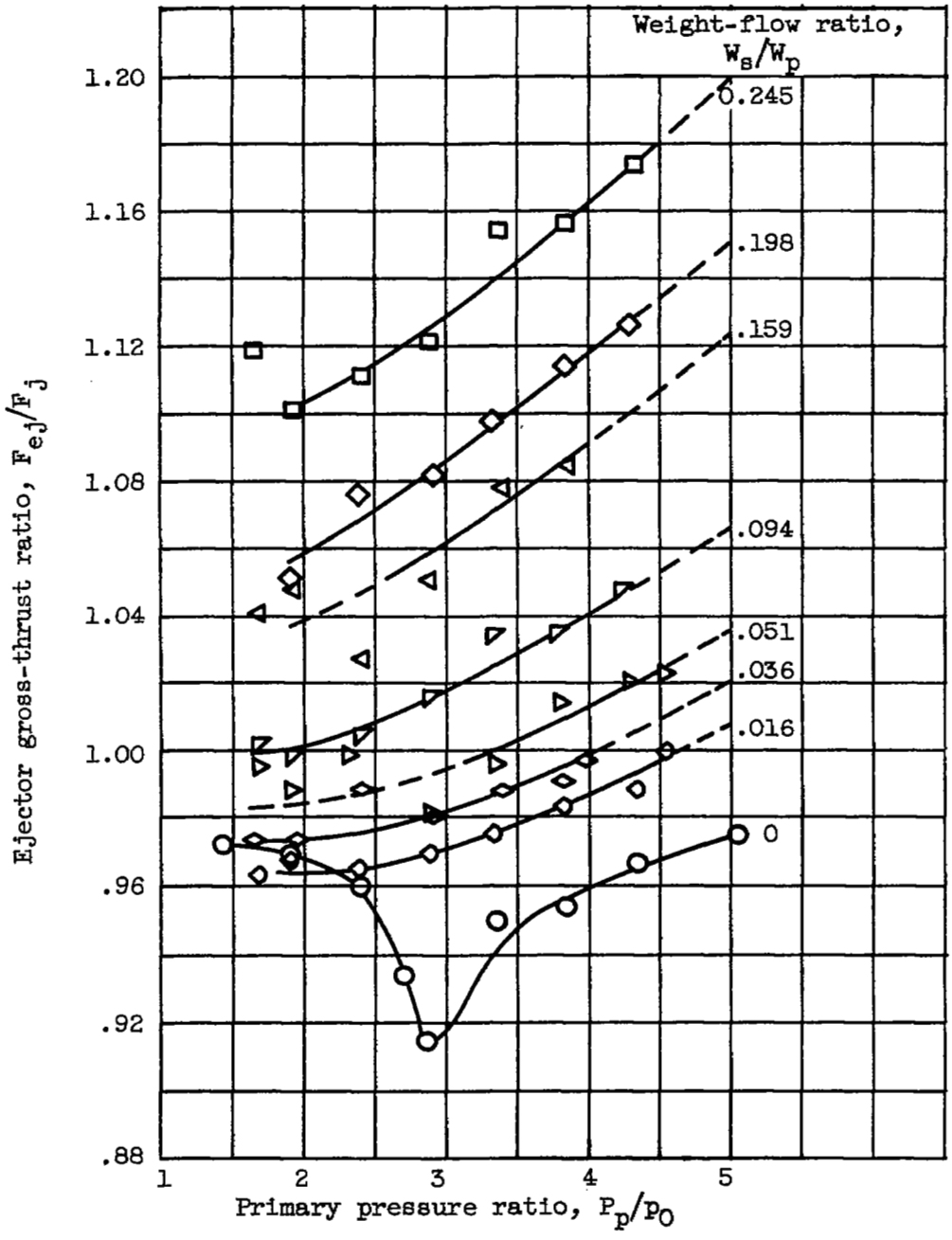

(a) Primary gas temperature, 1120° R.

Figure 32. - Ejector gross-thrust ratio at constant values of weight-flow ratio for configuration E. Diameter ratio, 1.195; spacing ratio, 0.403.

[redacted]

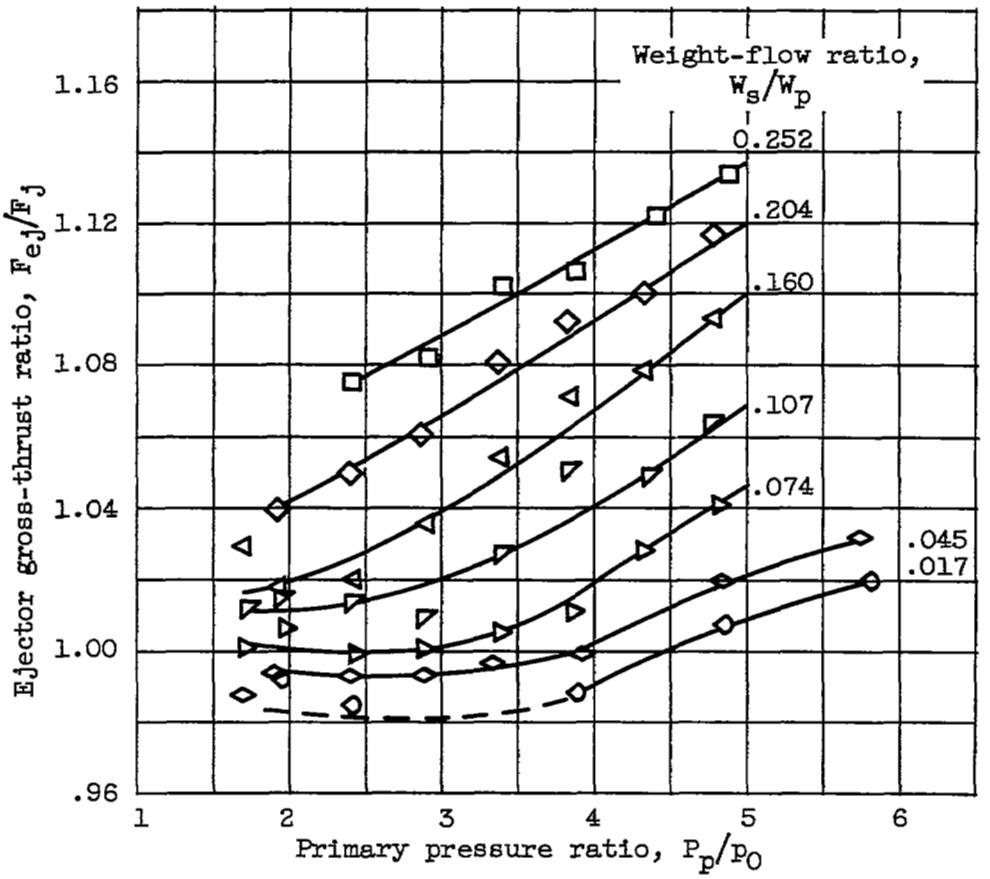

(b) Primary gas temperature, 2100° to 2200° R.

Figure 32. - Continued. Ejector gross-thrust ratio at constant values of weight-flow ratio for configuration E. Diameter ratio, 1.195; spacing ratio, 0.403.

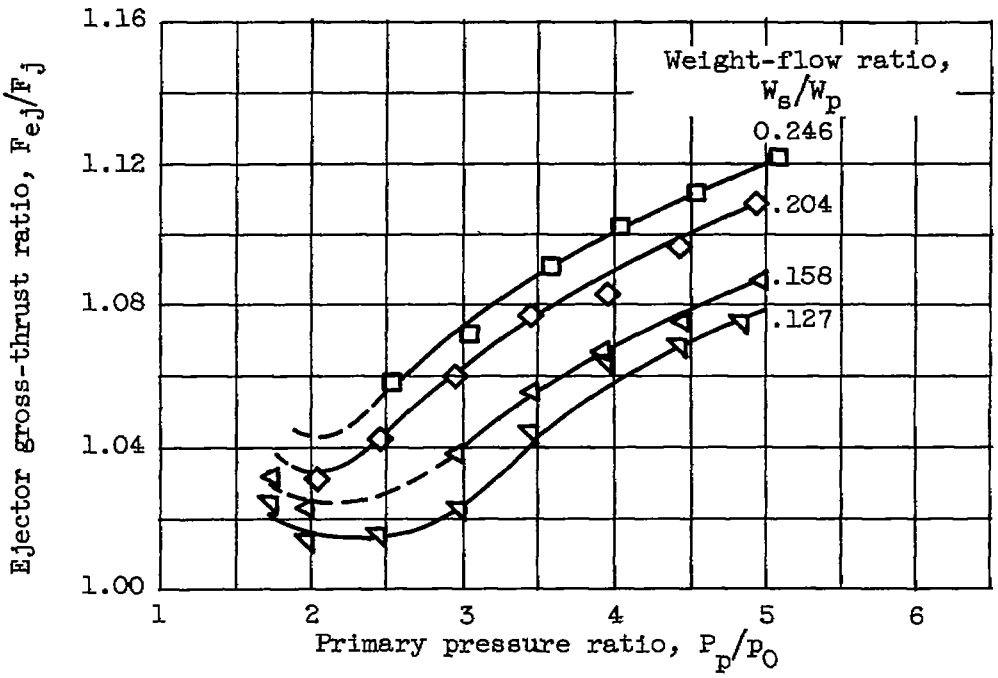

(c) Primary gas temperature, 3050° to 3150° R.

Figure 32. - Concluded. Ejector gross-thrust ratio at constant values of weight-flow ratio for configuration E. Diameter ratio, 1.195; spacing ratio, 0.403.

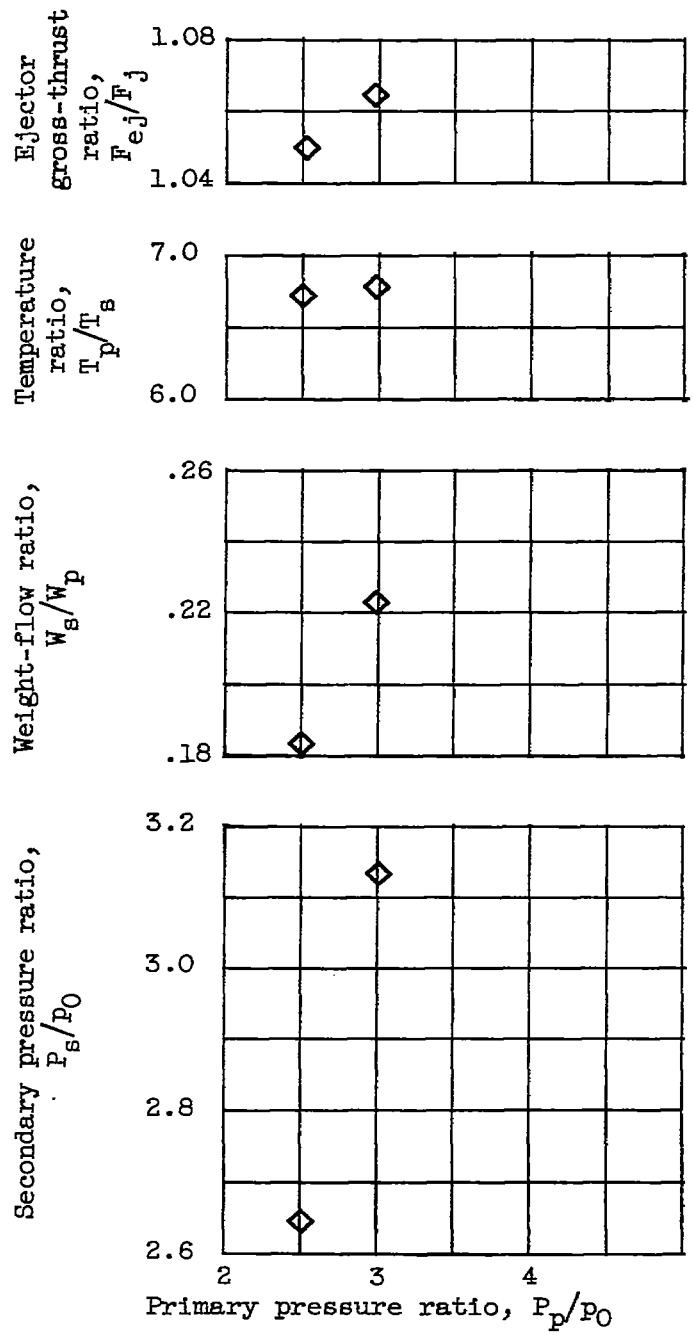

Figure 33. - Limited data for configuration C at a primary gas temperature of 3600° R. Diameter ratio, 1.195; spacing ratio, 0.403.

[redacted]

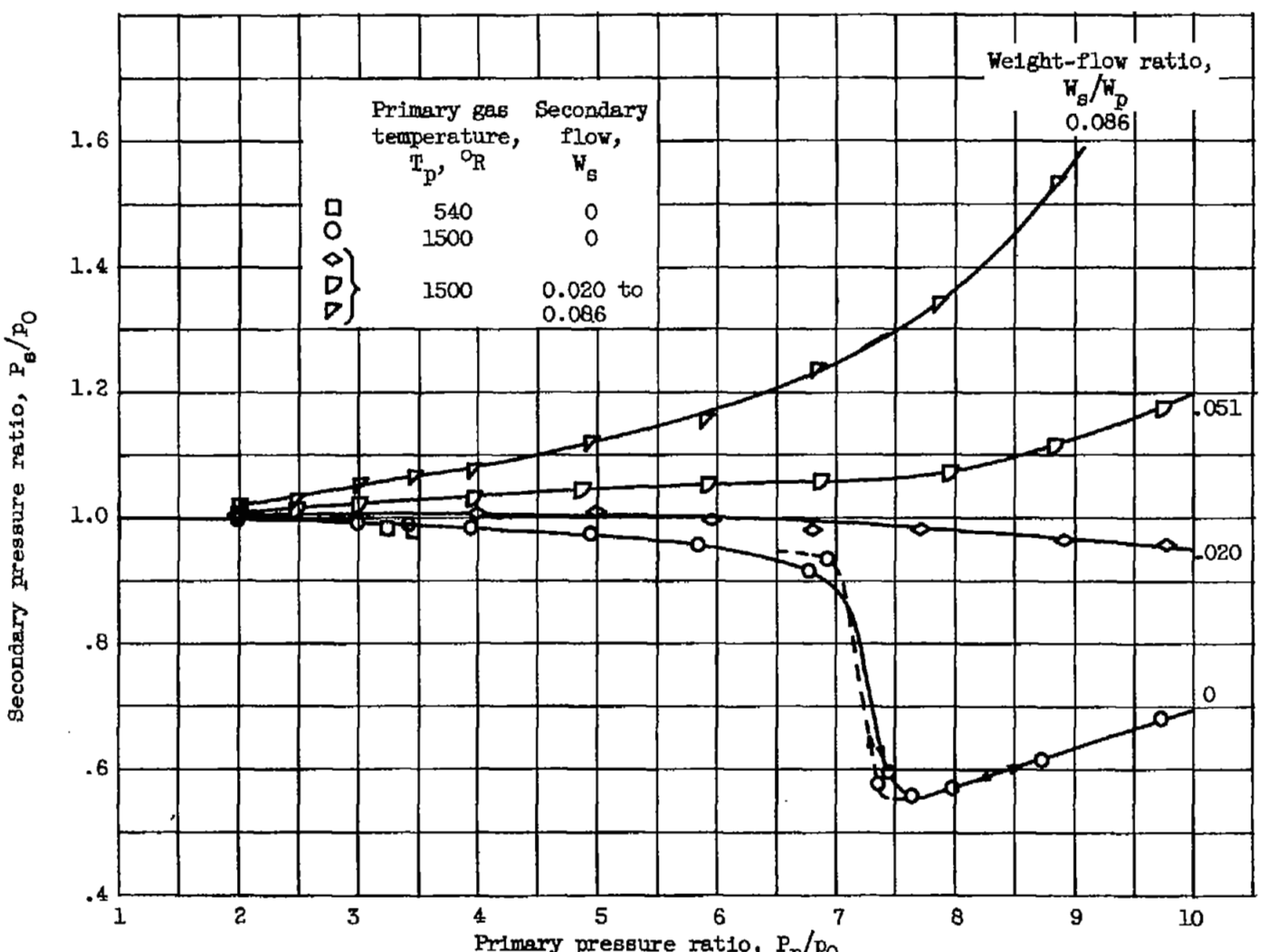

Figure 34. - Ejector pumping characteristics at constant values of weight-flow ratio for configuration F. Diameter ratio, 1.60; spacing ratio, 0.587.

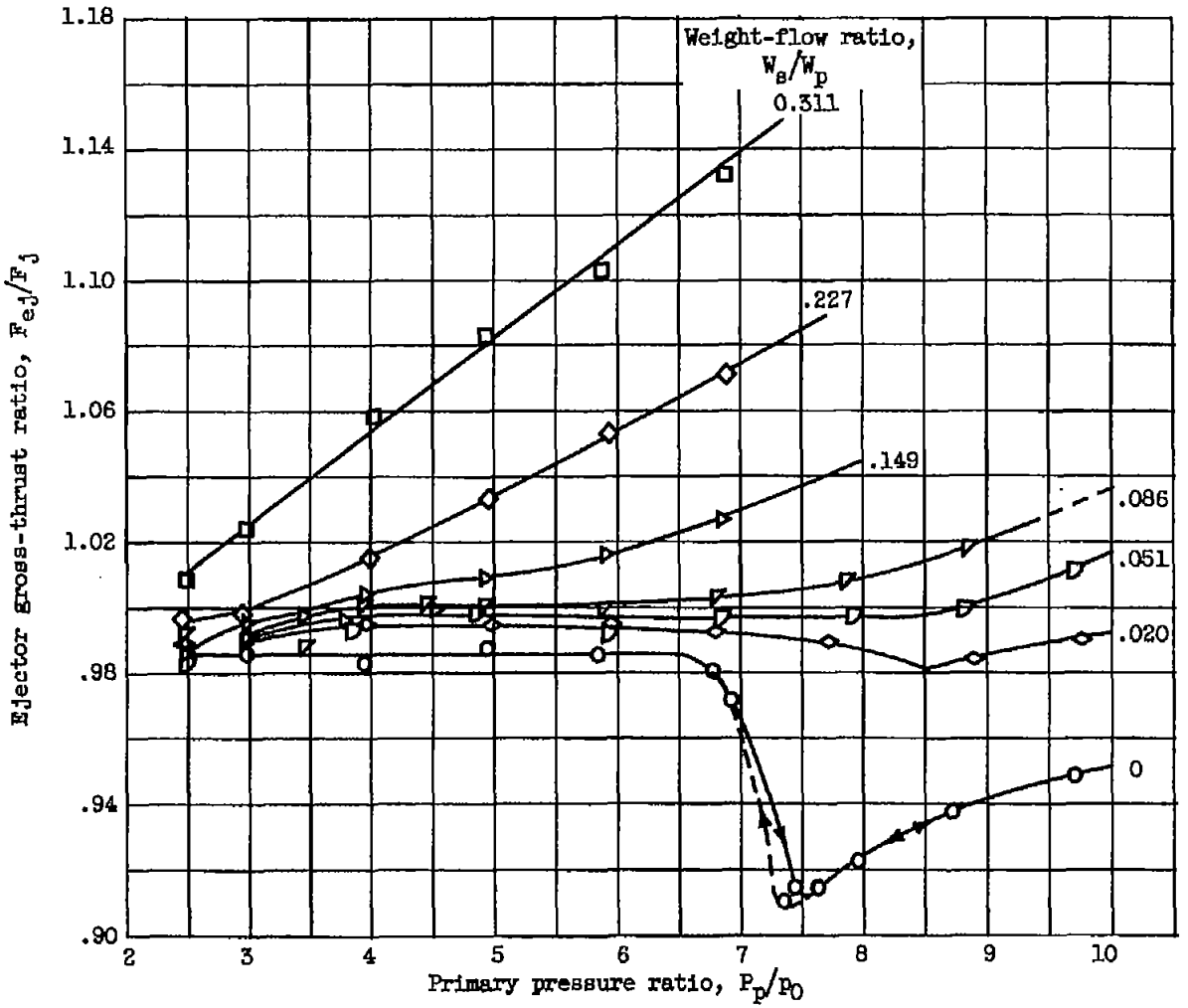

Figure 35. - Ejector gross-thrust ratio at constant values of weight-flow ratio for configuration F. Primary gas temperature, 1500° R. Diameter ratio, 1.60; spacing ratio, 0.587.

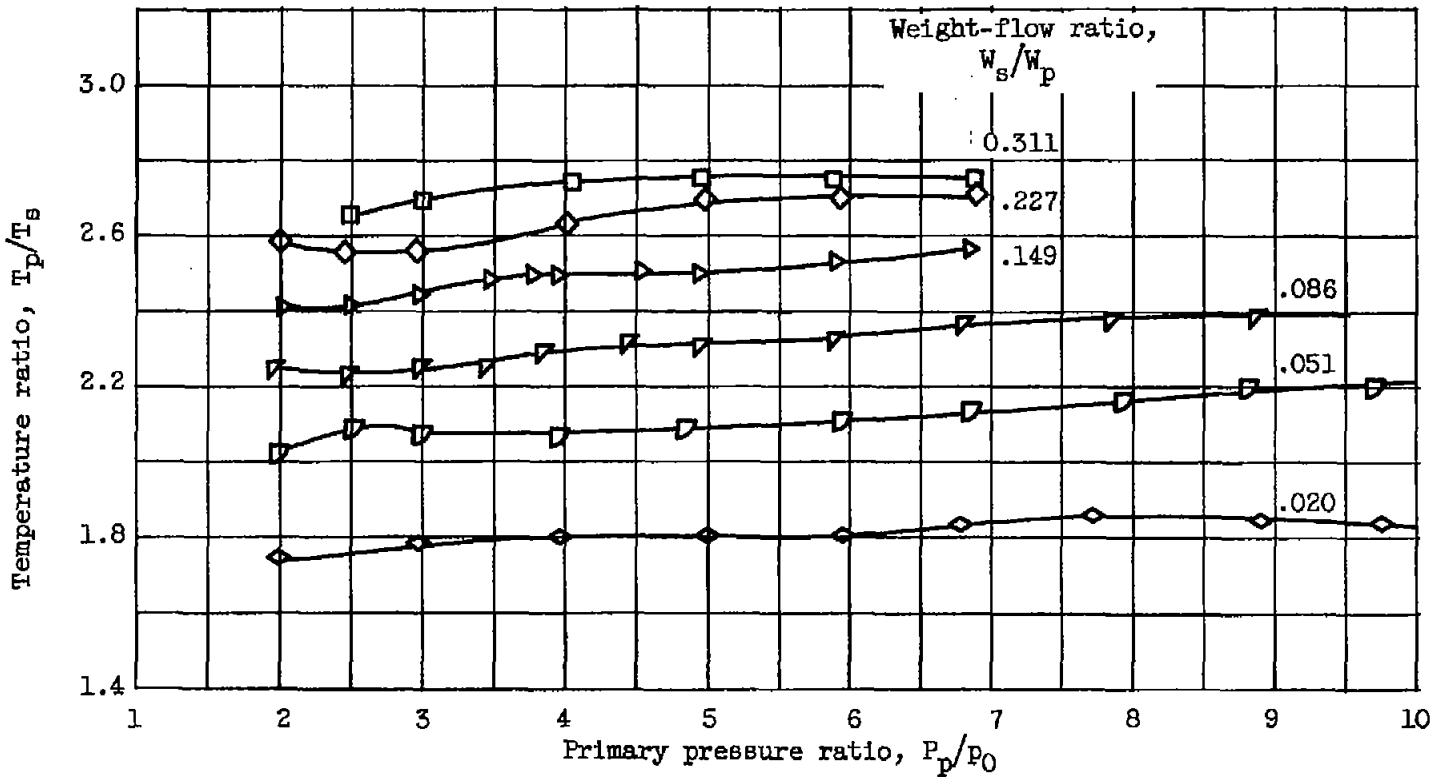

Figure 36. - Ejector temperature ratio at constant values of weight-flow ratio for configuration F. Diameter ratio, 1.60; spacing ratio, 0.587.

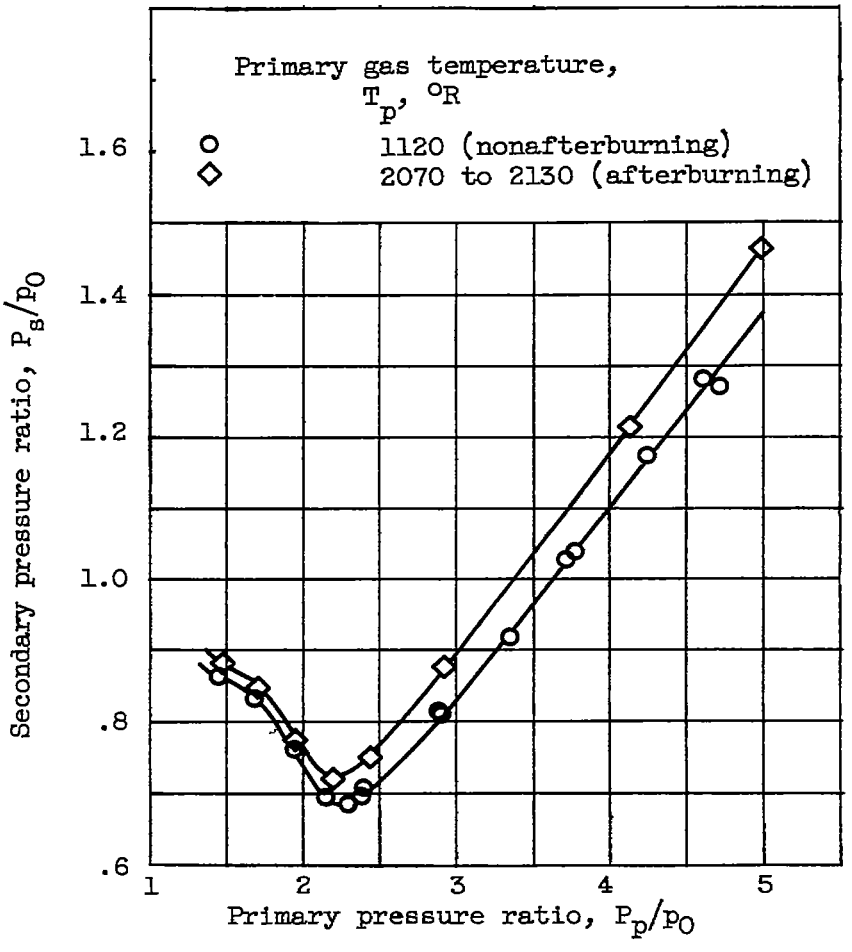

Figure 37. - Ejector pumping characteristics of configuration G at zero secondary flow. Diameter ratio, 1.10; spacing ratio, 0.408.

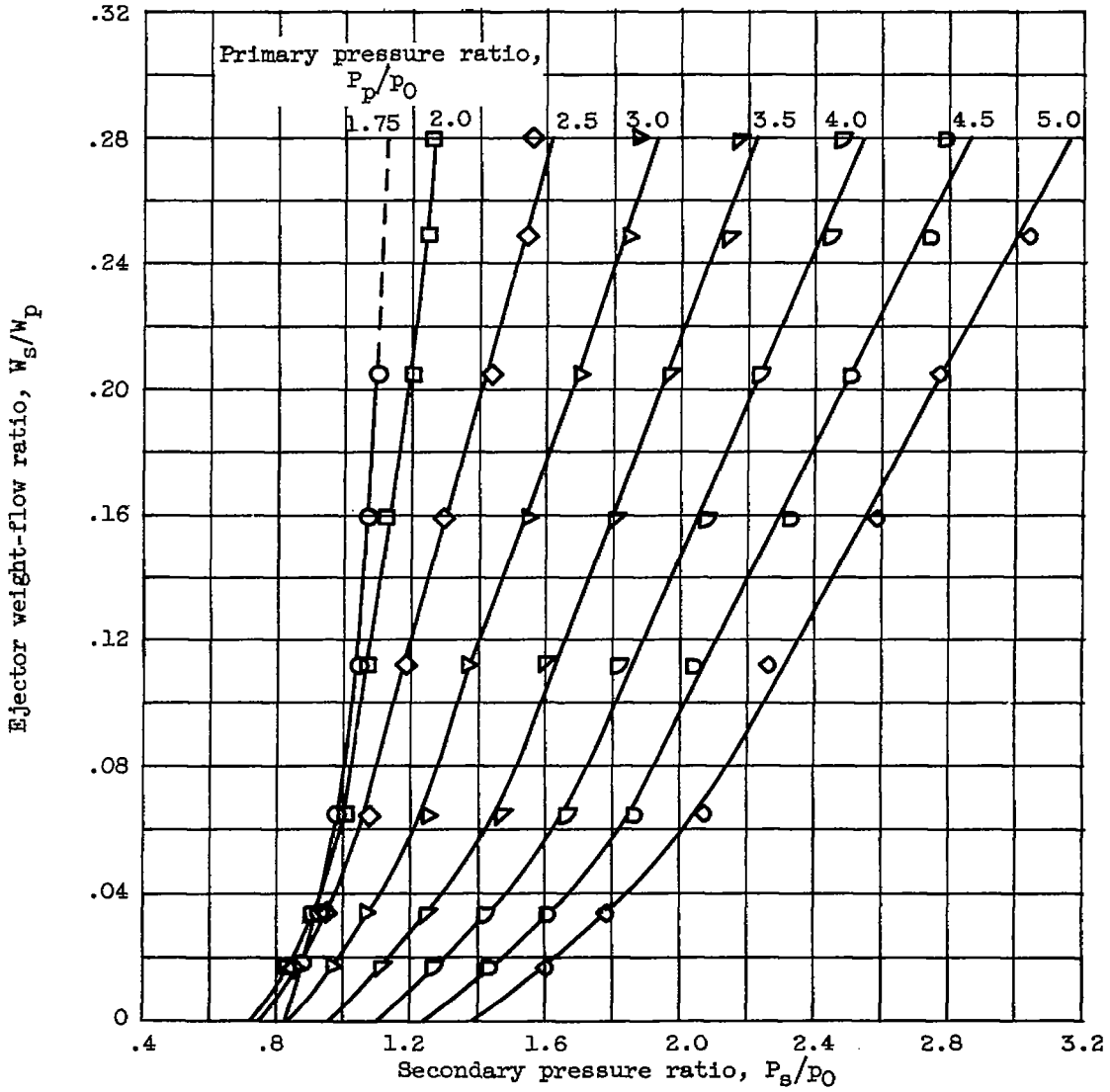

(a) Primary gas temperature, 1120° R.

Figure 38. - Effect of primary and secondary pressure ratio on ejector weight-flow ratio for configuration G. Diameter ratio, 1.10; spacing ratio, 0.408.

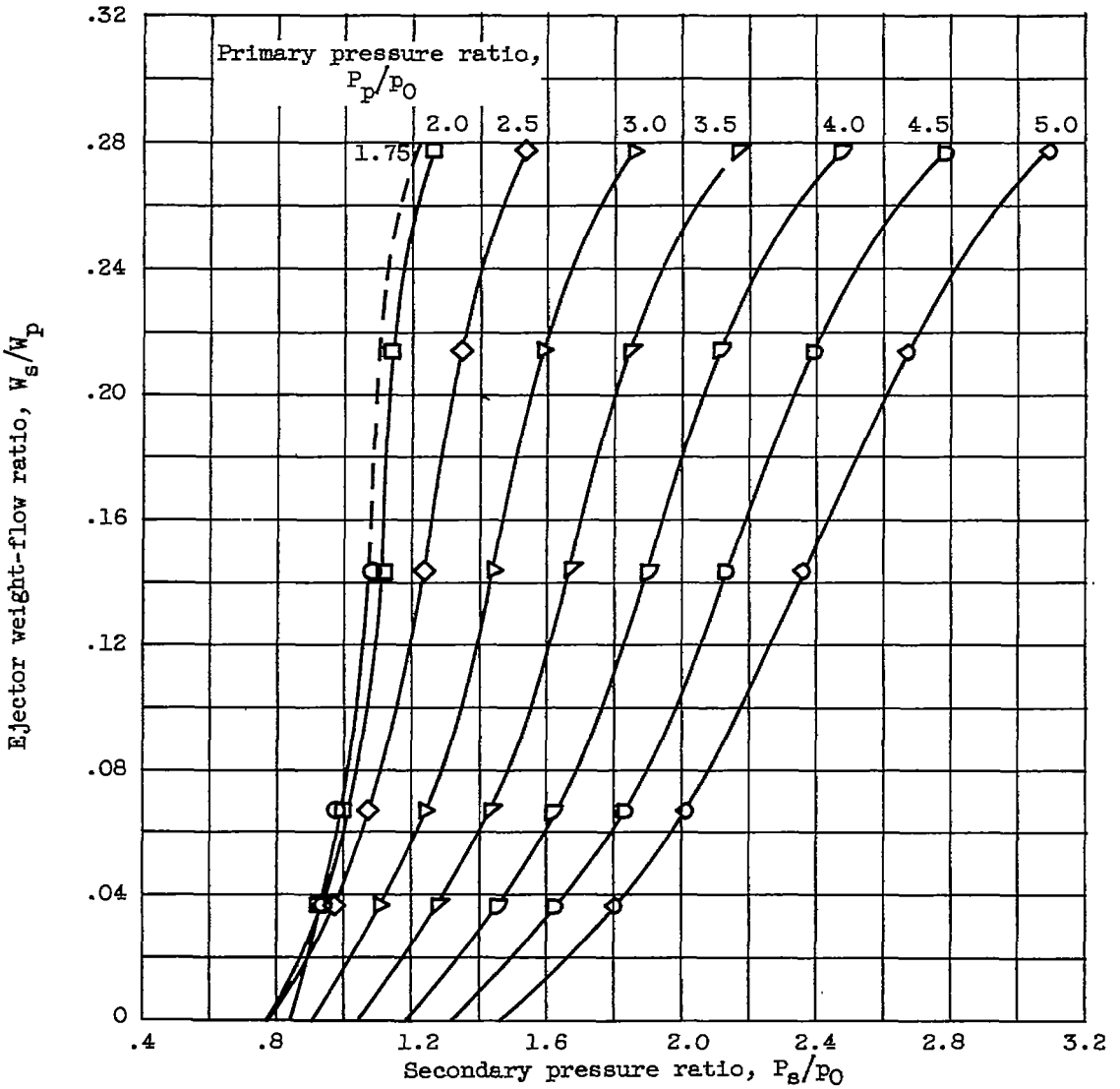

(b) Primary gas temperature, 2200° R.

Figure 38. - Continued. Effect of primary and secondary pressure ratio on ejector weight-flow ratio for configuration G. Diameter ratio, 1.10; spacing ratio, 0.408.

[redacted]

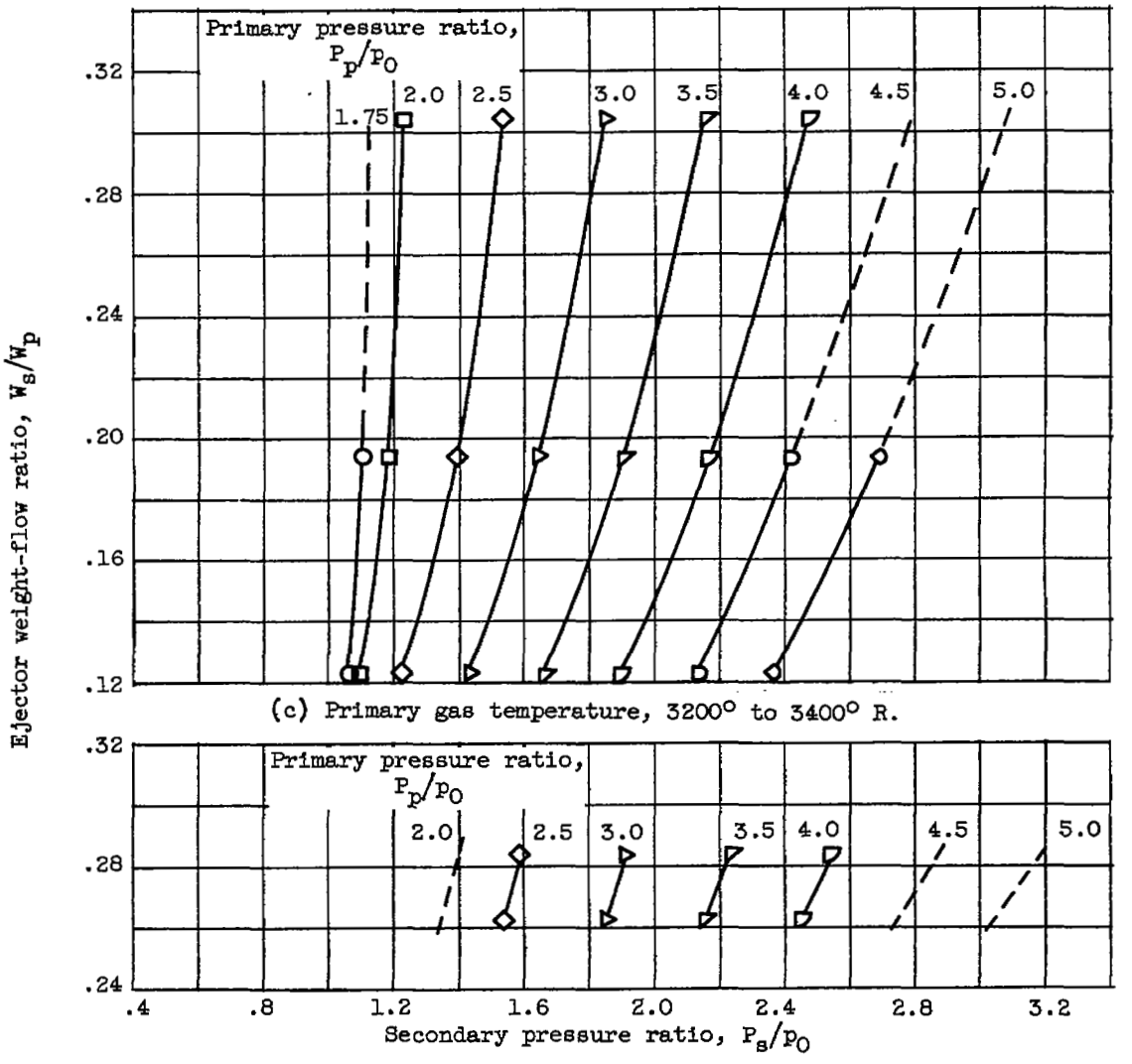

(c) Primary gas temperature, 3200° to 3400° R.

(d) Primary gas temperature, 3750° R.

Figure 38. - Concluded. Effect of primary and secondary pressure ratio on ejector weight-flow ratio for configuration G. Diameter ratio, 1.10; spacing ratio, 0.408.

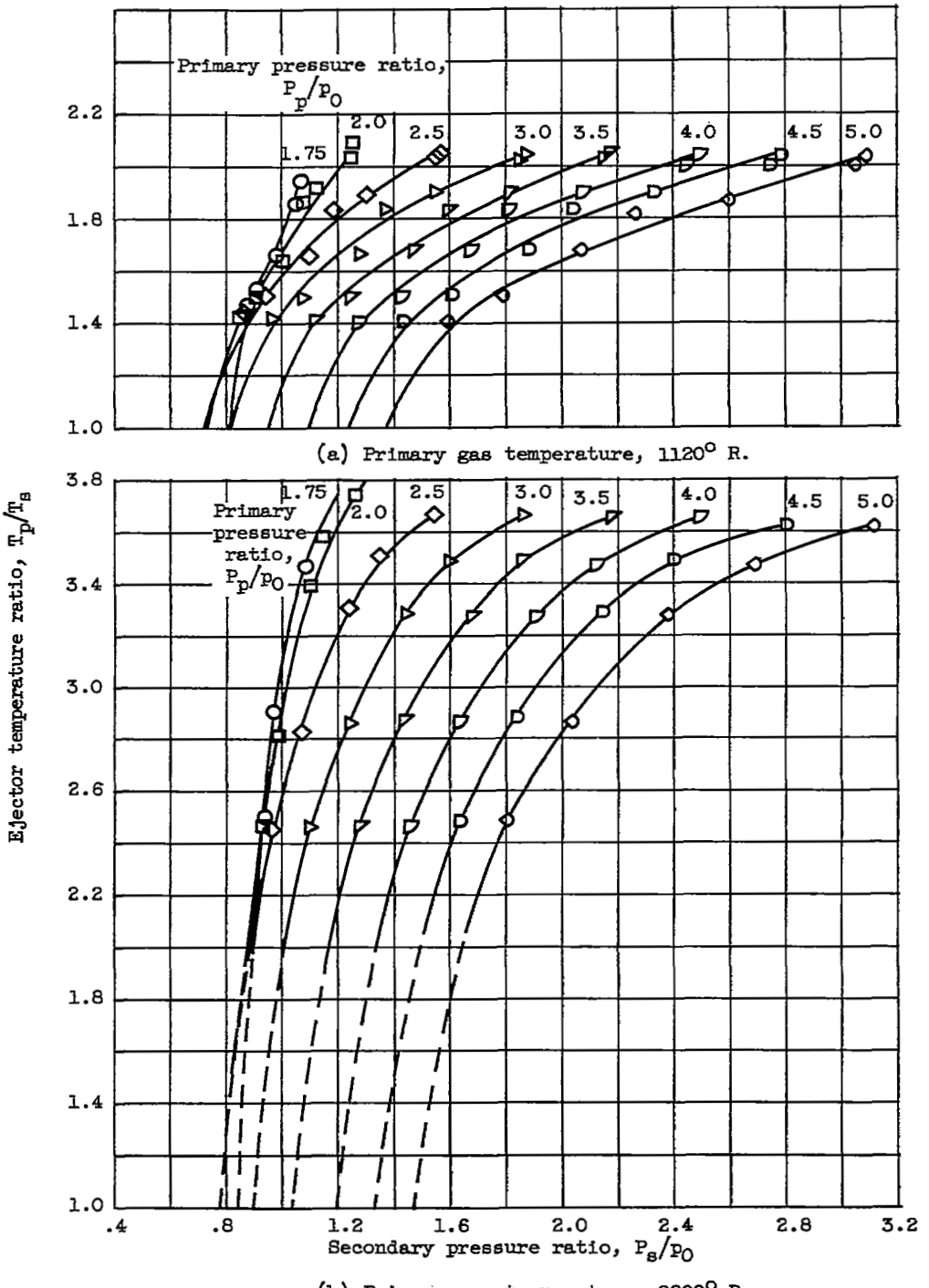

(a) Primary gas temperature, 1120° R.

(b) Primary gas temperature, 2200° R.

Figure 39. - Ratio of primary gas temperature to secondary air temperature as a function of operating conditions for ejector configuration G. Diameter ratio, 1.10; spacing ratio, 0.408.

[redacted]

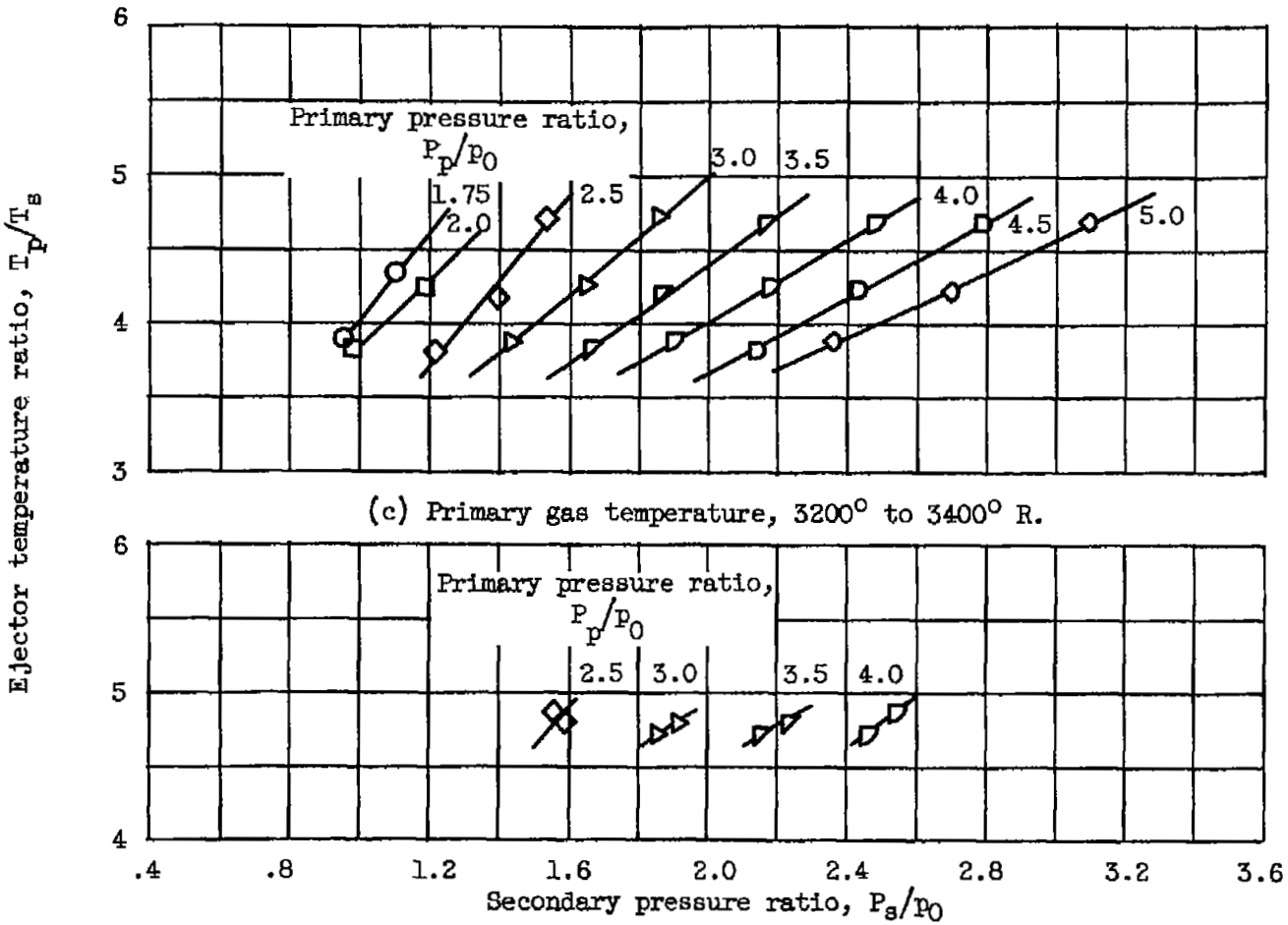

(c) Primary gas temperature, 3200° to 3400° R.

(d) Primary gas temperature, 3750° R.

Figure 39. - Concluded. Ratio of primary gas temperature to secondary air temperature as a function of operating conditions for ejector configuration G. Diameter ratio, 1.10; spacing ratio, 0.408.

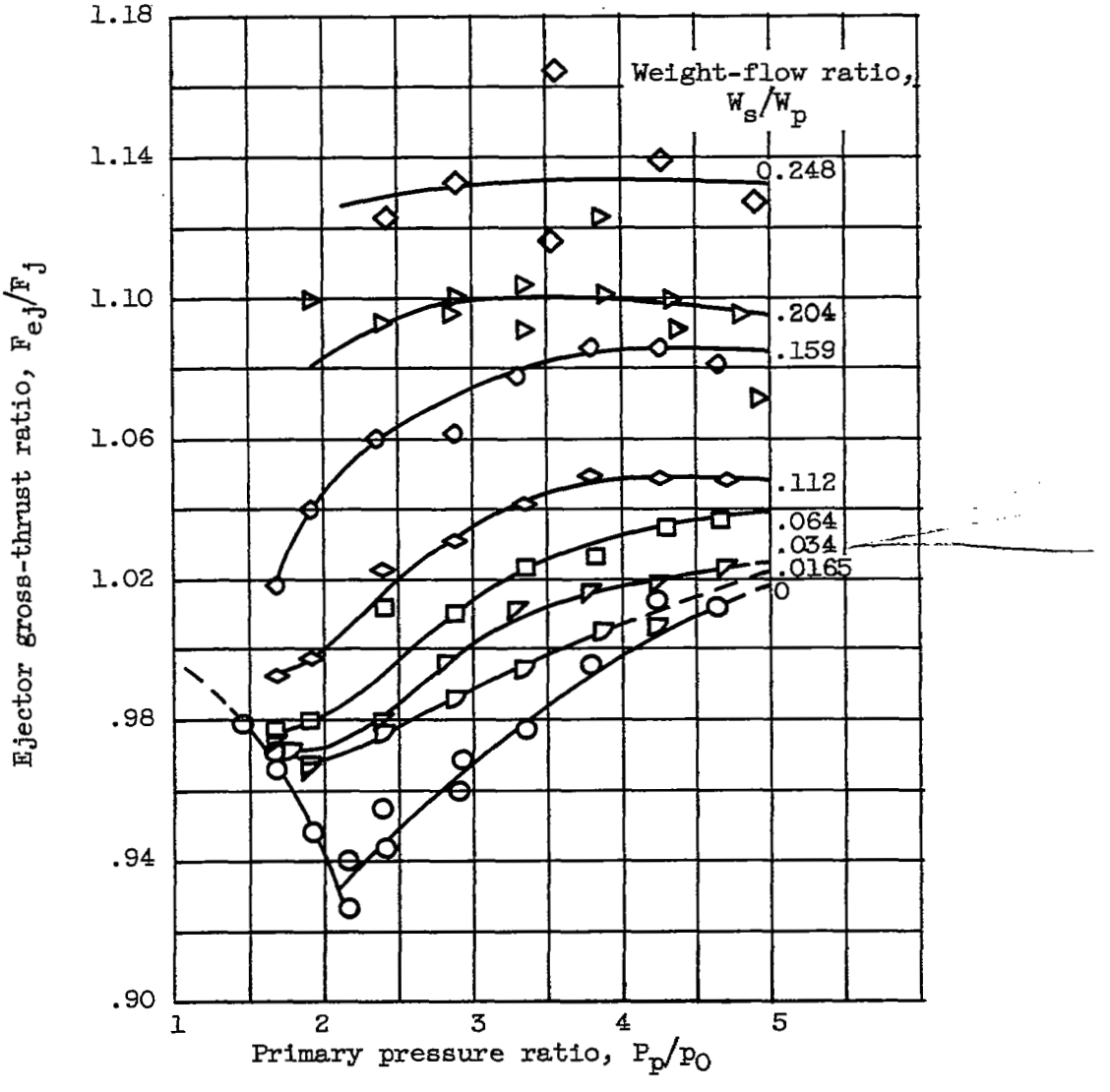

(a) Primary gas temperature, 1120° R.

Figure 40. - Ejector gross-thrust ratio at constant values of weight-flow ratio for configuration G. Diameter ratio, 1.10; spacing ratio, 0.408.

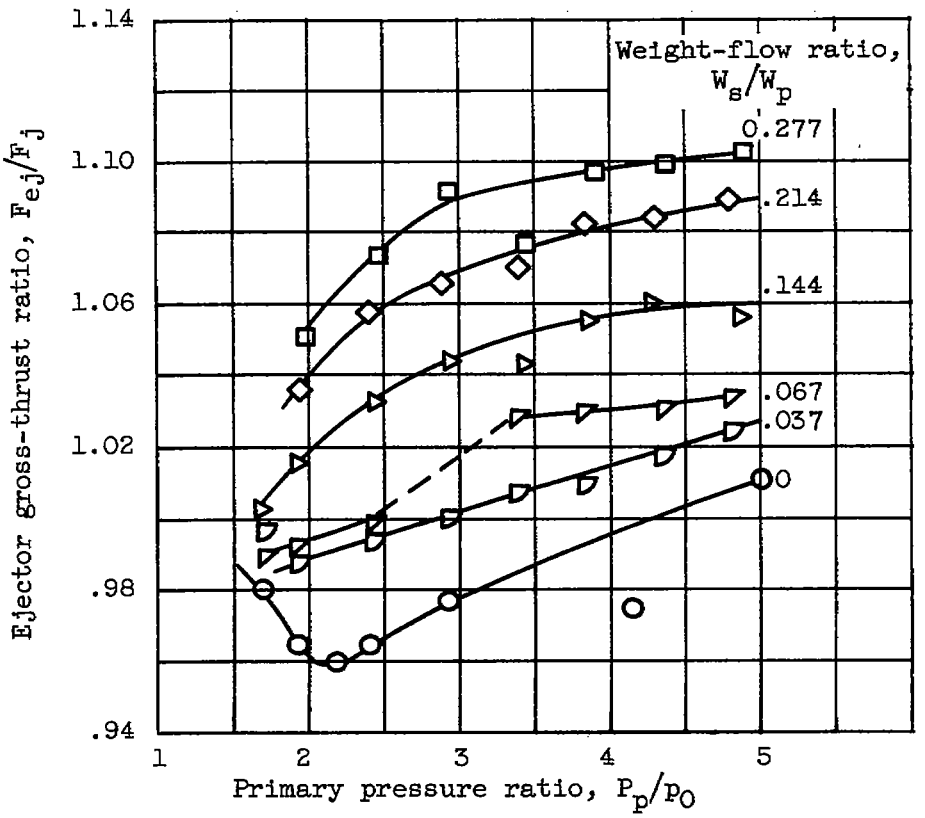

(b) Primary gas temperature, 2200° R.

Figure 40. - Continued. Ejector gross-thrust ratio at constant values of weight-flow ratio for configuration G. Diameter ratio, 1.10; spacing ratio, 0.408.

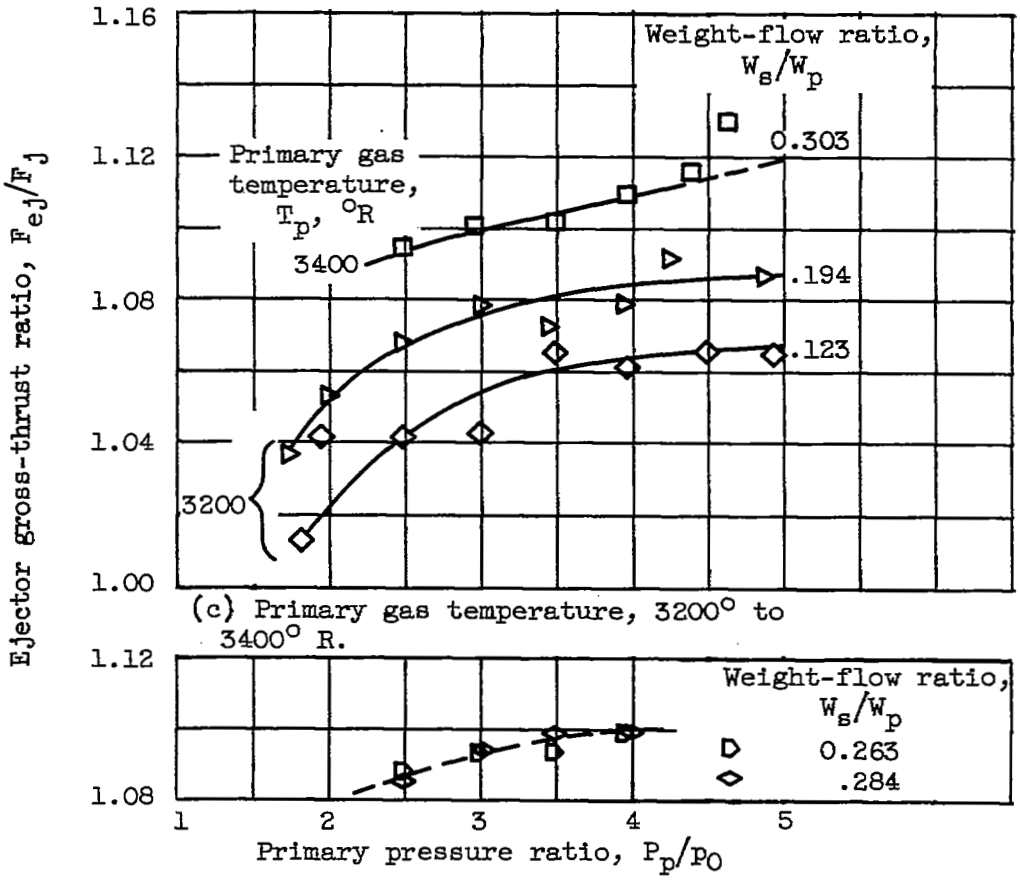

(c) Primary gas temperature, 3200° to 3400° R.

(d) Primary gas temperature, 3750° R.

Figure 40. - Concluded. Ejector gross-thrust ratio at constant values of weight-flow ratio for configuration G. Diameter ratio, 1.10; spacing ratio, 0.408.

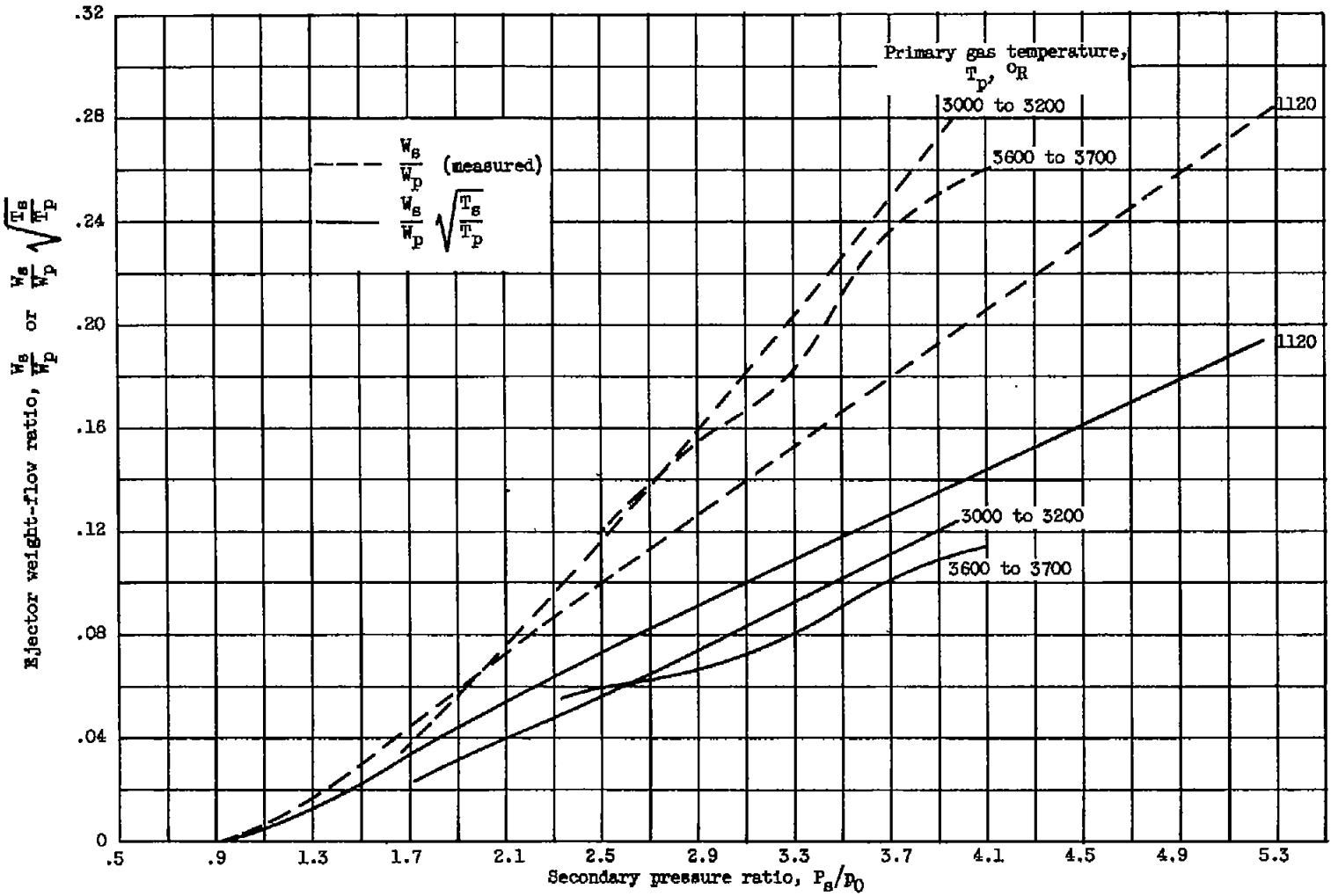

(a) Constant primary pressure ratio, 3.5.

Figure 41. - Comparison of measured and corrected weight-flow ratio over range of primary and secondary pressure ratio for configuration A. Diameter ratio, 1.048; spacing ratio, 0.445.

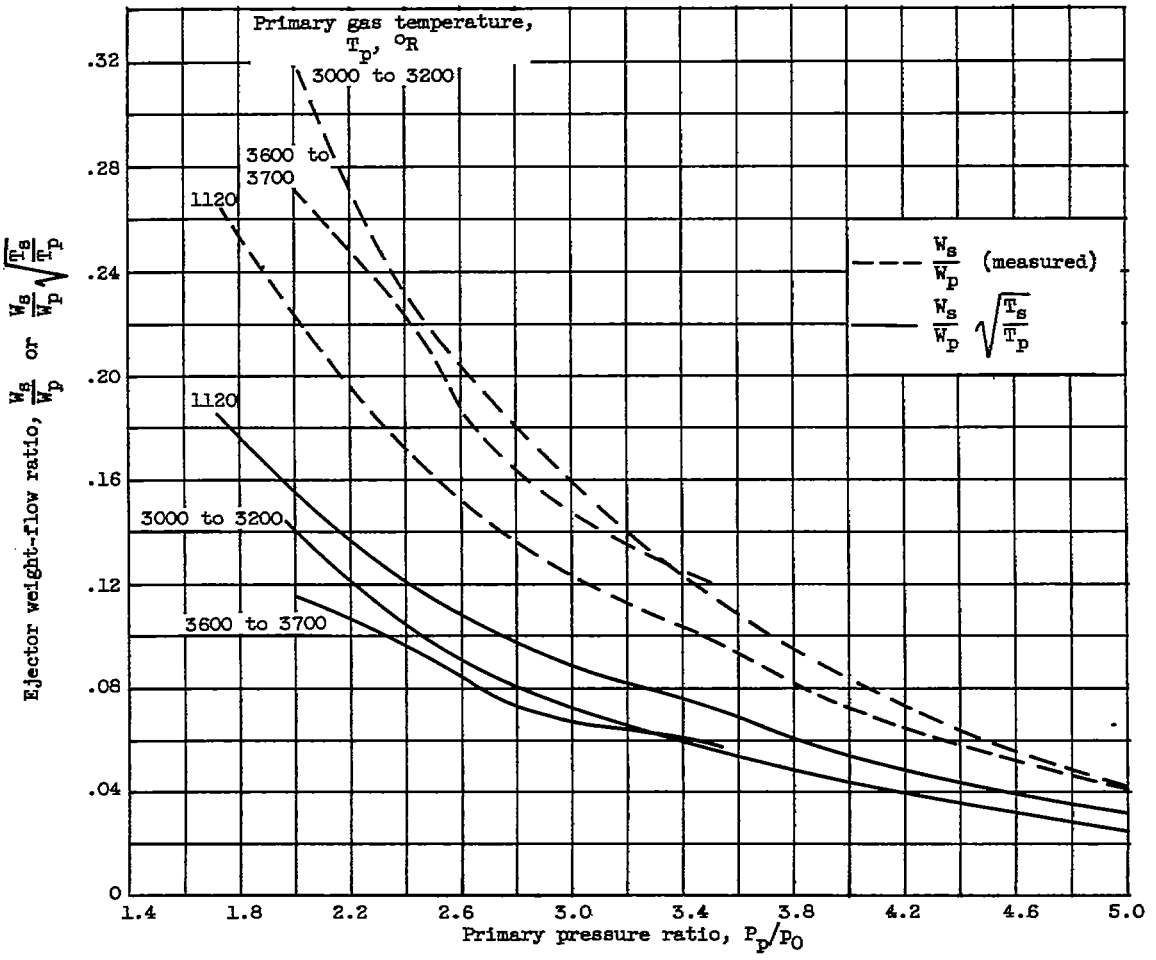

(b) Constant secondary pressure ratio, 2.5.

Figure 41. - Concluded. Comparison of measured and corrected weight-flow ratio over range of primary and secondary pressure ratio for configuration A. Diameter ratio, 1.048; spacing ratio, 0.445.

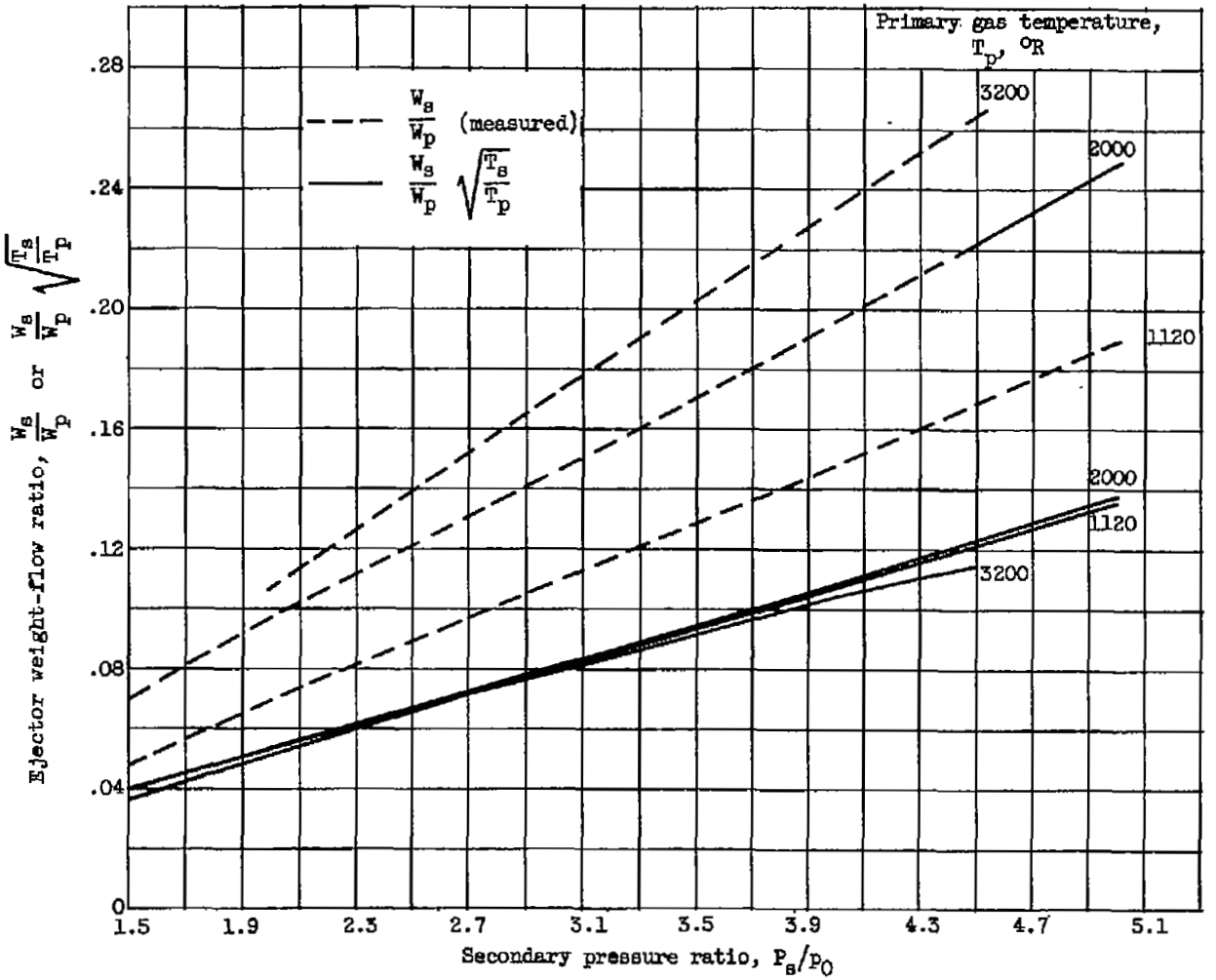

(a) Constant primary pressure ratio, 3.5.

Figure 42. - Comparison of measured and corrected weight-flow ratio over range of primary and secondary pressure ratio for configuration B. Diameter ratio, 1.095; spacing ratio, 0.213.

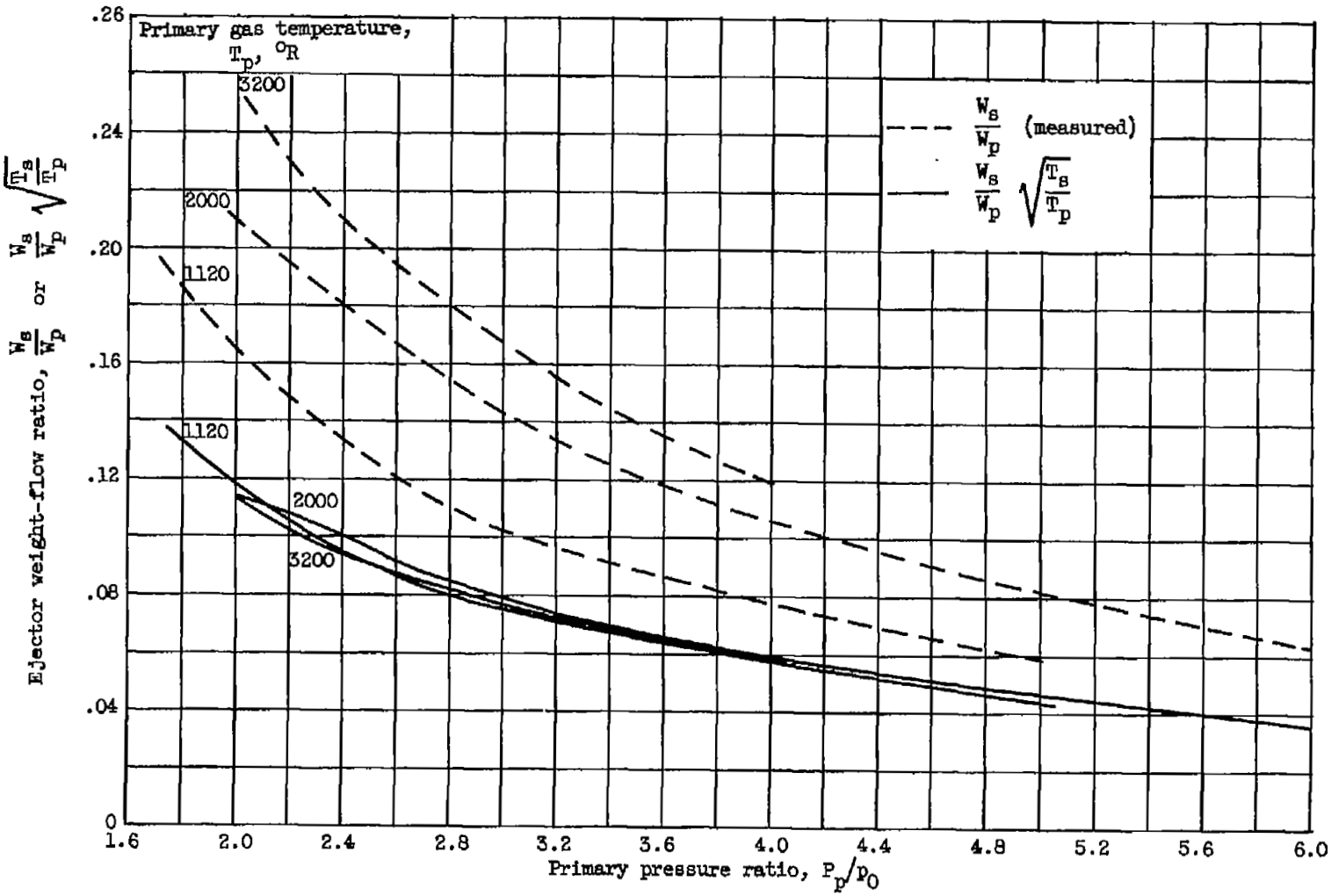

(b) Constant secondary pressure ratio, 2.5.

Figure 42. - Concluded. Comparison of measured and corrected weight-flow ratio over range of primary and secondary pressure ratio for configuration B. Diameter ratio, 1.095; spacing ratio, 0.213.

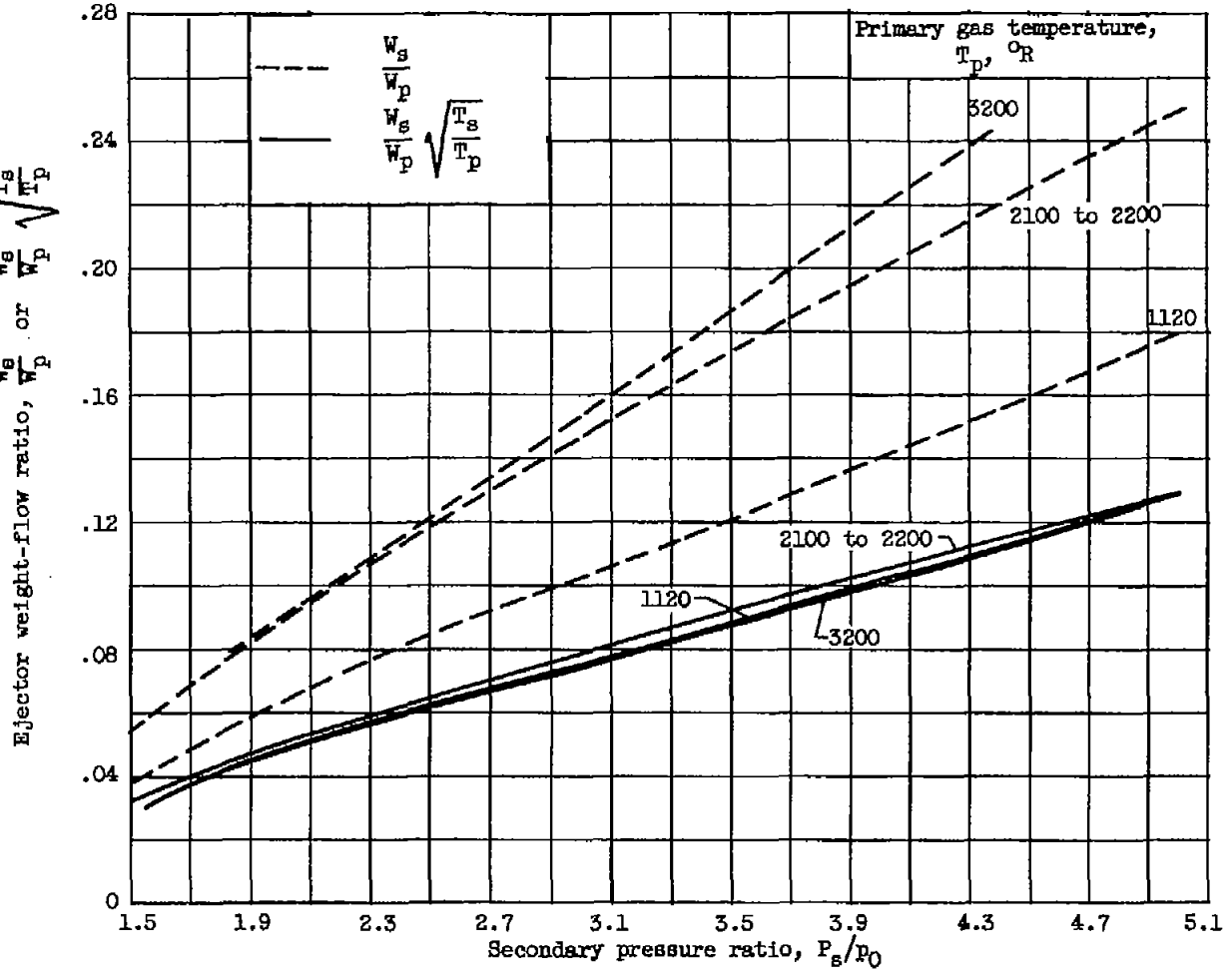

(a) Constant primary pressure ratio, 3.5.

Figure 43. - Comparison of measured and corrected weight-flow ratio over range of primary and secondary pressure ratio for configuration C. Diameter ratio, 1.095; spacing ratio, 0.408.

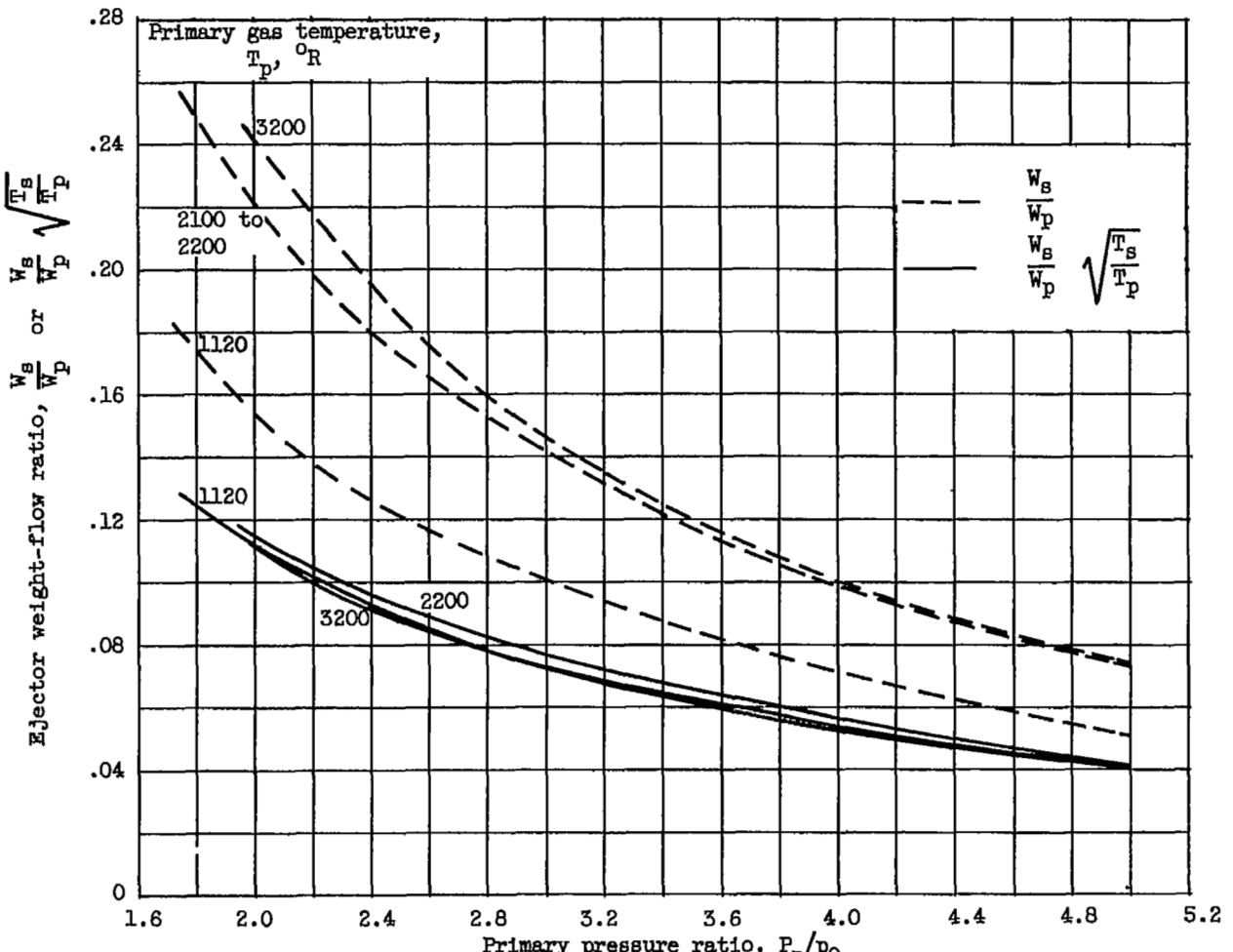

(b) Constant secondary pressure ratio, 2.5.

Figure 43. - Concluded. Comparison of measured and corrected weight-flow ratio over range of primary and secondary pressure ratio for configuration C. Diameter ratio, 1.095; spacing ratio, 0.408.

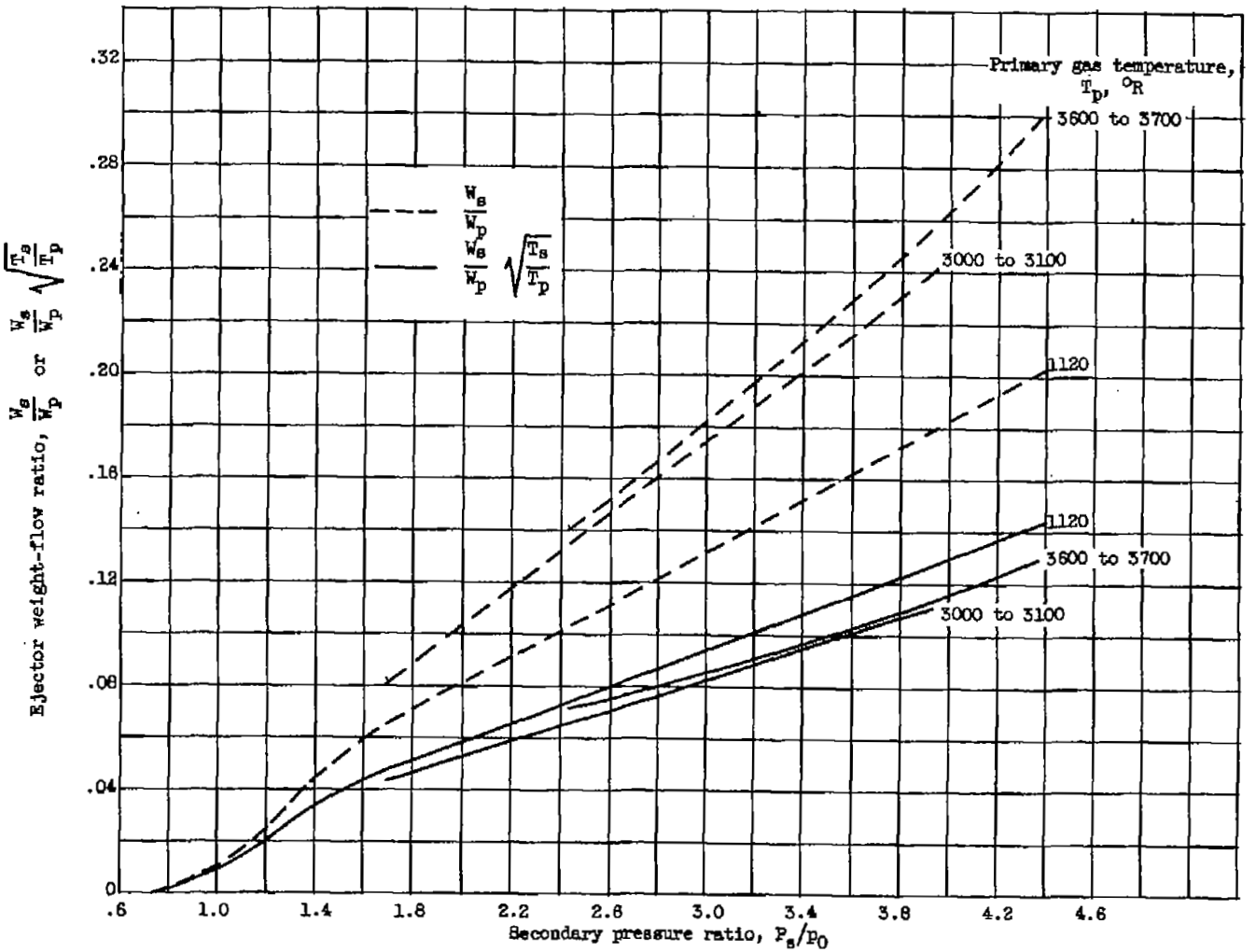

(a) Constant primary pressure ratio, 3.5.

Figure 44. - Comparison of measured and corrected weight-flow ratio over range of primary and secondary pressure ratio for configuration D. Diameter ratio, 1.095; spacing ratio, 0.810.

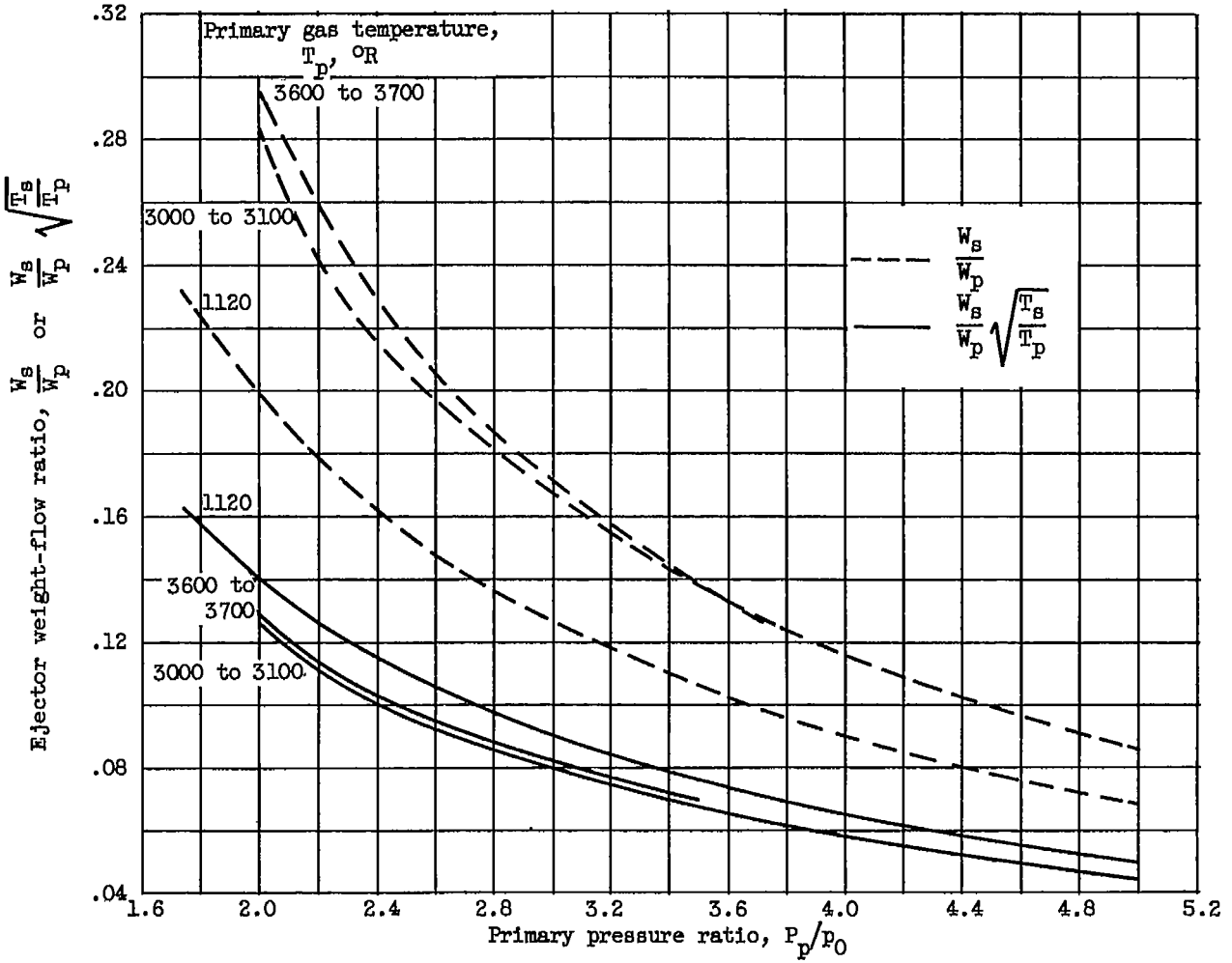

(b) Constant secondary pressure ratio, 2.5.

Figure 44. - Concluded. Comparison of measured and corrected weight-flow ratio over range of primary and secondary pressure ratio for configuration D. Diameter ratio, 1.095; spacing ratio, 0.810.

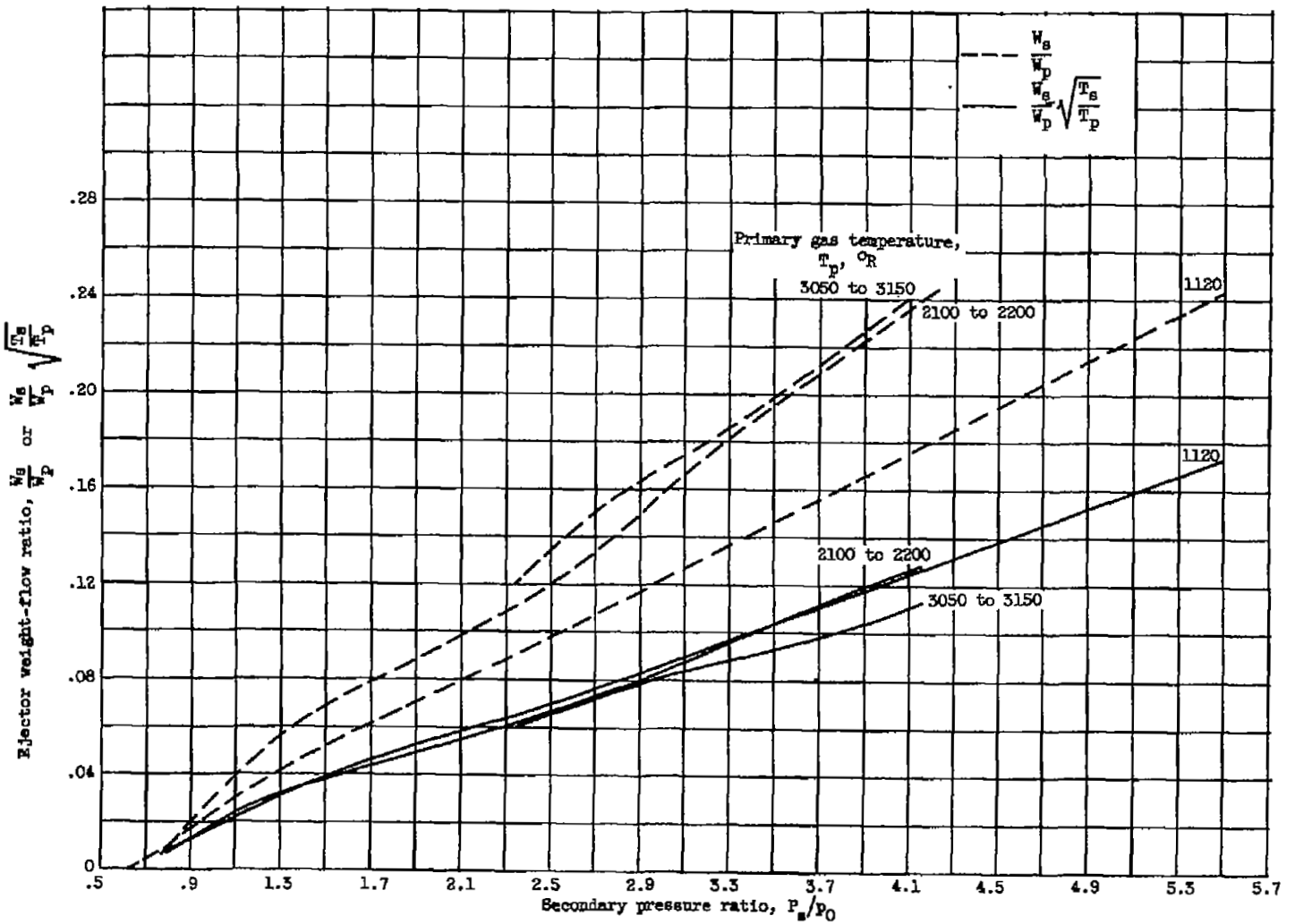

(a) Constant primary pressure ratio, 3.5.

Figure 45. - Comparison of measured and corrected weight-flow ratio over range of primary and secondary pressure ratio for configuration E. Diameter ratio, 1.195; spacing ratio, 0.405.

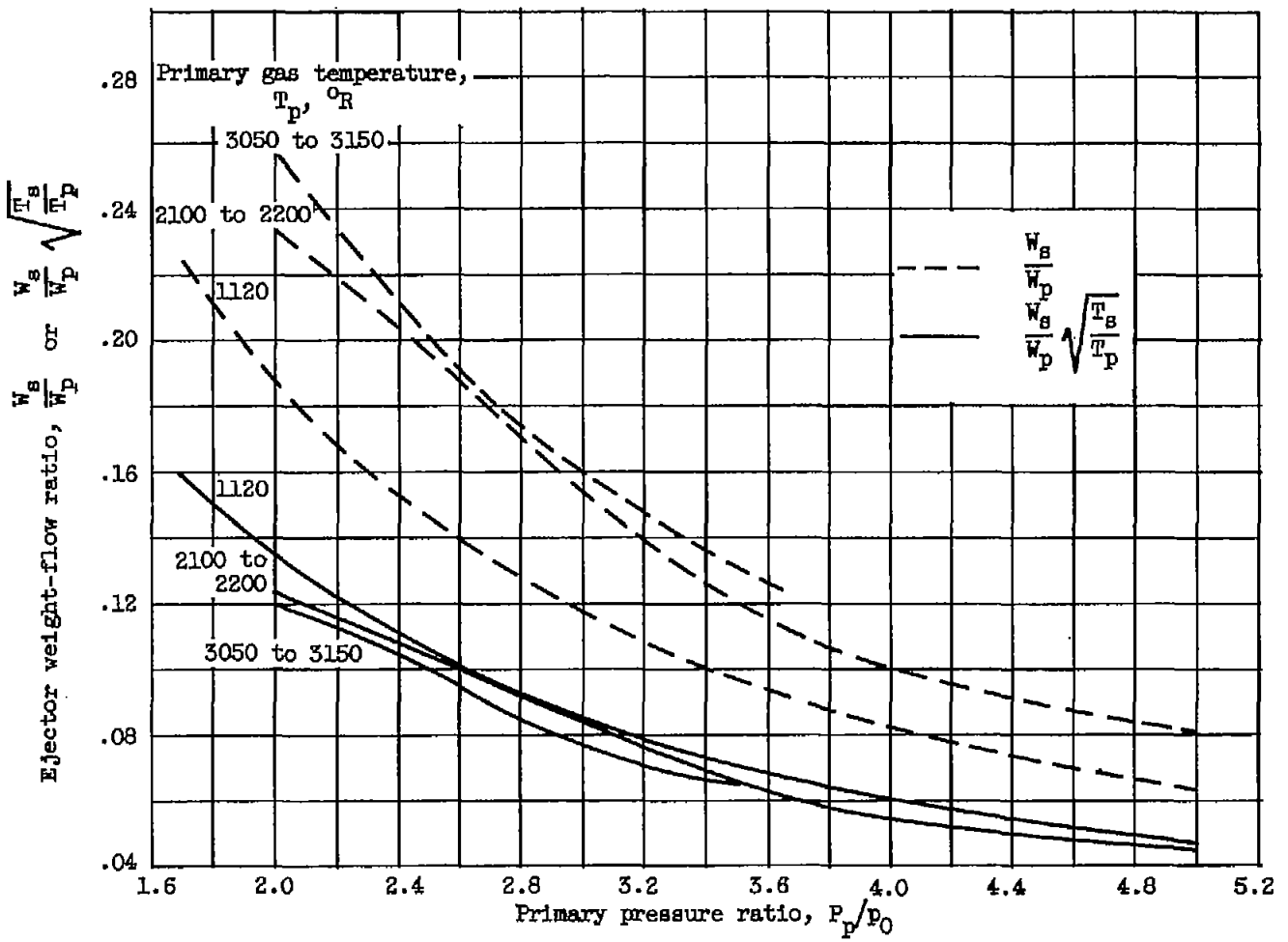

(b) Constant secondary pressure ratio, 2.5.

Figure 45. - Concluded. Comparison of measured and corrected weight-flow ratio over range of primary and secondary pressure ratio for configuration E. Diameter ratio, 1.195; spacing ratio, 0.403.

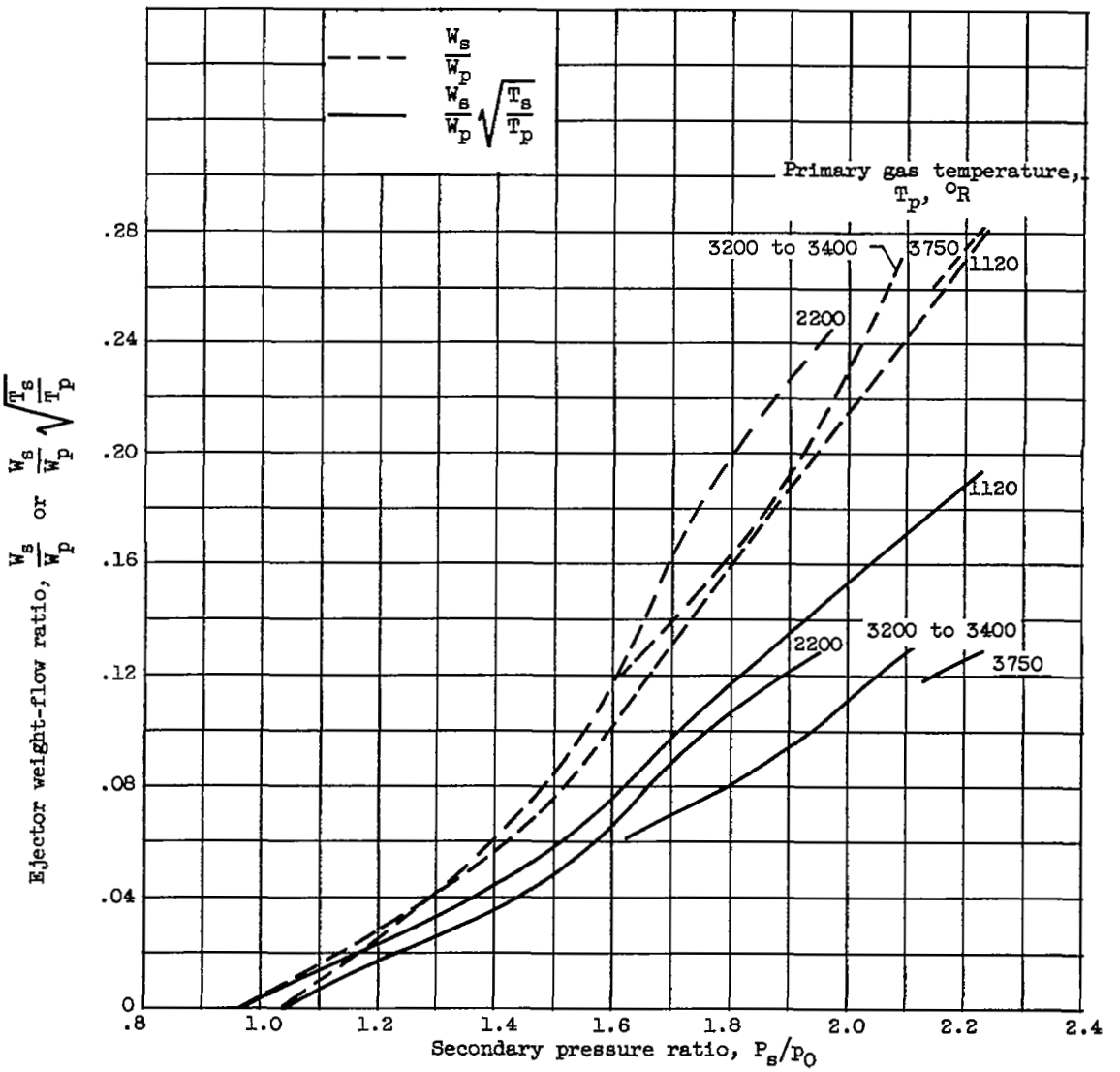

(a) Constant primary pressure ratio, 3.5.

Figure 46. - Comparison of measured and corrected weight-flow ratio over range of primary and secondary pressure ratio for configuration G. Diameter ratio, 1.10; spacing ratio, 0.408; conical.

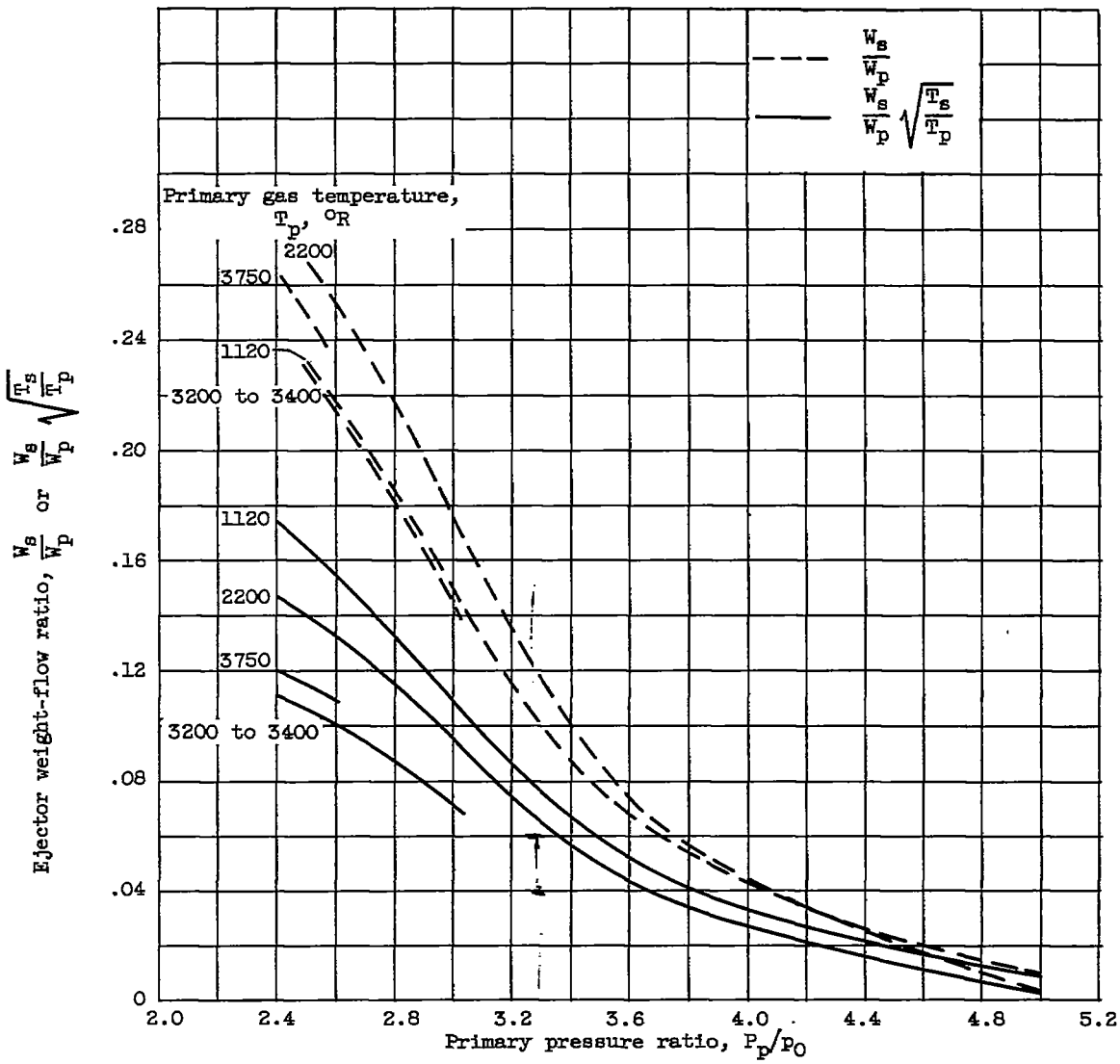

(b) Constant secondary pressure ratio, 1.5.

Figure 46. - Concluded. Comparison of measured and corrected weight-flow ratio over range of primary and secondary pressure ratio for configuration G. Diameter ratio, 1.10; spacing ratio, 0.408; conical.

[redacted]

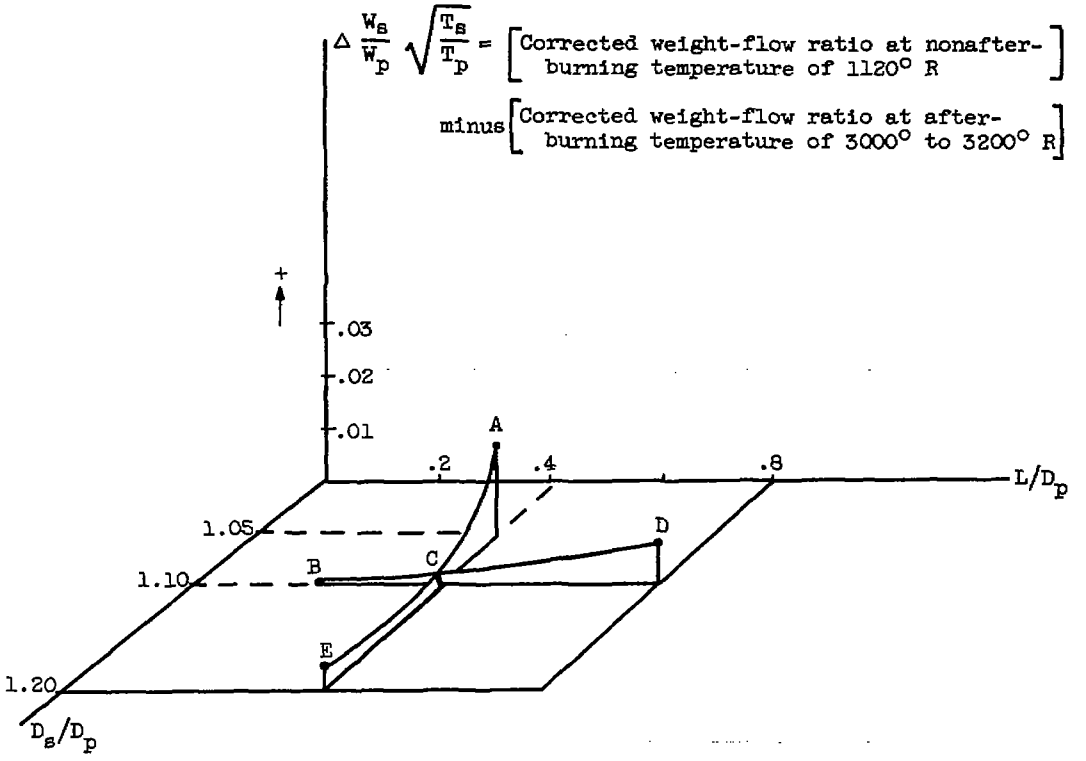

Configuration	Diameter ratio, D_s/D_p	Spacing ratio, L/D_p	$\Delta \frac{W_s}{W_p} \sqrt{\frac{T_s}{T_p}}$
A	1.048	0.445	0.017
B	1.095	.213	.0005
C	1.095	.408	.001
D	1.095	.810	.008
E	1.195	.408	.004

Figure 47. - Effect of diameter ratio and spacing ratio on degree of correlation of cylindrical-ejector air-flow characteristics obtained with the corrected weight-flow parameter. Primary pressure ratio, 3.5; secondary pressure ratio, 2.5.

[redacted]

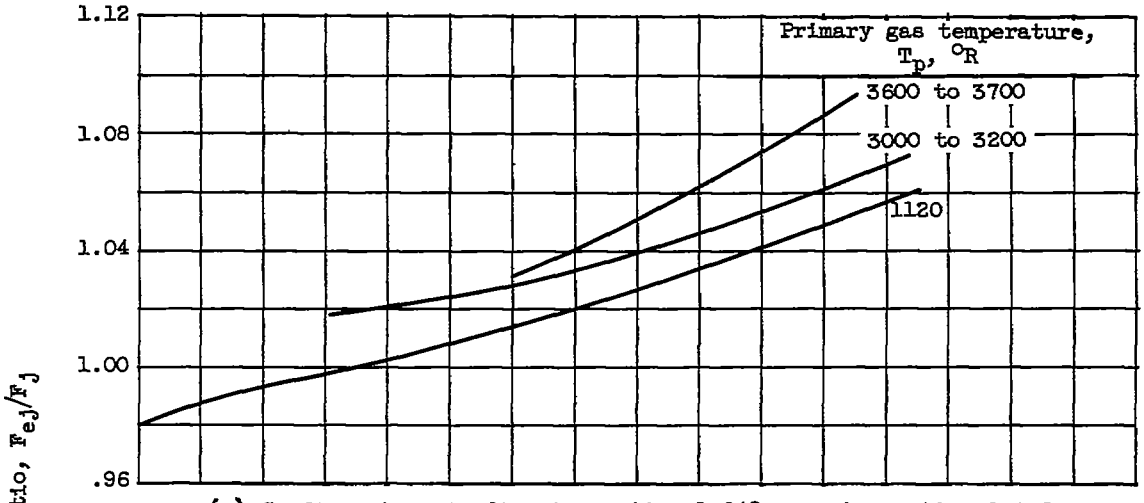

(a) Configuration A; diameter ratio, 1.048; spacing ratio, 0.445.

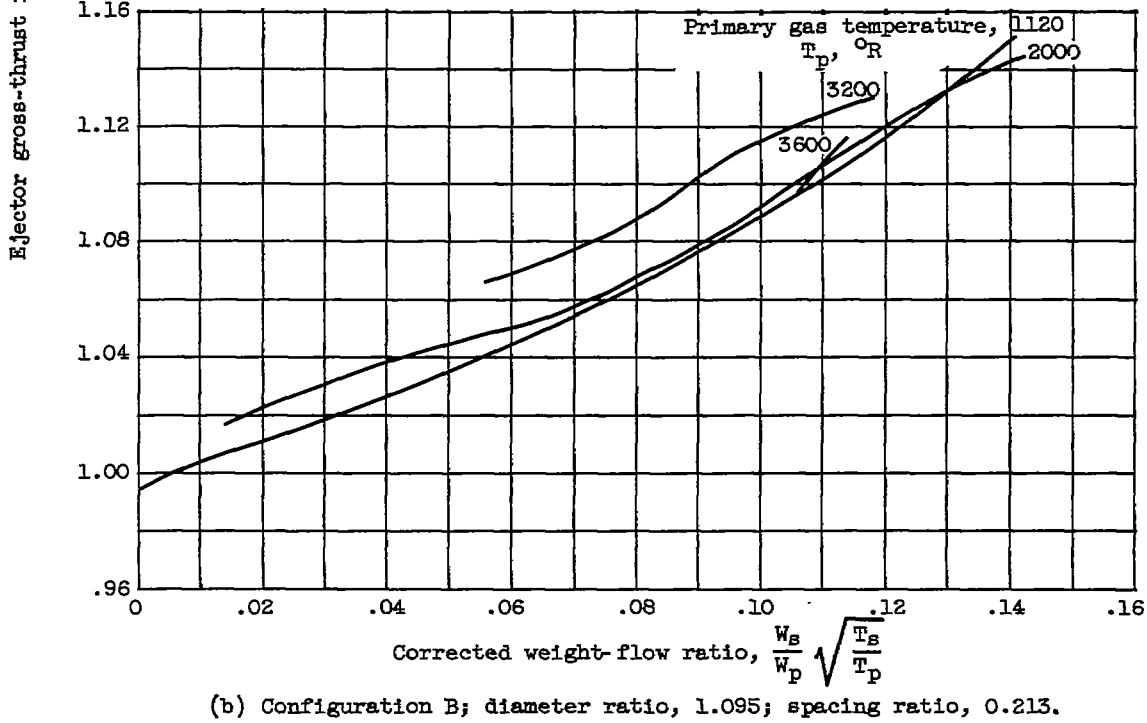

(b) Configuration B; diameter ratio, 1.095; spacing ratio, 0.213.

Figure 48. - Gross-thrust ratio of ejector configurations with various primary gas temperatures at primary pressure ratio of 5.0.

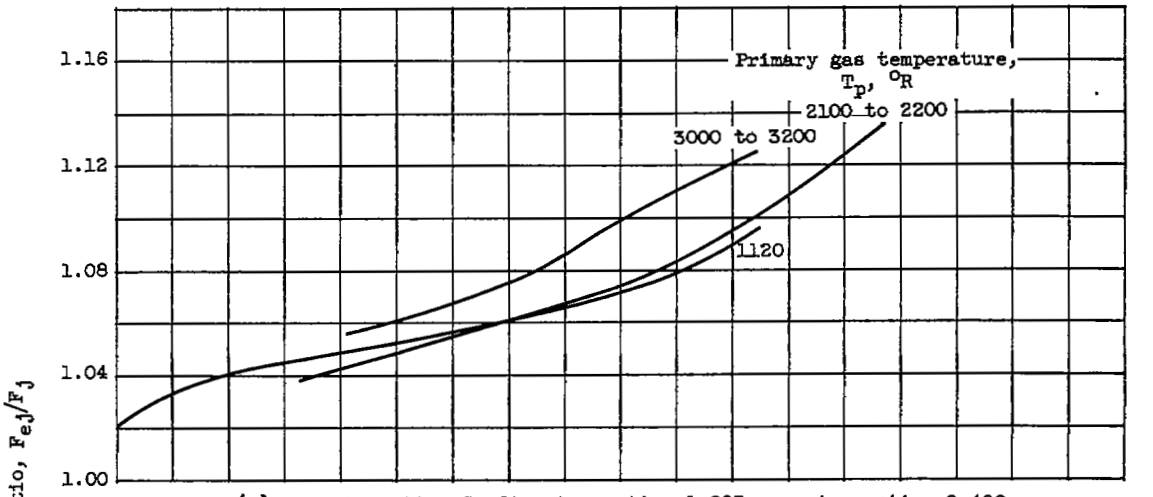

(c) Configuration C; diameter ratio, 1.095; spacing ratio, 0.406.

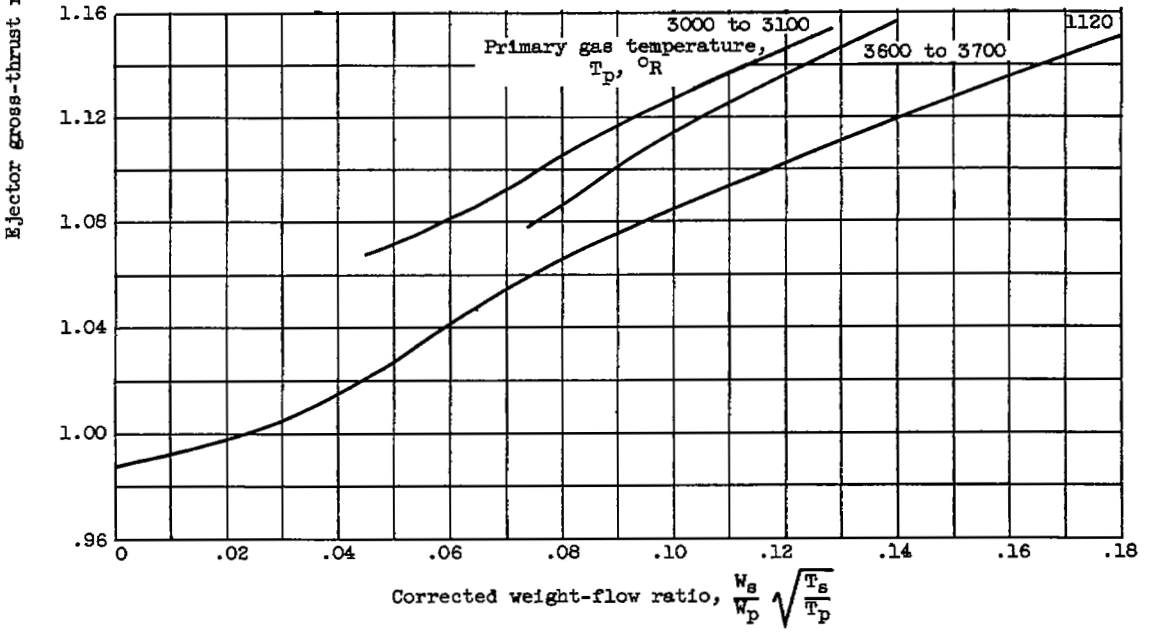

(d) Configuration D; diameter ratio, 1.095; spacing ratio, 0.810.

Figure 48. - Continued. Gross-thrust ratio of ejector configurations with various primary gas temperatures at primary pressure ratio of 5.0.

[redacted]

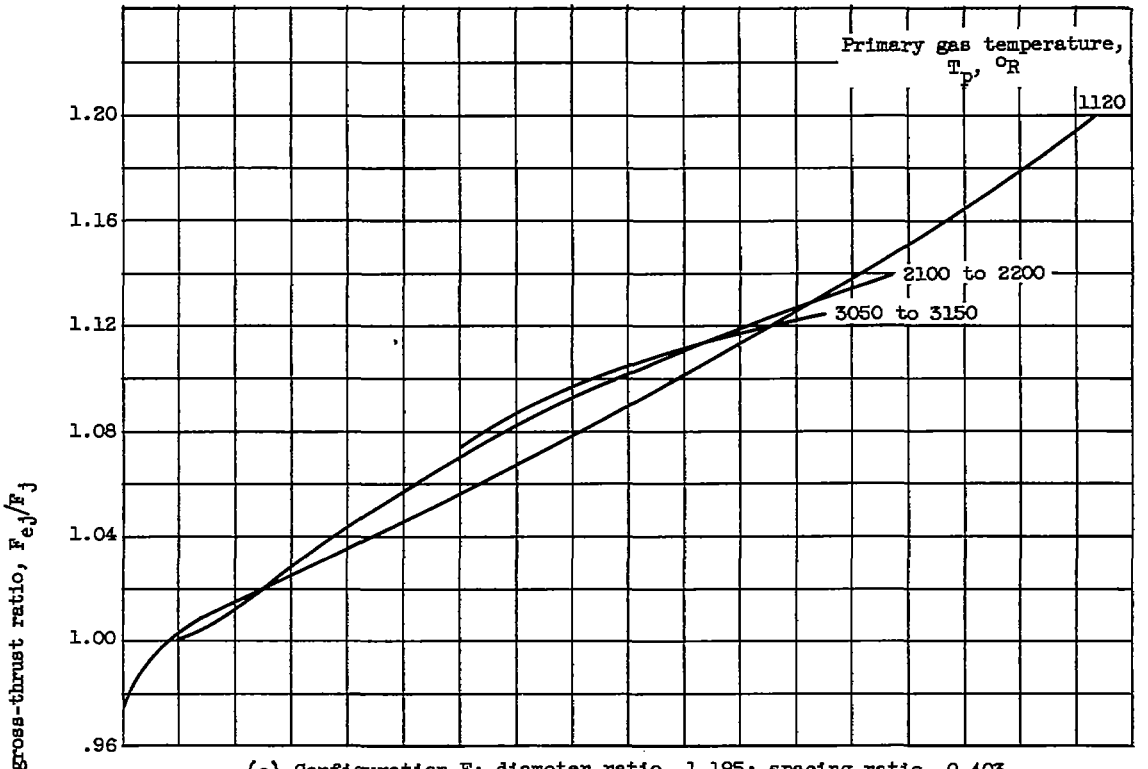

(e) Configuration E; diameter ratio, 1.195; spacing ratio, 0.403.

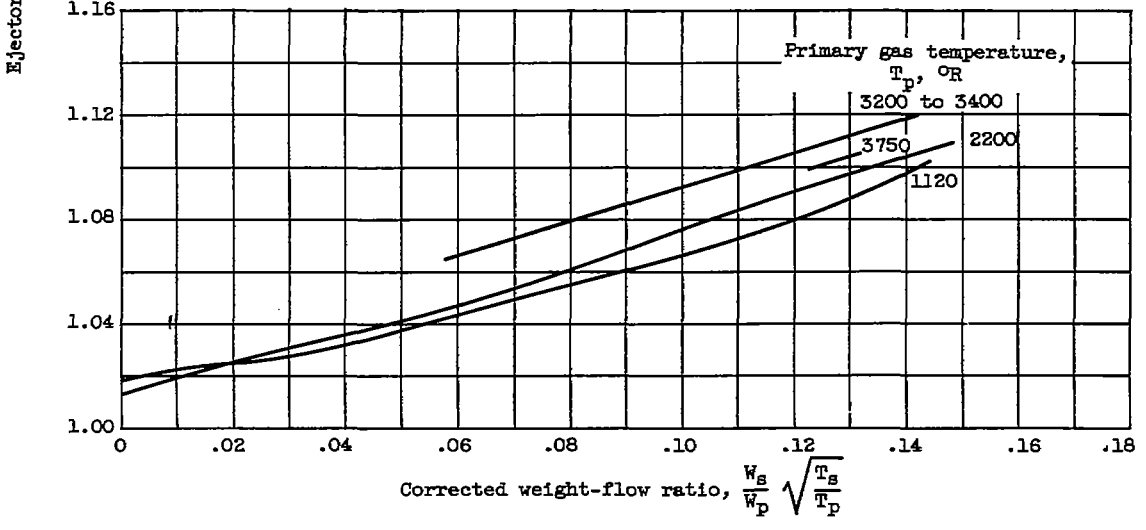

(f) Configuration G; conical ejector; diameter ratio, 1.10; spacing ratio, 0.408.

Figure 48. - Concluded. Gross-thrust ratio of ejector configurations with various primary gas temperatures at primary pressure ratio of 5.0.

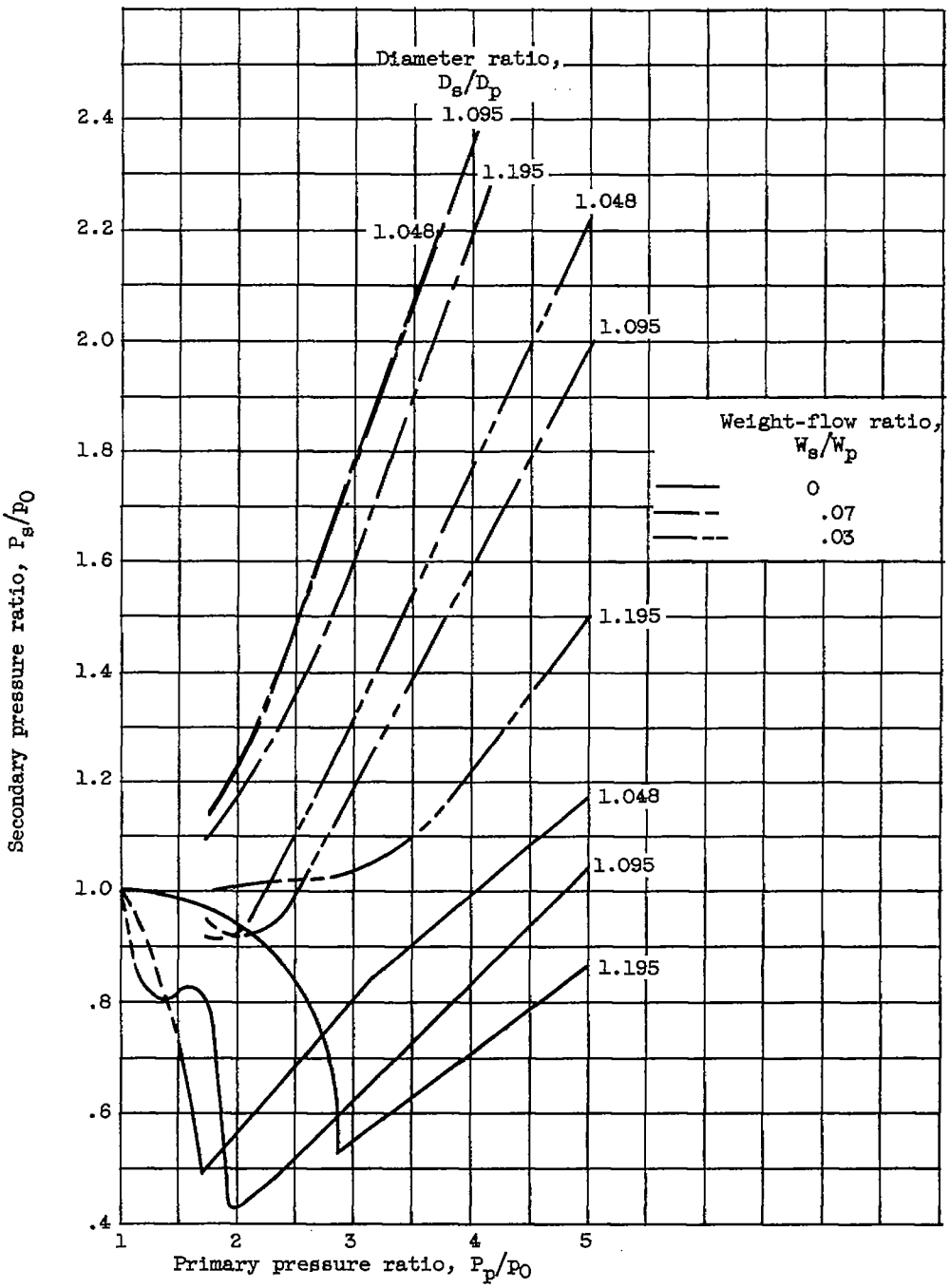

(a) Pumping characteristics.

Figure 49. - Comparison of ejector characteristics for three cylindrical ejectors having approximately the same spacing ratio of 0.4 at diameter ratios of 1.048, 1.095, and 1.195. Primary gas temperature, 1120° R.

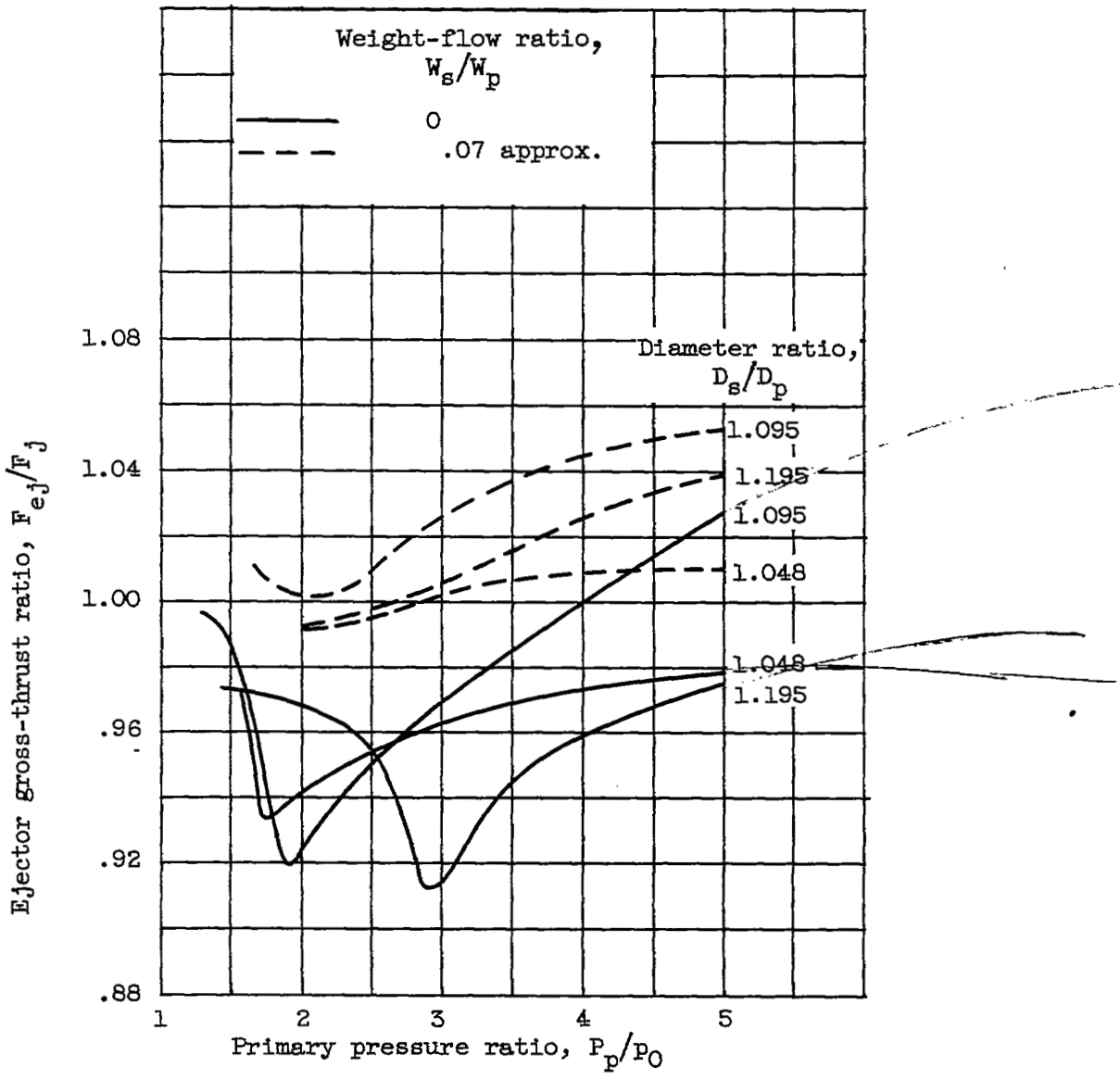

(b) Thrust characteristics.

Figure 49. - Concluded. Comparison of ejector characteristics for three cylindrical ejectors having approximately the same spacing ratio of 0.4 at diameter ratios of 1.048, 1.095, and 1.195. Primary gas temperature, 1120° R.

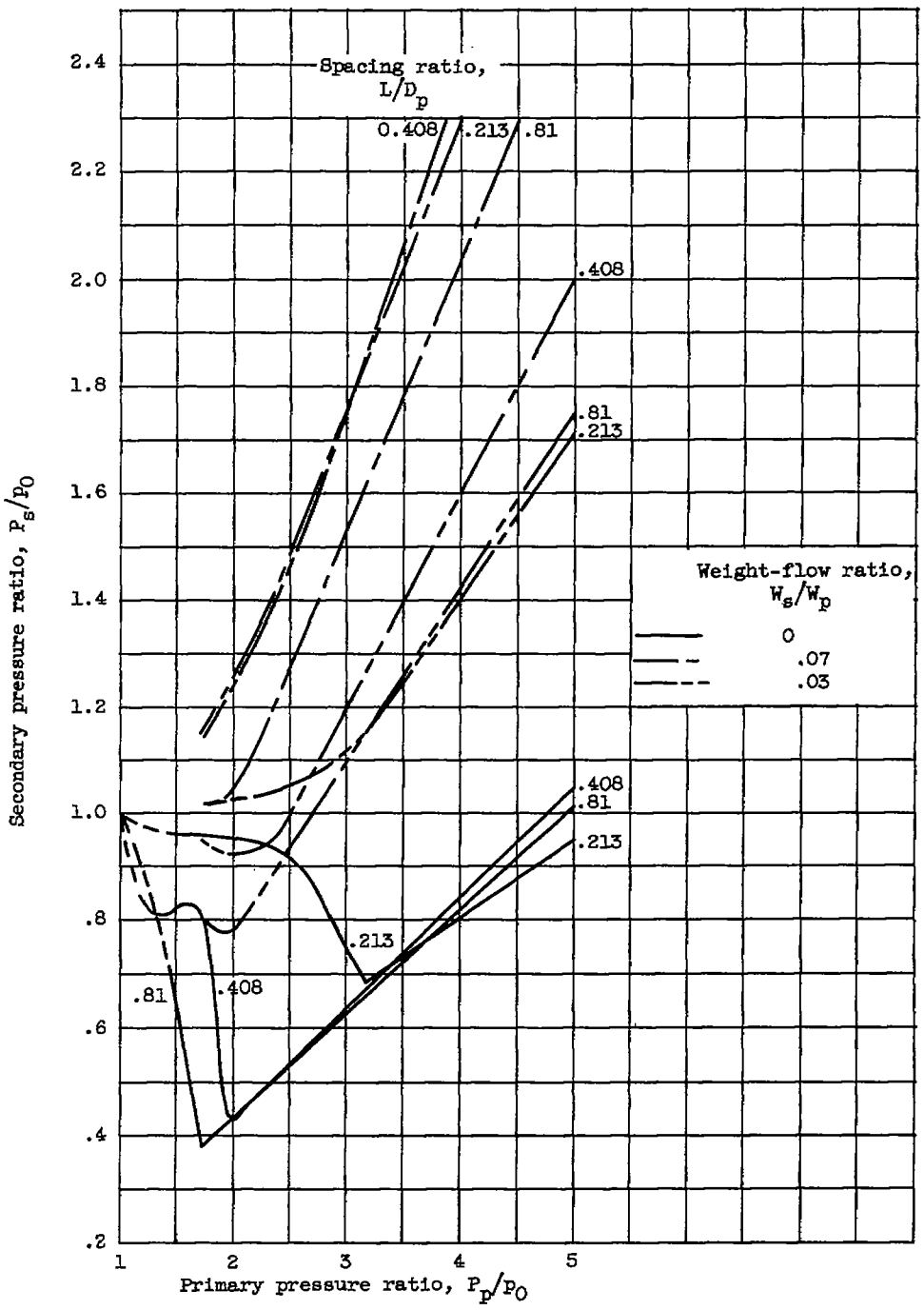

(a) Pumping characteristics.

Figure 50. - Comparison of ejector characteristics for three cylindrical ejectors having the same diameter ratio of 1.095 at spacing ratios of 0.213, 0.408, and 0.810. Primary gas temperature, 1120° R.

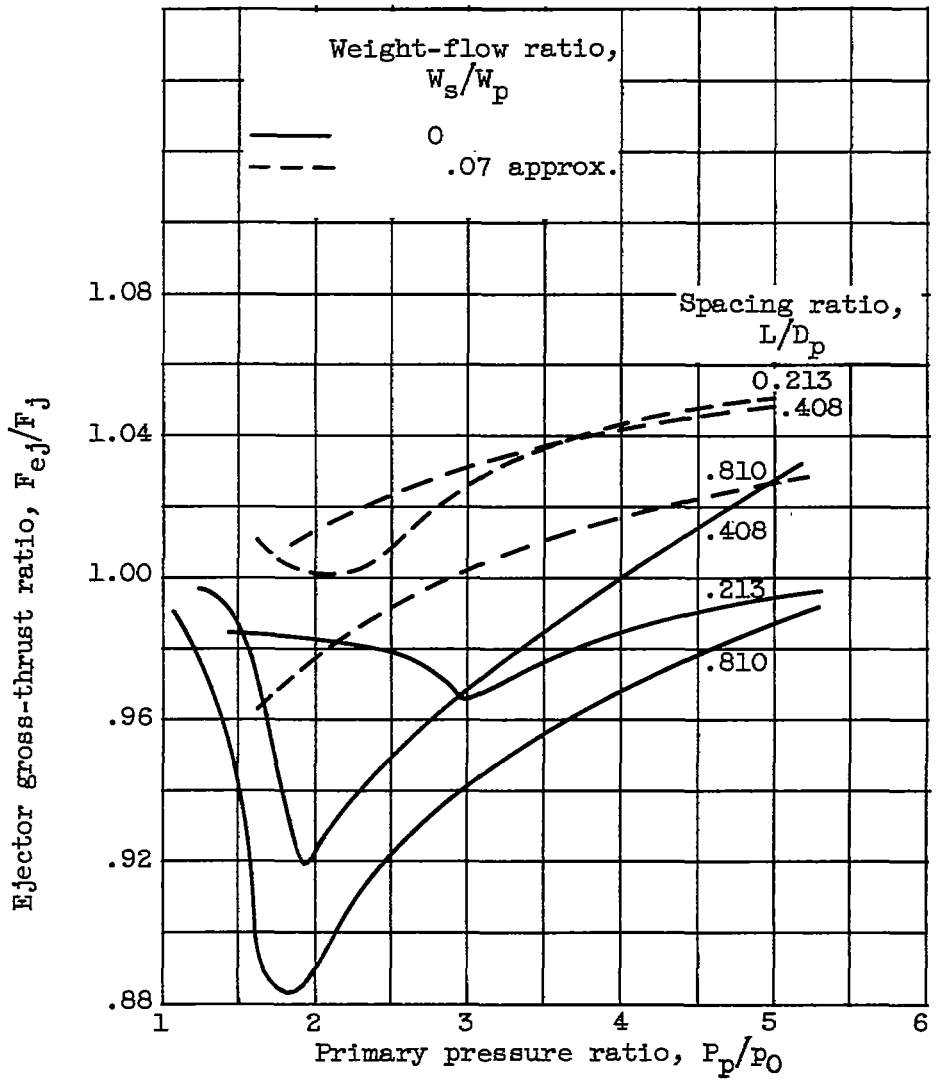

(b) Thrust characteristics.

Figure 50. - Concluded. Comparison of ejector characteristics for three cylindrical ejectors having the same diameter ratio of 1.095 at spacing ratios of 0.213, 0.408, and 0.810. Primary gas temperature, 1120° R.

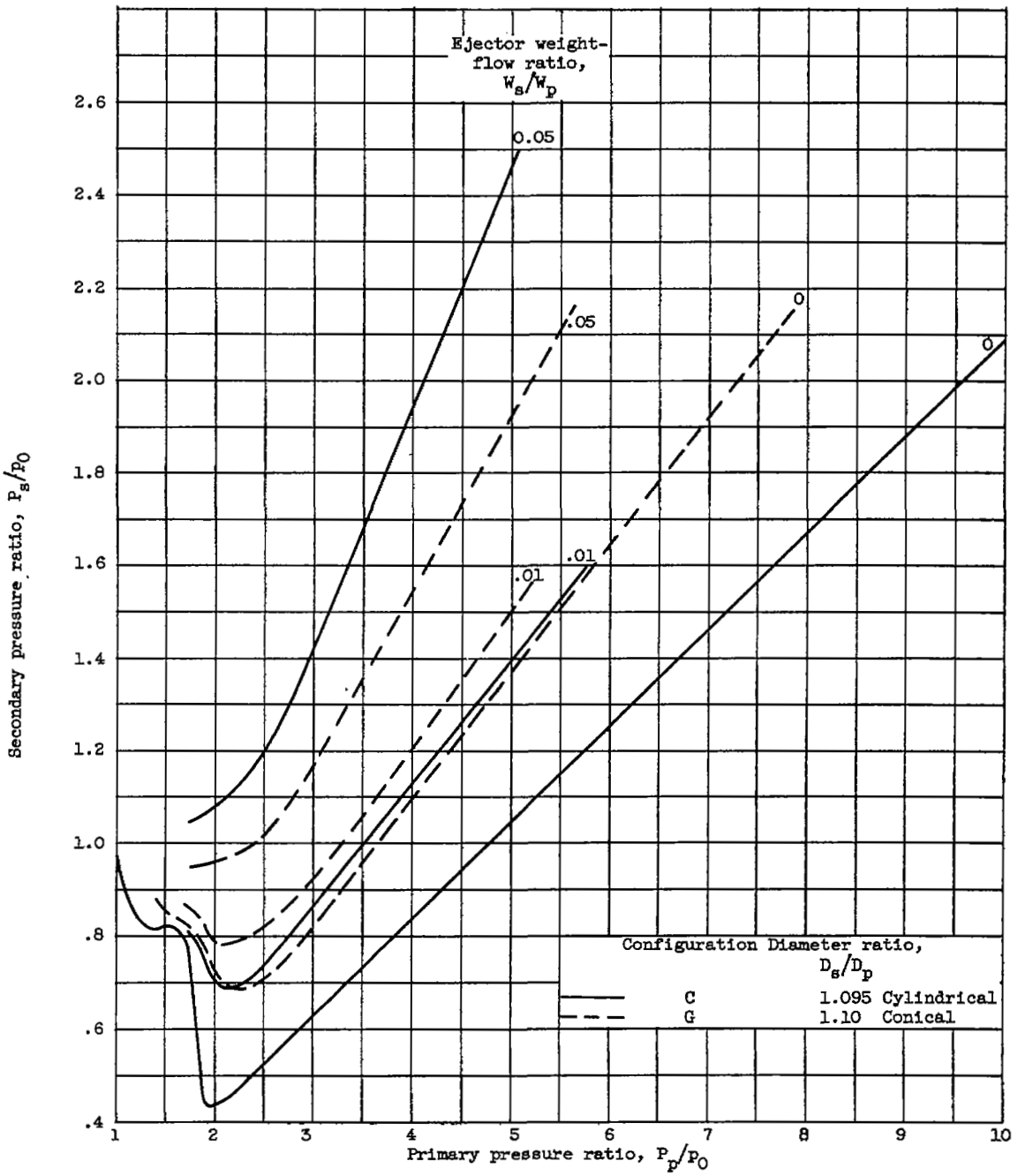

(a) Pumping characteristics.

Figure 51. - Comparison of cylindrical- and conical-ejector characteristics at approximately the same diameter ratio and spacing ratio. Primary gas temperature, 1120° R; spacing ratio, 0.408.

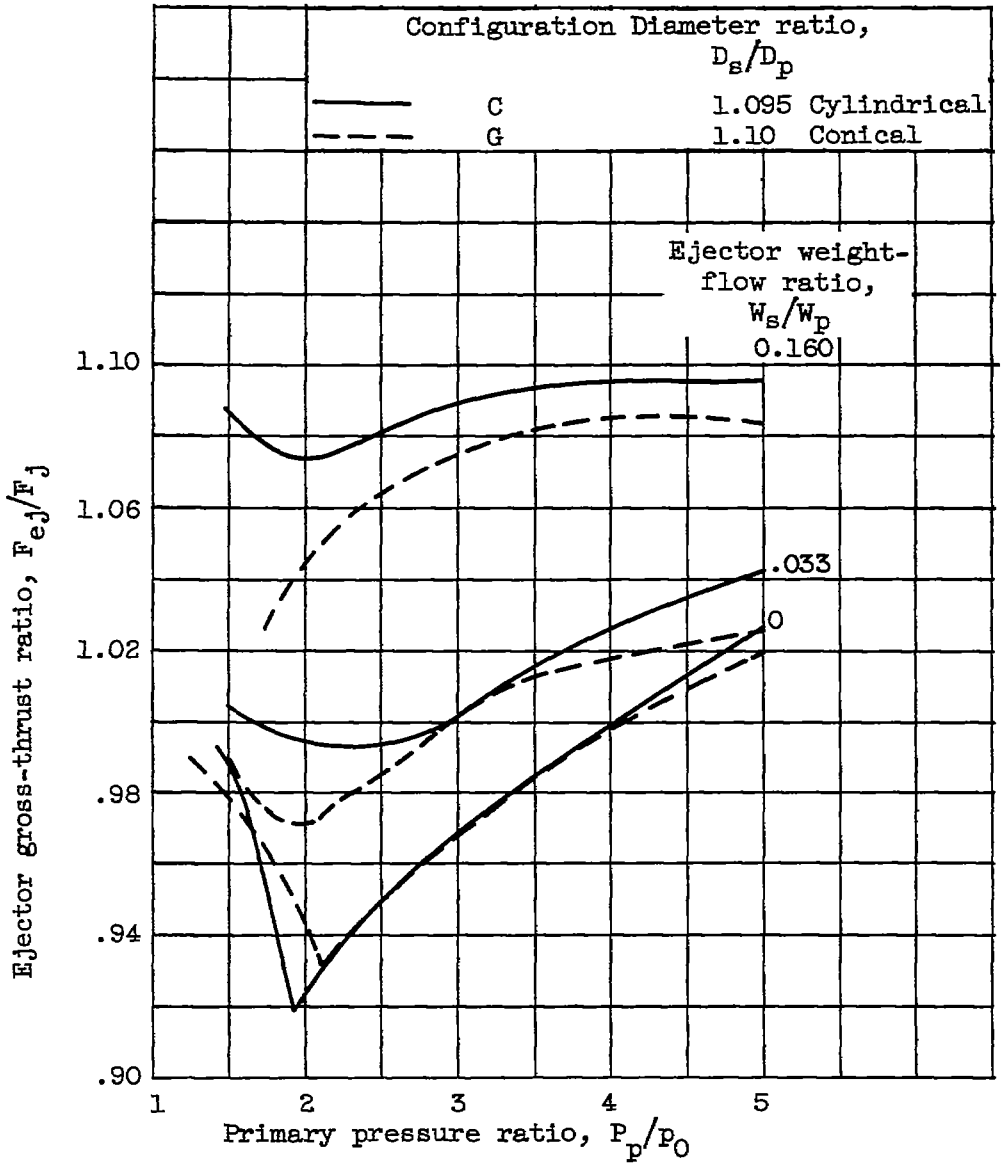

(b) Thrust characteristics.

Figure 51. - Concluded. Comparison of cylindrical- and conical-ejector characteristics at approximately the same diameter ratio and spacing ratio. Primary gas temperature, 1120° R; spacing ratio, 0.408.

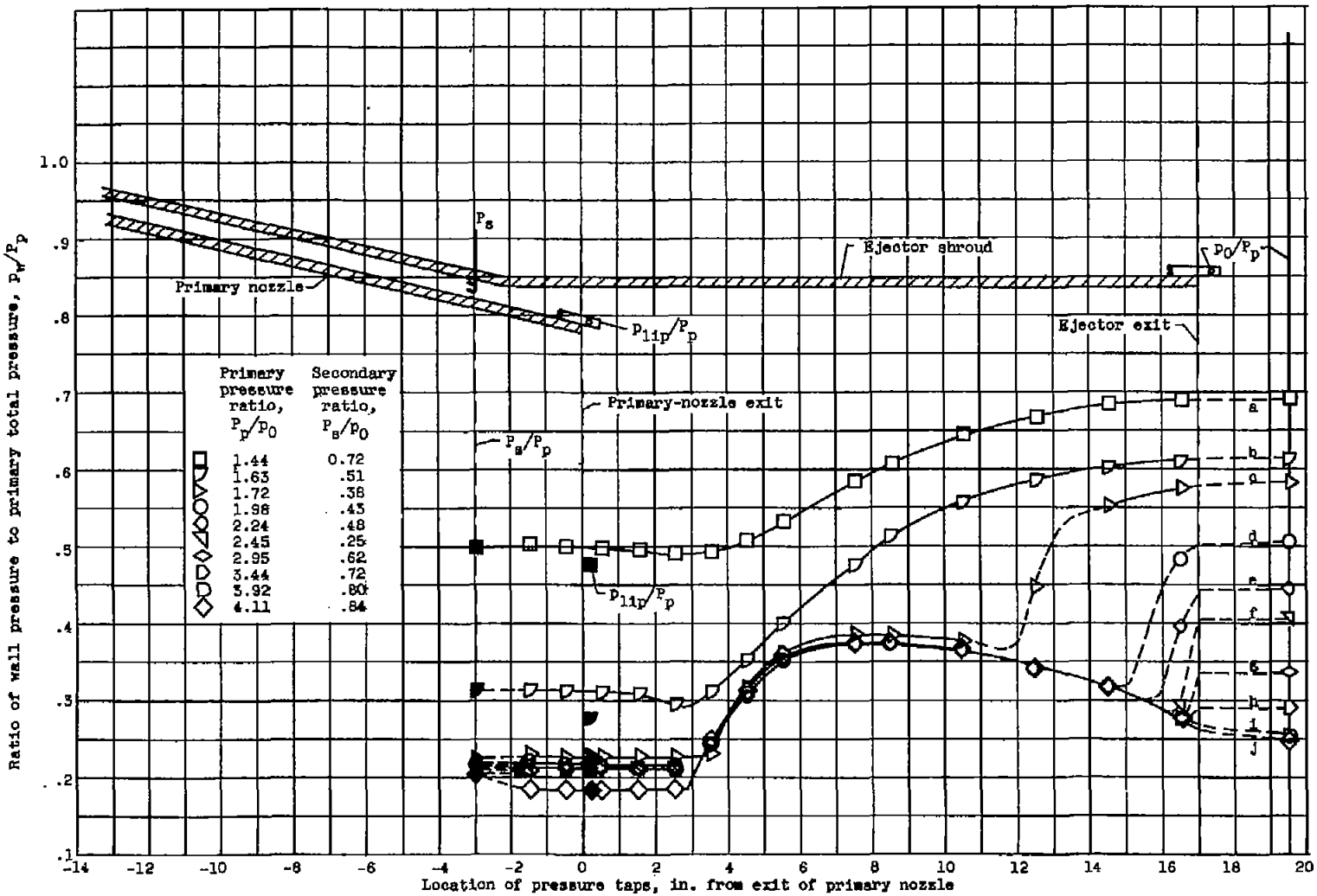

Figure 52. - Wall-pressure profile along ejector shroud of configuration D at primary gas temperature of 1120° R and zero secondary flow. Diameter ratio, 1.095; spacing ratio, 0.810.

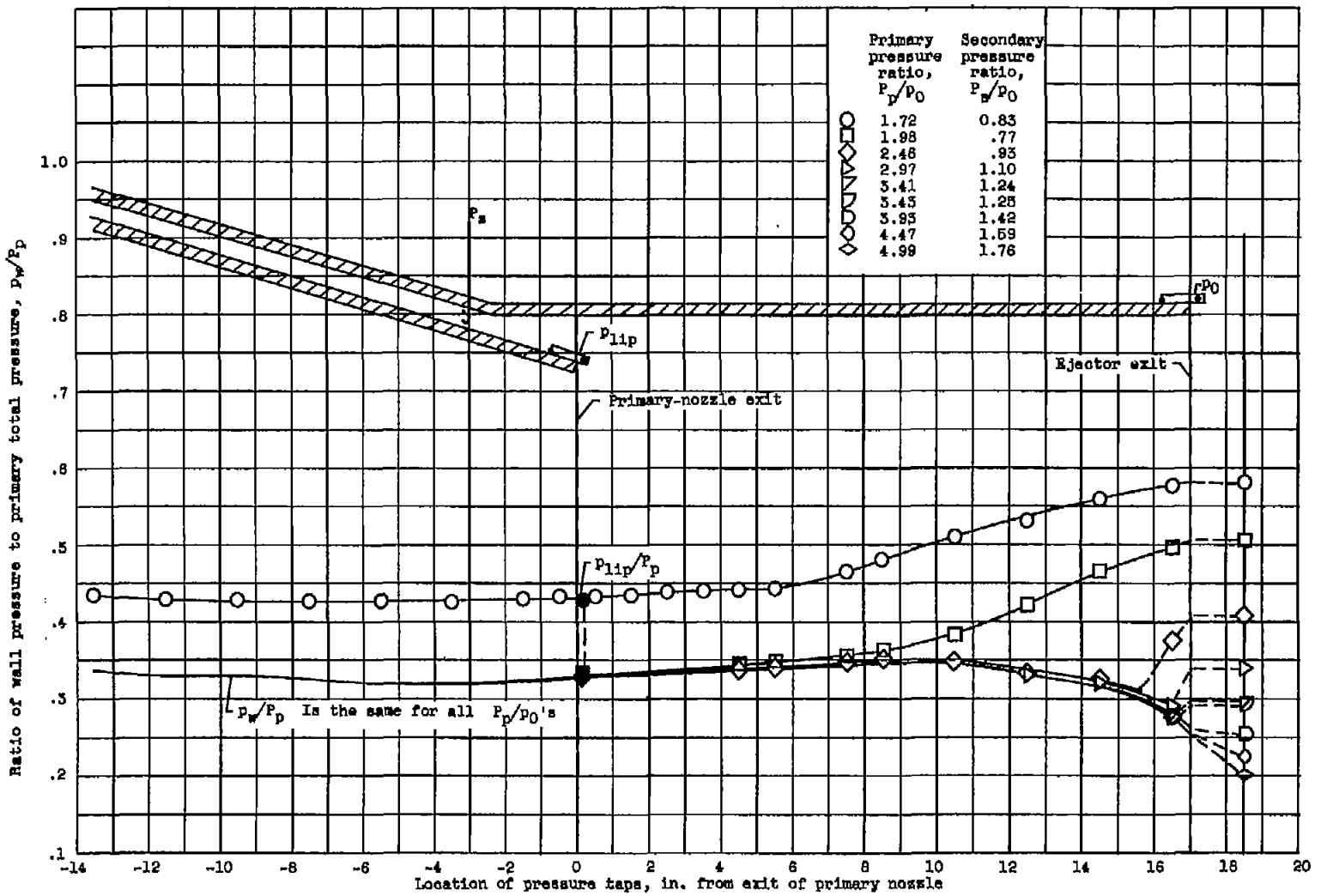

Figure 53. - Wall-pressure profile along ejector shroud of configuration D at primary gas temperature of 1120° R and ejector weight-flow ratio of approximately 0.031. Temperature ratio, 1.61 to 1.66; diameter ratio, 1.095; spacing ratio, 0.810.

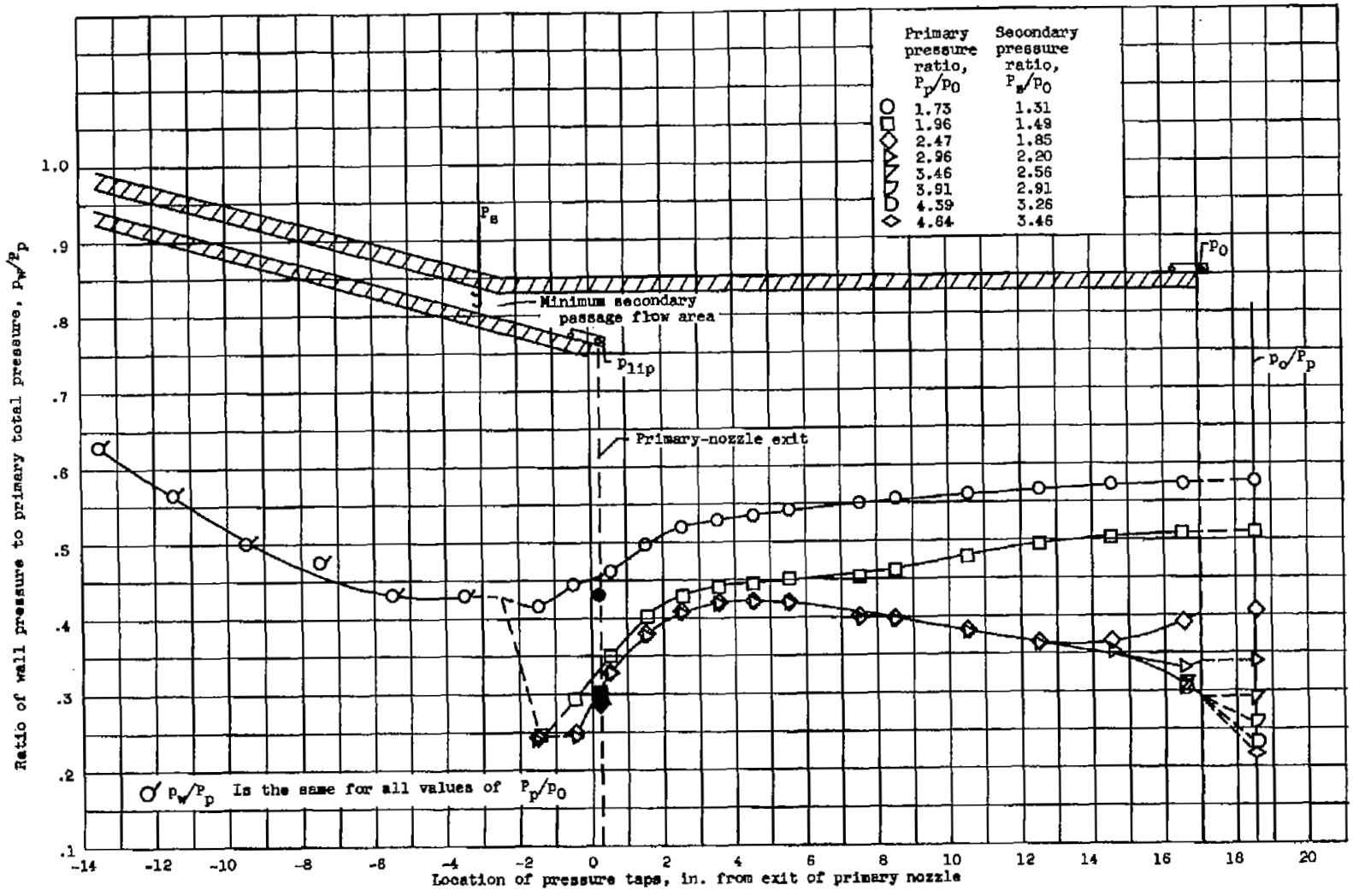

Figure 54. - Wall-pressure profile along ejector shroud of configuration D at primary gas temperature of 1120° R and ejector weight-flow ratio of approximately 0.112. Temperature ratio, 1.92 to 1.96; diameter ratio, 1.095; spacing ratio, 0.810.